

2006

Kinematics of curved flexible beam

Saurabh Jagirdar

University of South Florida

Follow this and additional works at: <http://scholarcommons.usf.edu/etd>



Part of the [American Studies Commons](#)

Scholar Commons Citation

Jagirdar, Saurabh, "Kinematics of curved flexible beam" (2006). *Graduate Theses and Dissertations*.
<http://scholarcommons.usf.edu/etd/2572>

This Thesis is brought to you for free and open access by the Graduate School at Scholar Commons. It has been accepted for inclusion in Graduate Theses and Dissertations by an authorized administrator of Scholar Commons. For more information, please contact scholarcommons@usf.edu.

Kinematics of Curved Flexible Beam

by

Saurabh Jagirdar

A thesis submitted in partial fulfillment
of the requirements for the degree of
Master of Science in Mechanical Engineering
Department of Mechanical Engineering
College of Engineering
University of South Florida

Major Professor: Craig P. Lusk, Ph.D.
Rajiv Dubey, Ph.D.
Autar K. Kaw, Ph.D.

Date of Approval:
October 26, 2006

Keywords: Compliant mechanisms, Pseudo-rigid-body, Spherical,
MEMS, Out of plane

© Copyright 2006, Saurabh Jagirdar

Dedication

Dedicated to my parents and my major professor.

Acknowledgement

I wish to express my gratitude to everyone who contributed to making this thesis a reality. I must single out my professor Dr. Craig P. Lusk who supported and guided me right from the beginning to bring this thesis to fruition.

I also want to thank my supervisory committee Dr. Rajiv Dubey and Dr Autar K. Kaw and all other professors for their encouragement and guidance.

I am especially grateful to our department staff Ms Susan Britten, Ms Shirley Tervort and Mr. Wes Frusher who helped me through all the official procedures and setting up our compliant mechanisms laboratory.

I thank Ms Cherine Chehab from the College of Engineering, USF to edit and improve the format of the thesis.

I am indebted to Mr Prateek Asthana of CSEE, Dept, USF to help me generate large number of input files by writing just one program. This program saved me enormous amount of time that it would have taken to generate them one by one.

I thank my friends and colleagues of the Mechanical engineering department and other departments for making my life fun and also

helping me through various ways, a special reference to Daniel Vilceus who continuously kept me pepped up with his sense of humour, Hari Patel, John Daly, Shantanu Shevade, Aditya Bansal, Cesar Hernandez and Son Ho.

I also thank my laboratory mates Joe, Alex, Diego, Sebastian, Patricia and Issa for their help and support.

I am deeply indebted to my roommates Dr Apurva Panchal and Phaninder Injeti for their patience to bear and take all my eccentricities and help me through my tough times.

I once again thank the Mechanical Engineering Department., the College of Engineering and University of South Florida, Tampa Florida.

Table of Contents

List of Tables	ii
List of Figures	iii
Abstract	vi
1. Introduction	1
1.1 Scope	2
1.2 Background	4
1.3 Roadmap	15
2. Methodology and Model Development	16
2.1 Correspondence between spherical and planar PRBMs	16
2.2 Kinematics of compliant circular arc	18
2.3 Spherical kinematics of the pseudo-rigid-body model	21
2.4 Spherical loading condition analogous to planar vertical end load	23
3. Finite Element Analysis (FEA)	24
4. Parametric Approximation of the Curved Beam's Deflection Path	33
5. Results and Discussion	40
6. Conclusion	50
References	51
Appendices	56
Appendix A Spherical Triangles and Napier Rules	57
Appendix B Manual for FEA	62
Appendix C Algorithms to Find γ	100
Appendix D Summary	119

List of Tables

Table 1:	Spherical PRBM	119
Table 2:	Planar PRBM	120

List of Figures

Figure 1:	A PRBM for a cantilever beam with a vertical end load (Howell 2001)	7
Figure 2:	Planar Mechanism with sliders moving on perpendicular straight lines	9
Figure 3:	Spherical mechanism with sliders moving on perpendicular circular arcs	10
Figure 4:	Geodesics	11
Figure 5:	Parallel transport (Henderson 1998)	13
Figure 6:	Parallel transport along the same longitude	14
Figure 7:	Relationship between existing planar PRBM and the spherical PRBM developed in this work	17
Figure 8:	Reference frames describing the motion of the end of a compliant circular cantilever	20
Figure 9:	The pseudo-rigid-body model of the compliant curved beam	22
Figure 10:	Path followed by beam the dotted line from Q to Q''	25
Figure 11:	Reference frames used to model the spherical mechanism and its planar equivalent	26
Figure 12:	Cross-section of beam for various aspect ratios	29
Figure 13:	Finite element model	30
Figure 14:	Deflection of curved segment	35
Figure 15:	Deflection of PRBM	37

Figure 16:	Final position of beam from fixed end α , v/s input displacement β	41
Figure 17:	Deflection of beam about neutral axis, θ_0 ,v/s input displacement β	41
Figure 18:	γ v/s Arc-lengths showing various colors for aspect ratios	42
Figure 19:	C_θ v/s Arc-lengths showing various colors for aspect ratios	43
Figure 20:	θ_{max} v/s Arc-lengths showing various colors for aspect ratios	43
Figure 21:	γ v/s Arc-lengths, for 200 load-steps of input displacement	45
Figure 22:	C_θ v/s Arc-lengths, for 200 load-steps of input displacement	46
Figure 23:	θ_{max} v/s Arc-lengths, for 200 load-steps of input displacement	47
Figure 24:	Trend-line of γ , for aspect ratio 0.1	48
Figure 25:	Trend-line of γ , for aspect ratio 0.4	48
Figure 26:	Trend-line of γ , for aspect ratio 0.7	49
Figure 27:	Spherical triangles	57
Figure 28:	Five parts arranged in order of occurrence	58
Figure 29:	Spherical right triangle	59
Figure 30:	Five parts for PRBM right spherical triangle	60
Figure 31:	Activating Graphical User Interface (GUI)	62
Figure 32:	Limiting the GUI options to structural preferences	63
Figure 33:	Adding or defining new element types	64

Figure 34: Beam elements	65
Figure 35: Defining real constants for respective elements	66
Figure 36: Inputting area and moment of inertia values to elements	67
Figure 37: Defining material properties	68
Figure 38: Creating key-points on work-plane through GUI	69
Figure 39: Creating key-points using command line	70
Figure 40: Pan, zoom, rotate	71
Figure 41: Defining of orthogonal triad at beam end	72
Figure 42: Creating lines	73
Figure 43: Creating arcs	74
Figure 44: Meshing	75
Figure 45: Mesh attributes for line	76
Figure 46: Allocating specific material to mesh (elements)	77
Figure 47: Selecting analysis type	78
Figure 48: Large displacement analysis selected	79
Figure 49: Equation chosen solvers	80
Figure 50: Applying loads to the beam	81
Figure 51: Solve	82
Figure 52: During solve	83
Figure 53: Output	84
Figure 54: To get the log-file	85

Kinematics of Curved Flexible Beam

Saurabh Jagirdar

ABSTRACT

Compliant mechanism theory permits a procedure called rigid-body replacement, in which two or more rigid links of the mechanism are replaced by a compliant flexure with equivalent motion. Methods for designing flexure with equivalent motion to replace rigid links are detailed in Pseudo-Rigid-Body Models (PRBMs). Such models have previously been developed for planar mechanisms. This thesis develops the first PRBM for spherical mechanisms.

In formulating this PRBM for a spherical mechanism, we begin by applying displacements are applied to a curved beam that cause it to deflect in a manner consistent with spherical kinematics. The motion of the beam is calculated using Finite Element Analysis. These results are analyzed to give the PRBM parameters. These PRBM parameters vary with the arc length and the aspect ratio of the curved beam.

1. Introduction

Mechanisms have been defined as “mechanical devices for transferring motion and/or force from a source to an output” (Erdman et al. 2001). Mechanisms form an important part of how our modern society interacts with the world, whether it is the steering wheel, the computer keyboard, or even the handle of a door. Most mechanisms are systems of levers, cams and gears, which move and rotate, and which have rigid parts. *Compliant mechanisms* are mechanisms that “gain some or all of their ability to move from the deflection of flexible segments” (Salamon 1989). In compliant mechanisms, individual parts not only move and rotate, but also undergo elastic deformations in response to the forces which are imposed on them. Some common compliant mechanisms are binder clips, paper clips, backpack latch, lid, nail-clippers, etc. Compliant mechanisms can have improved performance, lower costs and greater potential functional integration when compared with rigid-body mechanisms (Her 1986, Sevak and McLarman 1974).

1.1 Scope

Compliant mechanism theory permits a procedure called rigid-body replacement, in which two or more rigid links of the mechanism are replaced by a compliant flexure with equivalent motion (Howell 2001). Methods for designing flexure with equivalent motion to replace rigid links are detailed in Pseudo-Rigid-Body Models (PRBMs). In many texts, (Boettama and Roth, Mc Carthy 2000), rigid body analysis of synthesis techniques have been classified as planar, spherical and spatial according to the type of vector algebra used to describe the mechanisms. In a planar mechanism, the path of any single part of a link lies in a plane and in a spherical mechanism, the path of any single part of a link lies on the surface of a sphere.

Numerous PRBMs have been developed for planar mechanisms by Midha et al (1992, 2000), Howell and Midha (1994a, 1994b, 1995) Saxena and Kramer (1998), and Dado (2001) and used in applications such as Microelectromechanical Systems (MEMS) (Baker et al. 2000, Hubbard 2005, Ananthasuresh et al, 1993, Ananthasuresh and Kota 1996, Jensen et al. 1997, Salmon et al. 1996 and Kota et al. 2001), prosthetics (Guerinot et al. 2004), clutches (Roach et al. 1998, Crane et al. 2004), micro-bearings (Cannon et al. 2005), constant-force mechanisms (Millar et al. 1996), parallel mechanisms (Derderian et al. 1996), and bi-stable mechanisms (Jensen et al. 1999) and used in

various other applications like thermal and electrical actuating mechanisms for MEMS (Brocket and Stokes (1991) and Saggere and Kota (1997)). Thus, extensive research has been done on planar compliant mechanisms using PRBMs.

A prime advantage of compliant mechanisms is the part count reduction, that is, flexures can replace rigid links and reduce the number of joints (Howell 2001). This plays a significant role in the fabrication of MEMS. In MEMS design, the increase in the number of joints directly increases the complexity to manufacture MEMS. (Howell 2001). Compliant mechanisms also have increased precision, increased reliability, reduced weight and reduced maintenance (Howell 2001). These advantages make compliant mechanisms ideal for MEMS design and hence the applications for MEMS using compliant mechanisms are abundant.

The PRBM concept has been particularly fruitful in the design of surface micro-machined MEMS. Surface micromachining is less expensive and more versatile than alternative forms of fabrication (Howell 2001). For these reasons much of current MEMS research is devoted to this technique. But MEMS designs, fabricated by surface micro-machining are limited to moving back-and-forth and side-to-side (two dimensional motion) i.e. surface micro-machined devices are essentially flat (or in-plane or planar). For applications that need a

micro mechanism that rotates out of the plane of fabrication with an in-plane rotational input, or that rotates spatially about a point, existing planar compliant mechanisms are not suitable. Given that all current PRBMs relate compliant mechanisms to planar rigid-body mechanisms, we are led to ask is it possible to derive PRBMs that relate compliant mechanisms to spherical rigid-body mechanisms. No such PRBMs have been developed for spherical mechanisms. It is anticipated that the description of compliant spherical mechanisms with spherical motion will simplify the design of MEMS with out of plane motion.

In this thesis, the first PRBM for a spherical compliant mechanism is developed. The kinematics of a curved flexure with the equivalent of a vertical end load is studied and a spherical PRBM for a curved cantilever beam is developed by approximating the motion of the compliant flexure as an equivalent rigid-body mechanism.

1.2 Background

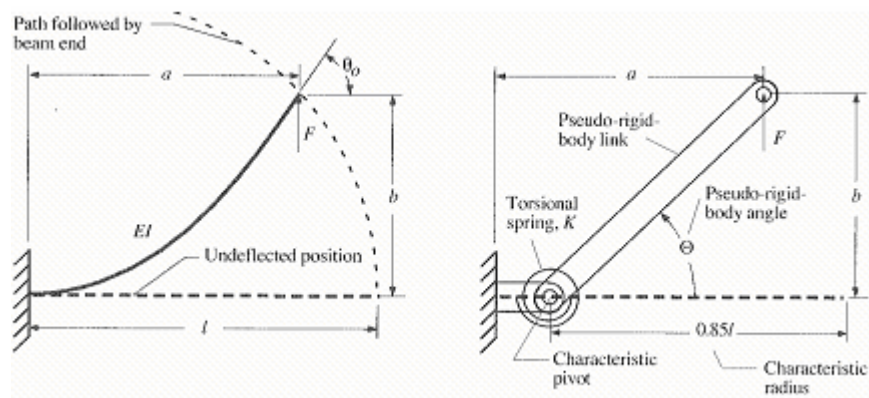
The motion of rigid-body mechanisms can be analyzed with *matrix algebra* (McCarthy 2000) or other techniques and more sophisticated techniques are required for spherical mechanisms than planar mechanisms. The analysis of the motion of compliant mechanisms, on the other hand, usually requires the solution of

differential equations, which describe the physics of an infinitely thin section of the mechanism (Frisch Fay 1962). Because the terms planar and spherical describe the gross motion of objects of finite size, it is not obvious *a priori* when or if these terms apply to compliant mechanisms. However, a compliant mechanism may be termed as planar or spherical mechanism when the solution of its governing differential equations can be reasonably approximated with rigid-body mathematical techniques i.e. matrix algebra. To convert the solution method of a compliant mechanism from a differential equation approach to an algebraic approach, a number of assumptions and specifications need to be made. The differential equation gives information about the relationships of a continuous series of points in the mechanism; the algebraic equation gives information about a few specific points. Thus, the transition requires the specification of the points of interest, typically the ends of the flexible segment. The solution to the differential equations requires that boundary conditions, i.e. information about applied loads and displacements, be specified (Howell 2001). Thus, the conversion to an algebraic solution is valid only for the specific loading conditions. These restrictions usually are placed on loading directions rather than magnitudes (Howell 2001). A validated and accurate identification between a spherical compliant

mechanism and a rigid-body mechanism with equivalent motion at the points of interest is a spherical PRBM.

The PRBM consists of diagrams and equations describing the flexible member and gives a rigid-link equivalent of the compliant mechanism which has the same motion and flexibility for a known range of motion and to a known mathematical tolerance. A PRBM can be used to perform analysis (i.e. given a compliant flexure, its motion can be found by treating it as the rigid body) or design (given a particular desired motion, a rigid body mechanism that performs the motion can be found, and the PRBM can be used to convert that rigid-body mechanism into a compliant mechanism). The creation of a PRBM entails steps beyond the typical mathematical analysis of motion of the compliant segment. These additional steps are necessary to find a simple and accurate rigid-body approximation of the motion of the compliant segment. Once that rigid-body approximation has been identified, it is optimized and validated so that its range of applicability and level of error is known and acceptable. This identification step requires proposing a topology for the rigid-body mechanism, i.e. specification of the number of links and joints. The optimization and validation of steps involve using a numerical optimization routine that insures that the rigid body approximation has a tolerable error (less than 0.5%) over as large a range of motion as possible. The creation

of such PRBMs is justified because they are easy to use in design and because the use of the PRBM in connection with rigid-body synthesis techniques produces compliant mechanism configurations that are unlikely to be produced in any other way. An example of this approach is the PRBM for a straight cantilever beam with vertical end load (Howell 2001), which associates motion of a compliant flexure with a rigid-link mechanism as shown in Figure 1. Figure 1(a) shows a straight cantilever beam subjected to a vertical end load F . Figure 1(b) shows the pseudo-rigid-body equivalent of the straight cantilever beam. The distance from the fixed end to the beam end in the x -direction is a , the distance from the fixed end to the beam end in the y -direction is b , length of the straight beam is l , θ is the pseudo-rigid-body angle and γ is the characteristic radius factor. The angle of inclination of the beam at the beam end is given by θ_0 .



(a) Compliant

(b) PRBM equivalent

Figure 1: A PRBM for a cantilever beam with a vertical end load (Howell 2001)

The co-ordinates of the beam end of the compliant beam are given in terms of the PRB angle, Θ , as:

$$a = l[1 - \gamma(1 - \cos \Theta)] \quad (1.1)$$

$$b = \gamma l \sin \Theta \quad (1.2)$$

Where $\gamma=0.85$ for a vertical end load.

The relationship between Θ and θ_0 is given by:

$$\theta_0 = 1.24\Theta \quad (1.3)$$

These relations are accurate to less than 0.5% error for $\Theta < 64.3^\circ$.

These rigid-body link equations help us to calculate the precise motion of the compliant cantilever i.e. for a given pseudo-rigid-body angle, Θ , we can calculate the final co-ordinates of the beam end from the fixed end, a in the x -direction and b in the y -direction. We can also calculate the angle of inclination of the beam, θ_0 .

There are analogies between planar mechanisms and spherical mechanisms that make it possible to develop a spherical PRBM from the planar PRBM of a cantilever with a vertical end load. A key component of the analogies between planar and spherical mechanisms is that straight lines in planar mechanisms become great circles or circular arcs in spherical mechanisms (Chiang 1992). Also, angles between lines become angles between planes (containing great

circles). For example, a planar mechanism may have an input in the y -direction and an output in the x -direction as shown in Figure 2.

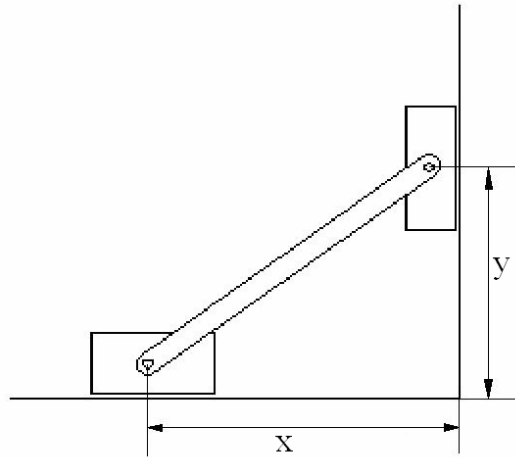


Figure 2: Planar Mechanism with sliders moving on perpendicular straight lines

The analogous spherical mechanism will travel on two perpendicular circular arcs Y -direction (equivalent of y direction) and an output in the X -direction (equivalent of x -direction) as shown in Figure 2 as shown in Figure 3.

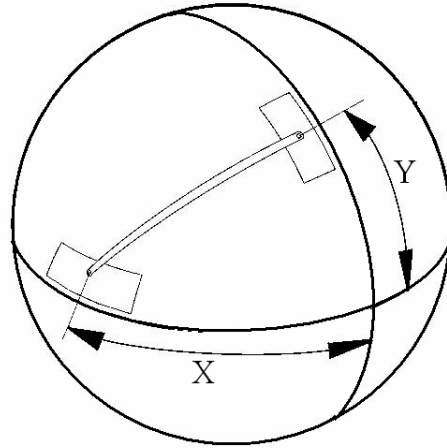
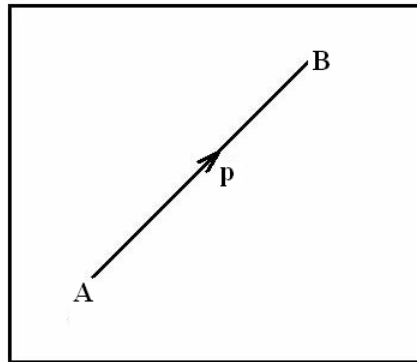


Figure 3: Spherical mechanism with sliders moving on perpendicular circular arcs

Note that spherical mechanisms whose size is very small compared to the radius of the sphere closely approximate planar mechanisms. In fact, spherical kinematics is identical to the planar kinematics in the limiting case when the radius of the sphere is infinite.

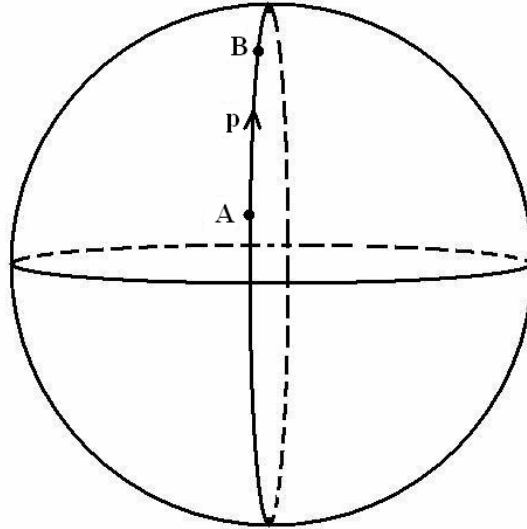
We are also motivated by the ideas that relate planes and spheres such as the *stereographic projections* used by cartographers to represent a spherical earth on a flat map or the mathematical identification between the complex plane and the *Riemann sphere* (Frankel 1997). Let us divide the sphere S just like the earth into latitudes, longitudes and equator. All longitudes and the equator are great circles (WordNet 2001). Great circles are circles that have the

same radius as the sphere and define a plane which cuts the sphere into two equal halves (Merriam-Webster Dictionary 2006). For example great circles on the surface of the earth have their radius equal to the radius of the earth. A great circle is also the shortest path between any two points on the surface of a sphere. The shortest line between two points on a mathematically defined surface is called a geodesic (Henderson 1998). A geodesic is a straight line on a plane and a great circle on sphere. On a sphere all and only great circles are geodesics (on the earth only longitudes and the equator are great circles (geodesics), latitudes other than the equator are not great circles and hence latitudes (except the equator) are not geodesics). Thus a great circle on a sphere is analogous to a straight line on a plane.



(a) Geodesic on a plane

Figure 4: Geodesics



(b) Geodesic on a sphere

Figure 4: (Continued)

Figure 4(a) shows the shortest path p between A and B , on a plane. Figure 4(b) shows the shortest path p between A and B , on a sphere. Moreover, on a sphere because “straight” lines are great circles (curved), there are no parallel lines. ‘Parallelism’ does not exist, that is, all great circles intersect on a sphere. Parallel transport on a sphere is an analogous concept to parallel lines on a plane. Lines that intersect a geodesic (great circles) with the same angle are *parallel transports* (Henderson 1998).

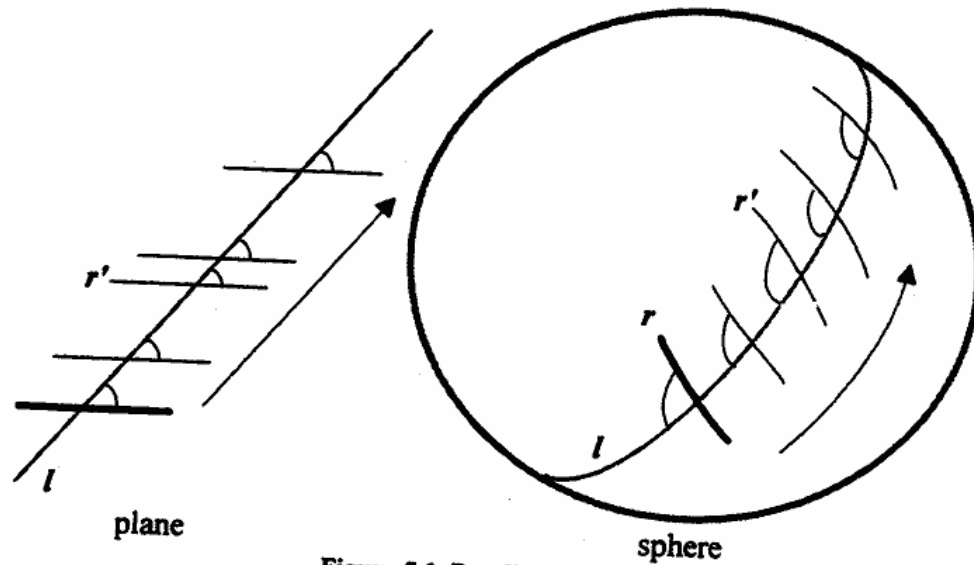


Figure 5.1. Parallel transport.

Figure 5: Parallel transport (Henderson 1998)

We use parallel transport to understand how forces and displacements should be applied to a spherical mechanism in a way that is analogous to a vertical displacement in a planar mechanism. In spherical mechanisms, force and velocity vectors in a particular tangent plane should continue to be tangent to the sphere and follow the motion of the mechanism. Hence the force and velocity vectors need to change direction as the mechanism moves. On a sphere, different tangent planes have different normal vectors. For the force and velocity vectors to be in the tangent plane, any normal component of the vector must be removed. Parallel transport of a vector along a longitude (great circle) can be found by copying the original vector and removing the normal component (Henderson 1998).

A vector m is parallel transported along a longitude to obtain a vector n as shown in Figure 6.

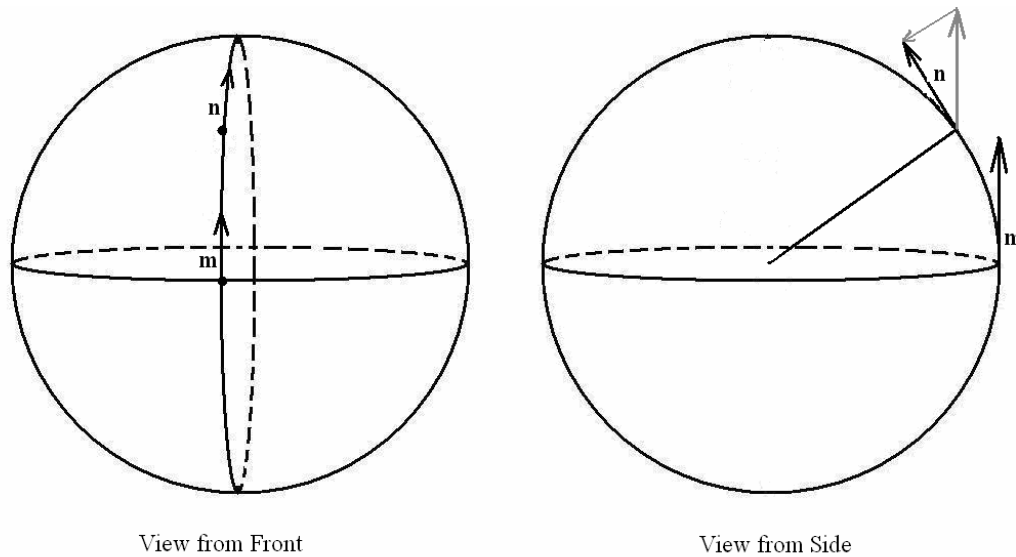


Figure 6: Parallel transport along the same longitude

All longitudes make the same angle with the equator (geodesic) (Henderson 1998). Thus, all longitudes are parallel transports of each other. At any point in the northern hemisphere, all vectors pointing to the North Pole will lie on longitudes, thus any vector in the northern hemisphere and pointing towards the North Pole is a parallel transport of any other such vector. Thus, a northward-pointing force-vector on the equator of a sphere can be parallel transported to a vector pointing north at any other point on the sphere. A vector pointing north on a sphere is analogous to a vertical force in a plane.

1.3 Roadmap

This chapter has presented background on PRBMs and spherical kinematics, Later chapters describe, how the spherical PRBM is modeled, analyzed and validated. Chapter 2 describes the analogy between planar PRBM and a spherical PRBM. It also gives the nomenclature and topology for the spherical PRBM. Chapter 3 describes the finite element model and how the displacements were applied to the model. Chapter 4 describes how the data was used to obtain the values for the PRBM parameters given in the second chapter. Chapter 5 describes the results obtained for different aspect ratios, b/h and arc lengths, λ . Chapter 6 is the conclusion based on the results.

2. Methodology and Model Development

2.1 Correspondence between spherical and planar PRBMs

Mechanisms whose joint axes are parallel to each other are known as planar mechanisms (Chiang 1992). In planar compliant mechanisms, this characteristic is usually achieved by designing straight cantilevers (flexures) that, at each point along their length, are most flexible about parallel lines and considerably more rigid in other directions. Mechanisms whose joint axes intersect at a point are spherical mechanisms (Chiang 1992). In spherical compliant mechanisms, this characteristic can be achieved by designing curved cantilevers (flexures) that, at each point along the arc, are most flexible about lines that point to the centre of the sphere. In both kinds of mechanisms it is necessary that the length (arc-length) of flexure be much greater than the width of the beam (flexure), and the width of the beam to be larger than its thickness.

It is hypothesized that a flexure which is a long, thin circular arc will move in a manner consistent with spherical kinematics when loaded appropriately. The process of obtaining the PRBM for a

spherical compliant mechanism is similar to planar compliant mechanism.

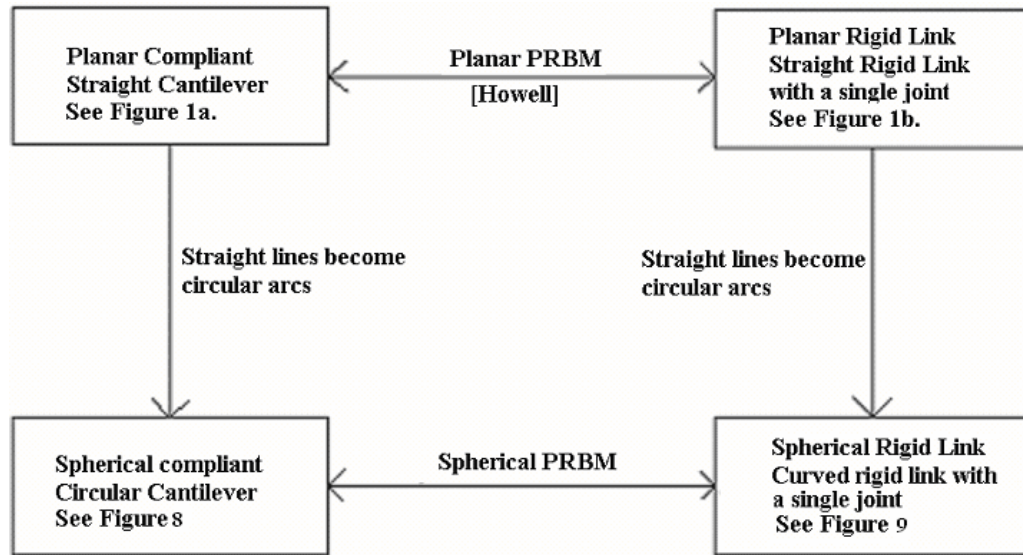


Figure 7: Relationship between existing planar PRBM and the spherical PRBM developed in this work

The spherical compliant mechanism and its rigid body counterpart are derived from the planar mechanism by making straight lines curved. There is a correspondence principle between spherical PRBMs and planar PRBMs. The correspondence principle is that when small angle assumption is used for spherical arcs. i.e. the arc length is much smaller than the radius of the sphere, the spherical PRBM becomes identical to planar PRBM. To emphasize the relationship between lines and arcs, the lengths in planar model are denoted with Roman letters, and the equivalent arcs in the spherical model are denoted with the Greek letter equivalents. For example the

arc length, β , that appears in some formulas for spherical mechanisms, can be related to the planar length, b . Thus, using small angle approximation.

$$\begin{aligned}\cos \beta &= 1, \\ \sin \beta &= \beta \rightarrow b\end{aligned}$$

Where b is the planar equivalent of the arc β . Similarly a and l are the planar equivalent of arcs α and λ respectively.

Additionally, similar terminology is used in planar and spherical PRBMs, for angles between lines (arcs) such as Θ , θ_0 , and for ratios such as γ and C_θ . These variables do not change in the small angle case. In the planar case, the deflected angle of beam end, θ_0 , is about an axis normal to the plane. Similarly, in the spherical case, the deflection of the beam end, θ_0 , is about an axis normal to the tangent plane to the sphere at the beam end.

2.2 Kinematics of compliant circular arc

The kinematics of the compliant circular cantilever, PQ , is described by using a series of co-ordinate frames, as shown in Figure 8. The fixed end of the curved cantilever beam is denoted as P and free end of the beam as Q . Let S be a sphere whose center is defined by O frame and the frames A , B , C and D are always on the surface of

the sphere. The position and orientation of the co-ordinate frames are related as follows:

The O frame is a fixed frame that locates the center of the sphere.

The A frame is a frame that locates the beam end Q , in undeformed co-ordinates with neutral axis of beam at Q is parallel to the a_3 direction and the a_1 direction is outward radial vector through the beam end.

The B frame is a frame that locates the deflected position of the beam end Q in the x - z plane (analogous to the translation in the x -direction in the planar model).

The C frame is a moving frame that describes movement of beam end Q in the b_2 - b_1 plane rotating about point O (analogous to the translation in the y -direction in the planar model).

The D frame is a moving frame at the same position as the C frame and tracks the deflection of the beam end about the radial axis through the beam end (analogous to the deflection about the z -axis in the planar model).

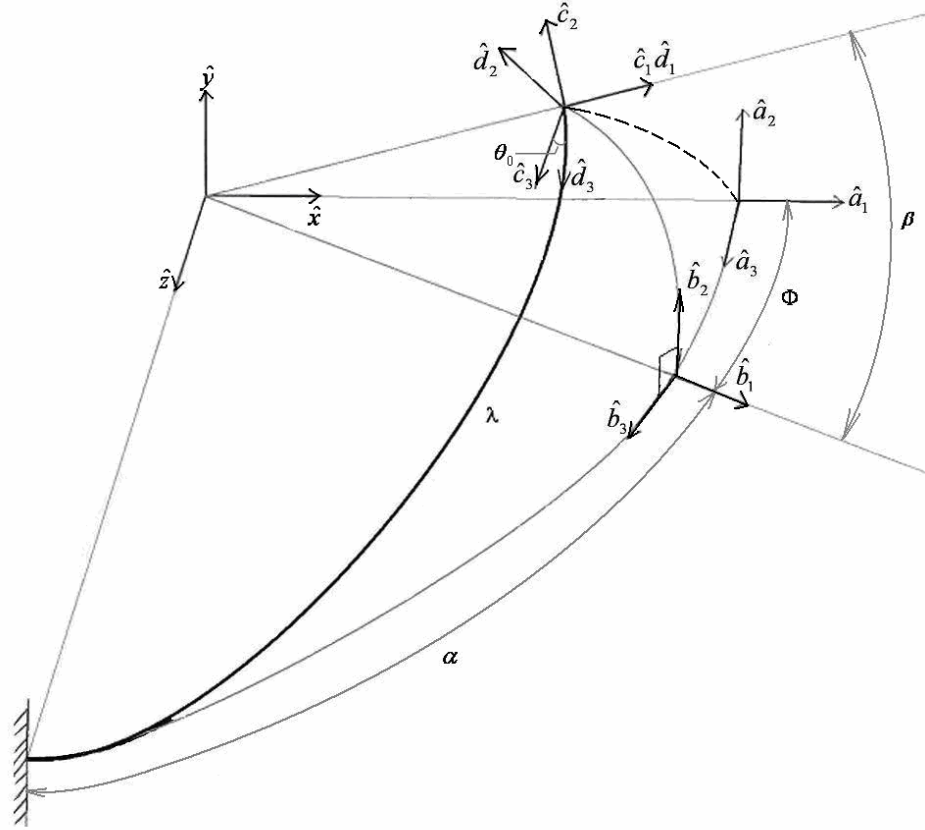


Figure 8: Reference frames describing the motion of the end of a compliant circular cantilever

The frames are described by the matrices A , B , C and D , where the columns of the matrix are the basis vectors. The transformations relating the frames are given by:

$$A = [\{a_1\}, \{a_2\}, \{a_3\}] = \begin{bmatrix} 1 & 0 & 0 \\ 0 & 1 & 0 \\ 0 & 0 & 1 \end{bmatrix}$$

$$B = [\{b_1\}, \{b_2\}, \{b_3\}] = \begin{bmatrix} \cos(-\Phi) & 0 & \sin(-\Phi) \\ 0 & 1 & 0 \\ \sin(-\Phi) & 0 & \cos(-\Phi) \end{bmatrix} A = R(\hat{a}_2, -\Phi)A$$

$$C = [\{c_1\}, \{c_2\}, \{c_3\}] = \begin{bmatrix} \cos(\beta) & -\sin(\beta) & 0 \\ \sin(\beta) & \cos(\beta) & 0 \\ 0 & 0 & 1 \end{bmatrix} B = R(\hat{b}_3, \beta)B$$

$$D = [\{d_1\}, \{d_2\}, \{d_3\}] = \begin{bmatrix} 1 & 0 & 0 \\ 0 & \cos(\theta_0) & -\sin(\theta_0) \\ 0 & \sin(\theta_0) & \cos(\theta_0) \end{bmatrix} C = R(\hat{c}_1, \theta_0)C$$

The transformations relating the frames are given by:

$$D = R(\hat{c}_1, \theta_0)R(\hat{b}_3, \beta)R(\hat{a}_2, -\Phi)A$$

Thus the motion of the cantilever beam is described by the parameter $\Phi = \lambda - \alpha$, β and θ_0 which are analogous to planar parameters $l-a$, b and θ_0 , respectively which are shown in Figure 1.

2.3 Spherical kinematics of the pseudo-rigid-body model

Now by analogy to the planar PRBM, in the spherical PRBM, Θ is defined as the pseudo-rigid-body angle of the beam end about the characteristic-pivot (pseudo-pivot) and γ is defined as the ratio of the arc length from the beam end to the pseudo-pivot to the entire arc length λ of the beam. The value of γ is chosen so that the motion of the beam end closely approximates the motion of the compliant beam. The details of selecting the value of γ are explained in chapter 4.

Thus the proposed topology for the pseudo-rigid-body model is shown in Figure 9.

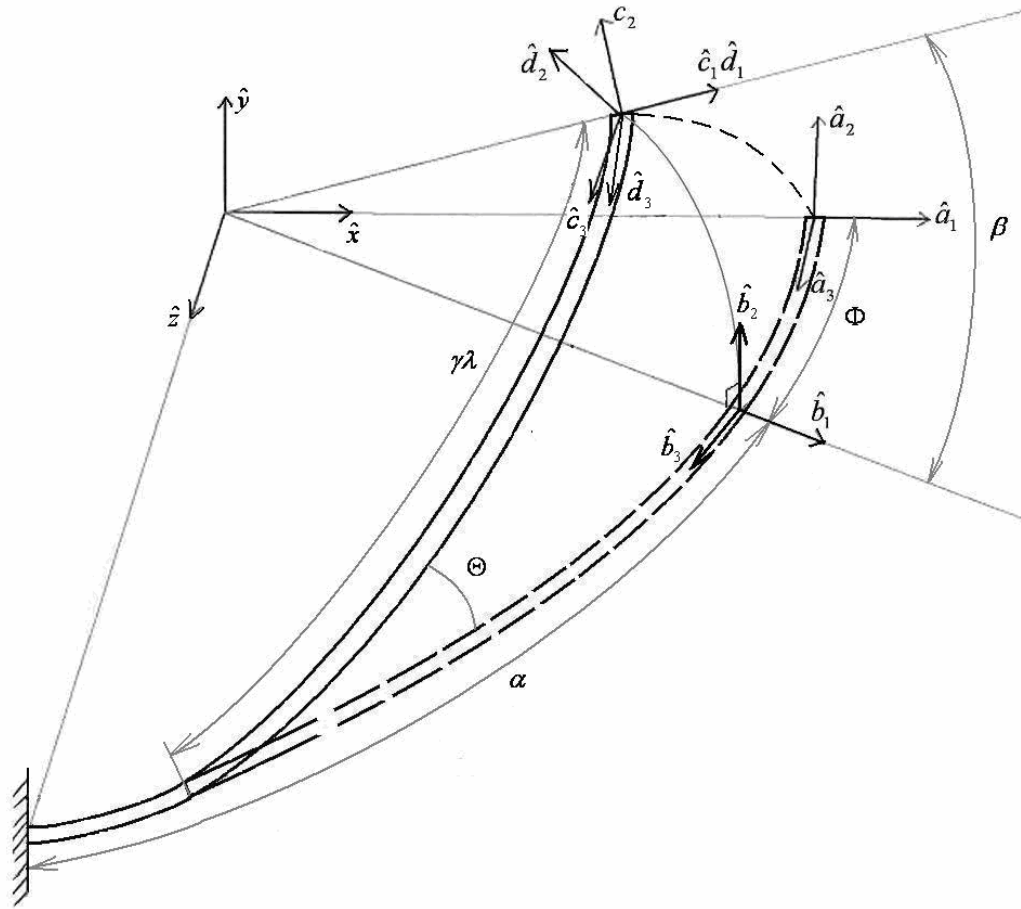


Figure 9: The pseudo-rigid-body model of the compliant curved beam

The relationships for α and β in terms of γ and Θ are obtained using Napier rules for right spherical triangle (Spiegel, 1968). The right spherical triangle in Figure 9 has sides $\gamma\lambda$, η , and β (See Appendix A) where

$$\eta = \alpha - (1 - \gamma)\lambda$$

Thus we find η as a function of $\gamma\lambda$ and Θ

$$\sin(90 - \Theta) = \tan \eta \tan(90 - \gamma\lambda)$$

$$\eta = \tan^{-1}(\tan \gamma\lambda \cos \Theta)$$

(2.1)

And α is obtained as

$$\begin{aligned}\alpha &= (1 - \gamma)\lambda + \eta \\ \alpha &= (1 - \gamma)\lambda + \tan^{-1}(\tan \gamma\lambda \cos \Theta)\end{aligned}\quad (2.2)$$

Also β is obtained as a function of $\gamma\lambda$ and Θ

$$\begin{aligned}\sin \beta &= \sin \gamma\lambda \sin \Theta \\ \beta &= \sin^{-1}(\sin \gamma\lambda \sin \Theta)\end{aligned}\quad (2.3)$$

2.4 Spherical loading condition analogous to planar vertical end load

Based on the discussion in chapter 2, the spherical equivalent of a vertical end load is northward-pointing end-load. An important distinction between planar and spherical loading conditions is that the planar load direction is constant; the spherical load direction must change. A vertical end load in the planar case always points upward, on a sphere there is no such one direction to which the load vector points. The direction of the force vector should change as the mechanism moves along the curvature of the sphere. In practice the change requires that any component of force in the direction normal to the sphere must be removed, perhaps by addition of load bearing members in the mechanism. Thus, at any other point on the sphere the vector initiating from that point and pointing towards the North Pole imitates a vertical end load in planar case.

3. Finite Element Analysis (FEA)

To deduce the accurate motion of the beam going through spherical motion the beam is modeled in a FEA software package. The parametric angle co-efficient, C_{θ} , the characteristic radius factor, γ , and the parameterization limit, θ_{max} , are obtained from the results of the FEA model. A major challenge in building the model in FEA package is to apply loads on the beam such that there is no reaction load at the fixed end, P , (see Figure 10) and the free end, Q , of curved cantilever beam moves in a manner consistent with spherical kinematics. For this study we focus on the motion of the beam (kinematics), the reaction loads will be studied in later work.

Development of the model is a paradox because the load direction depends on the displacement of the beam end, and the displacement of the beam end depends on the load direction. Thus, to ensure that there is no reaction load at the fixed end, P , we need to know the path (dotted line shown in Figure 10) followed by the beam end. The path followed is an arc on the sphere from the A frame (undeflected position Q) to the C or D frame (final position Q'').

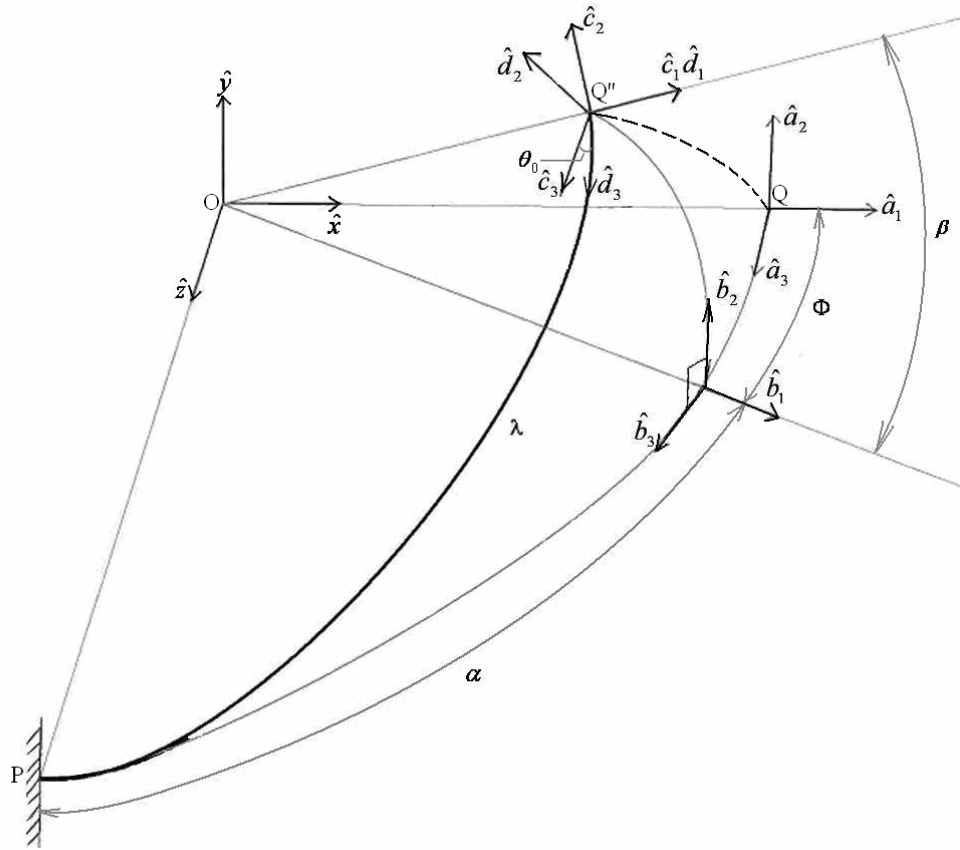
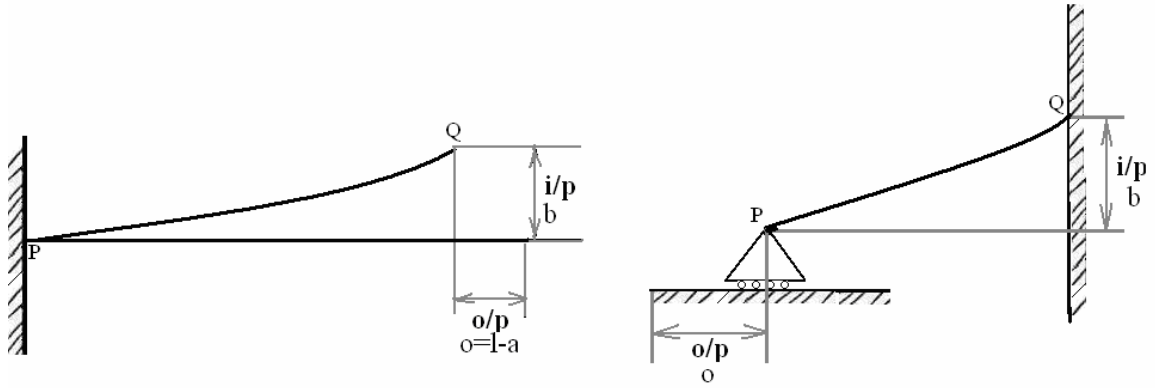


Figure 10: Path followed by beam the dotted line from Q to Q''

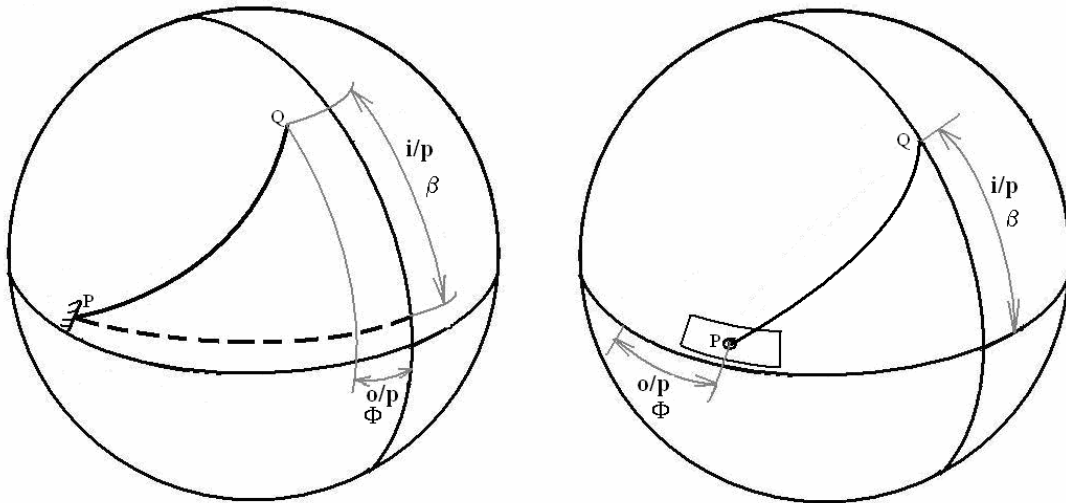
When the beam PQ is taken as fixed at P , the A -frame of reference is fixed. The motion of the beam can also be described in the B -frame of reference such that the end Q of the beam is allowed to move in the b_1 - b_2 plane. As a consequence of this the end P , of the beam now moves in the b_1 - b_3 plane, that is, the beam undergoes spherical motion such that the ends P and Q move on orthogonal great

circles. To illustrate clearly, the comparison with the planar case is shown.



(a) Planar Fixed reference frame

(b) Planar Moving reference frame



(c) Spherical Fixed reference frame

(d) Spherical Moving reference frame

Figure 11: Reference frames used to model the spherical mechanism and its planar equivalent

We can see from Figure 11(a) and 11(c) that if an input is given at the free end Q , the output obtained when the beam is fixed at P is a displacement at Q . On the other hand, in Figure 11(b) and 11(d) an

input is given at Q and the output is obtained at P . As we see from Figure 11, the difference between the fixed frame of reference and moving frame of reference is the location of the output displacements. In the planar case, when an input displacement of b is given the output obtained is $o=l-a$ in both the fixed frame of reference, shown in Figure 11(a), and the moving frame of reference Figure 11(b). In the spherical case, when an input displacement of β is given, the output obtained is $\phi=\lambda-\alpha$ in both the fixed frame of reference, shown in Figure 11(c), and the moving frame of reference, shown in Figure 11(d). Thus, the mechanisms are equivalent to each other and only the frame of reference has changed. It proves convenient to analyze the behavior of the flexible curved beam in a FEA model built to mimic the moving frame. In this frame of reference, we apply displacement loads at Q and measure the output displacement at P . The fixed frame of reference is the A frame in Figure 10 In order to get the spherical frame B .

When the B -frame is observed in a moving frame of reference it coincides with the A -frame for all northward-pointing input displacements. The initial position is such that both the ends of the beam are in the b_1 - b_3 plane. An input of displacement angle, β , is applied to the beam end Q . The motion of Q is a circular arc in b_1 - b_2 plane. The output obtained is the displacement angle ϕ (about the y -

axis of the O frame) observed at the other end P of the beam. The motion of this beam end, P , is a circular arc that lies in the b_1 - b_3 plane. The mechanism shown in 11(d) is modeled in FEA software package.

The ANSYS version 10.0, (ANSYS, 2006) FEA package was used. A major aspect of modeling in ANSYS is that it does not take inputs or outputs with respect to units. Hence the model itself has to be built in a single system of consistent units. Since this is a 'kinematic' model, the factors expected to affect the results would be dimensions of the curved beam and Modulus of Elasticity. Here the model dimensions were defined in millimetres (mm) and the modulus of elasticity in Newton per square millimetre (N/mm^2).

In this model we take the length of the rigid beam OP =1000mm, the radius of the arc PQ =1000mm. The Q end of the beam is always in the X - Y plane and its initial position for all arc-lengths of PQ , is $Q(1000,0,0)$. The initial position of the end P varies for different arc-lengths and is given by $P(R*\cos(\text{arclength}),0,R*\sin(\text{arclength}))$.

Where R is the radius of the arc (sphere) =1000mm and arclength is the angle created by the arc to the centre in radians.

The mechanism is modeled such that the circular segment PQ is highly compliant and the straight segment OP is highly rigid. This is done by maintaining the modulus of elasticity of the compliant circular segment at $300\text{N}/\text{mm}^2$ and that of the rigid straight segment at

300,000 N/mm². Various aspect ratios of the beam are obtained by varying the cross-section of the beam that is if an aspect ratio of 0.1 is desired then the thickness (or height h) of the beam is 1/10 th of the width b . When aspect ratio of the beam is 1 the beam has a square cross-section of sides 50mm, for successive values of aspect ratio the sides vary accordingly to obtain a rectangular cross-section of width b and height h given by $h = \text{aspect ratio} * b$ as shown in Figure 12.

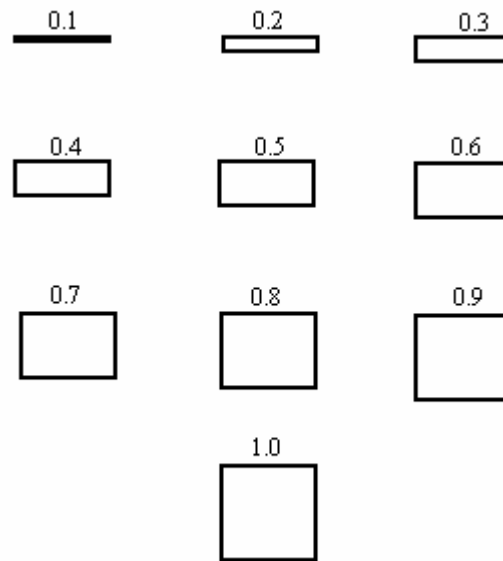


Figure 12: Cross-section of beam for various aspect ratios

This model is then meshed to define elements and nodes.

Displacement loads are applied according to the boundary conditions described below.

To apply the boundary conditions for the above model we denote the displacements in x , y and z directions by UX , UY and UZ and

rotations about x , y and z by ROTX, ROTY and ROTZ. Points O and P lie on the rigid straight segment and hence they are made to stay in the x - z plane and allowed to rotate about y -axis of O frame. The point O fixes the structure in space and hence all other degrees of freedom are constrained. The point Q is the end of the curved segment and hence it is made to lie in the x - y plane.

The boundary conditions applied to the finite element model shown in Figure 13 are:

Point O $U_X=0, U_Y=0, U_Z=0, ROTX=0, ROTZ=0$.

Point P $U_Y=0$,

Point Q $U_Z=0, ROTZ=\beta, ROTX=0, ROTY=0$.

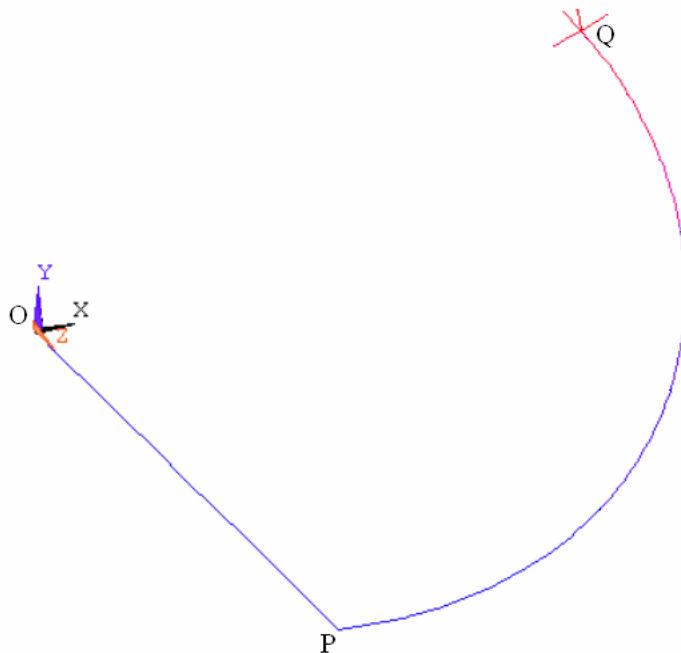


Figure 13: Finite element model

Rotational displacement loads, β , were applied at the Q end of the beam and analysis was conducted. For various inputs of β we get corresponding outputs of $\Phi=\lambda-\alpha$. The deflection θ_0 of the neutral axis of the beam at beam end (that moves in b_1 - b_2 plane) about the radial axis of the beam at the same beam end is also obtained as an output. The deflection of the beam is calculated from the rotation matrix generated by a pre-defined triad at the Q end of the beam.

Thus these outputs are noted for various inputs and this simulation is repeated for varying:

a) Initial arc length λ b) Cross-section of the curved flexible beam. The results from FEA model were used to calculate the parametric angle co-efficient, C_θ , the characteristic radius factor, γ and θ_{0max} . See Appendix C for a visual manual to conduct one simulation. A log file generated from one analysis (simulation) is then obtained from the file menu. This log file is then edited with new values of the parameters (aspect ratio and arc-length) and subsequently run in ANSYS by using an input command. Simulations were run for arc-lengths ranging from angle of 4 degrees to 112 degrees in increments of 2 degrees and for each arclength aspect ratios varying from 0.1 to 1 with increments of 0.1. The input displacement, β , is given such that it is equal to the angle created by the respective arc-length, that is, if an

arc-length of 90 degrees is to be analyzed then an input displacement of 90 degrees is applied.

4. Parametric Approximation of the Curved Beam's Deflection Path

We follow Howell's method (Howell 2001) for developing our parametric approximation of the curved beam's deflection path. An acceptable value for the characteristic radius factor, γ , may be found by first determining the maximum acceptable percentage error in deflection. The value of γ that would allow the maximum pseudo-rigid-body angle, Θ , while still satisfying the maximum error constraint is then determined. The problem may be formally stated as follows: Find the value of the characteristic radius factor γ which maximizes the pseudo-rigid-body angle, Θ , where Θ for a spherical mechanism is derived from Napier Rules. For right spherical triangle whose sides are $\gamma\lambda$, η , and β , and Θ is the angle between $\gamma\lambda$ and η it can be shown that:

$$\sin[\alpha - \lambda(1 - \gamma)] = \tan\beta\cot\Theta \quad (\text{See Appendix A})$$

where

$$\alpha = \lambda - \phi$$

to get

$$\Theta = \tan^{-1} \left[\frac{\tan\beta}{\sin[\alpha - \lambda(1 - \gamma)]} \right] \quad (4.1)$$

Equation (4.1) is valid for $\beta < 90^\circ$.

$$\Theta = \tan^{-1} \left[\frac{\sin \beta / \sin \gamma \lambda}{\tan \eta \cot \gamma \lambda} \right] \quad (4.2)$$

Equation (4.2) is applicable for all values of β (See Appendix-A), and is subject to the parametric constraint

$$g(\Theta) = \text{error} / \varepsilon_e \leq (\text{error} / \varepsilon_e)_{\max} \text{ for } (0 < \Theta < \Theta_{\max}) \quad (4.3)$$

where $\text{error} / \varepsilon_e$ is the relative deflection error, and ε_e for a spherical mechanism is defined as the vector difference of deflected position of the flexible curved segment and the original un-deflected position.

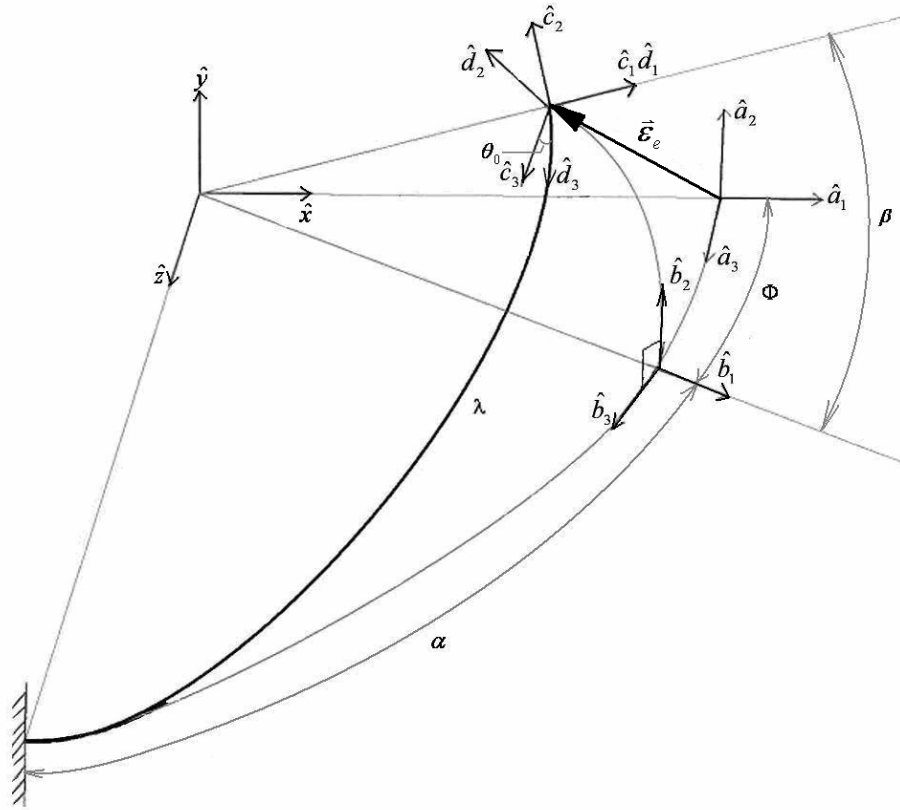


Figure 14: Deflection of curved segment

The deflection of curved segment ϵ_e as shown in Figure 14 is obtained using finite element analysis software. For various values of β , the corresponding values of ϕ are noted. These are then used to calculate the final position from rotation and transformation matrices. Finally the original co-ordinates of the beam end are subtracted from the final co-ordinates to obtain the deflection ϵ_e .

$$\vec{\varepsilon}_e = \begin{bmatrix} \cos \beta & -\sin \beta & 0 \\ \sin \beta & \cos \beta & 0 \\ 0 & 0 & 1 \end{bmatrix} \begin{bmatrix} \cos(-\phi) & 0 & \sin(-\phi) \\ 0 & 1 & 0 \\ -\sin(-\phi) & 0 & \cos(-\phi) \end{bmatrix} \begin{bmatrix} 1 \\ 0 \\ 0 \end{bmatrix} - \begin{bmatrix} 1 \\ 0 \\ 0 \end{bmatrix} = \begin{bmatrix} \cos \beta \cos \phi - 1 \\ \sin \beta \\ \cos \beta \sin \phi \end{bmatrix} \quad (4.4)$$

to get

$$\vec{\varepsilon}_e = \begin{bmatrix} \varepsilon_{ex} \\ \varepsilon_{ey} \\ \varepsilon_{ez} \end{bmatrix} = \begin{bmatrix} \cos \beta \cos \phi - 1 \\ \sin \beta \\ \cos \beta \sin \phi \end{bmatrix} \quad (4.5)$$

and the deflection for the PRBM, ε_a , is given by the vector difference of deflected position of the PRBM and the original un-deflected position of the beam end Q.

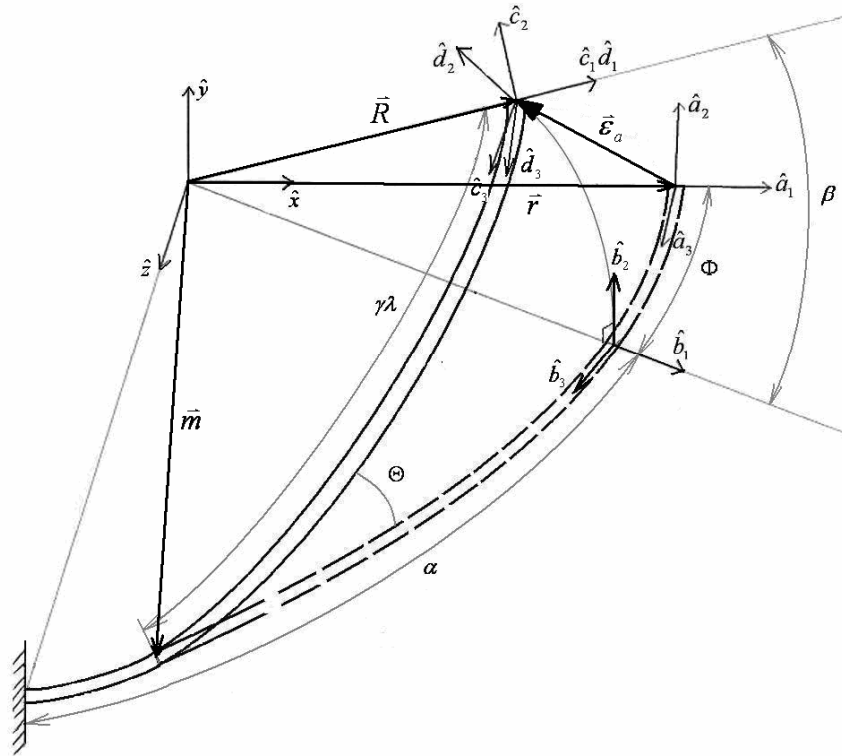


Figure 15: Deflection of PRBM

The vector difference between the estimated deflected position of PRBM and the original un-deflected position of beam end, Q , is calculated using the following transformations.

From Figure 15 we have $\vec{\varepsilon}_a = \vec{R} - \vec{r}$

and $\vec{R} = R\vec{r}$ where R is the rotation of the vector \vec{r} about the axis \vec{m} through angle θ (Lai, Rubin and Krempl, 1993).

$$\vec{R}(\vec{m}, \vec{r}, \Theta) = (1 - \cos \Theta)(\vec{m} \cdot \vec{r})\vec{m} + \cos \Theta \vec{r} + \sin \Theta (\vec{m} \times \vec{r})$$

where,

$$\vec{m} = \begin{bmatrix} \cos \hat{\gamma}\lambda \\ 0 \\ \sin \hat{\gamma}\lambda \end{bmatrix} \quad \text{and} \quad \vec{r} = \begin{bmatrix} 1 \\ 0 \\ 0 \end{bmatrix}$$

which reduces to

$$\vec{R} = R\vec{r} = \begin{bmatrix} \cos^2 \hat{\gamma}\lambda(1 - \cos \Theta) + \cos \Theta \\ \sin \hat{\gamma}\lambda \sin \Theta \\ \cos \hat{\gamma}\lambda \sin \hat{\gamma}\lambda(1 - \cos \Theta) \end{bmatrix}$$

Therefore,

$$\vec{\varepsilon}_a = \begin{bmatrix} \cos^2 \hat{\gamma}\lambda(1 - \cos \Theta) + \cos \Theta - 1 \\ \sin \hat{\gamma}\lambda \sin \Theta \\ \cos \hat{\gamma}\lambda \sin \hat{\gamma}\lambda(1 - \cos \Theta) \end{bmatrix} \quad (4.6)$$

error is simply defined as the vector difference between the final positions of the curved flexible segment and the pseudo-rigid body model.

The *error* in the deflection is calculated as

$$error = |\vec{\varepsilon}_e - \vec{\varepsilon}_a| = \left[(\varepsilon_{ex} - \varepsilon_{ax})^2 + (\varepsilon_{ey} - \varepsilon_{ay})^2 + (\varepsilon_{ez} - \varepsilon_{az})^2 \right]^{1/2} \quad (4.7)$$

A parameter relative error, $error/\varepsilon_e$ is defined to help in comparing with the planar flexible segment.

$$\frac{error}{|\vec{\varepsilon}_e|} = \frac{|\vec{\varepsilon}_e - \vec{\varepsilon}_a|}{|\vec{\varepsilon}_e|} \quad (4.8)$$

The value of the angular deflection of the beam's end, θ_0 , at the point at which the error equals or exceeds an acceptable amount, is the maximum angular deflection of the beam's end, or the parameterization limit θ_{max} .

5. Results and Discussion

For a given value of aspect ratio, h/b , and arc-length, λ , one can find a value of characteristic radius factor, γ and parametric angle coefficient, C_θ that best approximates the motion (position and orientation of beam at various input displacements) using the techniques described in the previous chapter.

For example for $h/b=1$, and $\lambda=90^\circ$, the final displacement of beam from the fixed end, α , and the rotation θ_0 are found for a given input displacement of β . They are plotted against β as shown in Figure 16 and Figure 17.

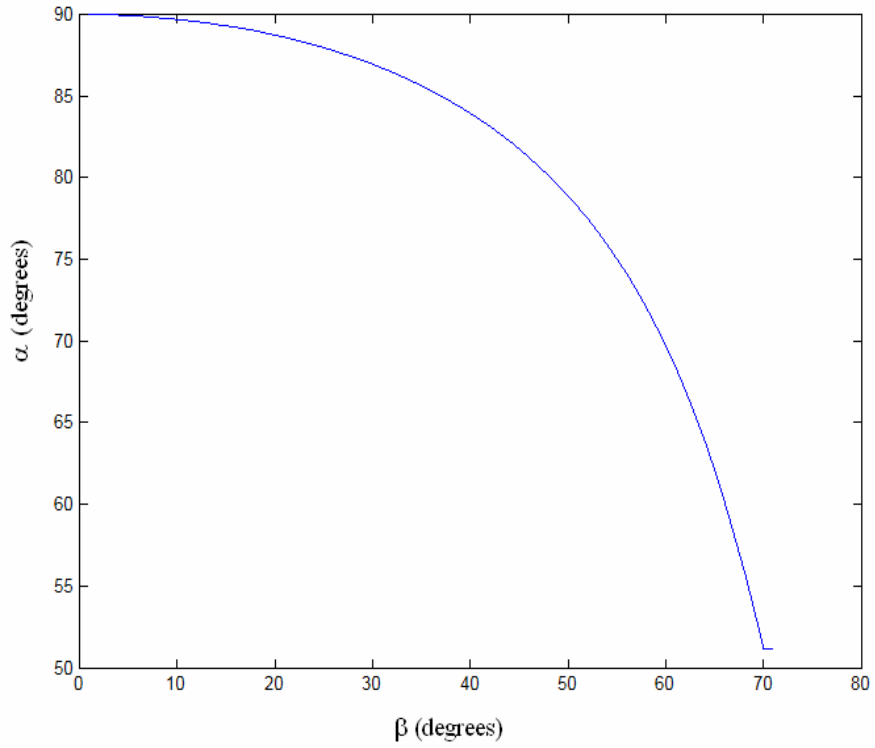


Figure 16: Final position of beam from fixed end α , v/s input displacement β

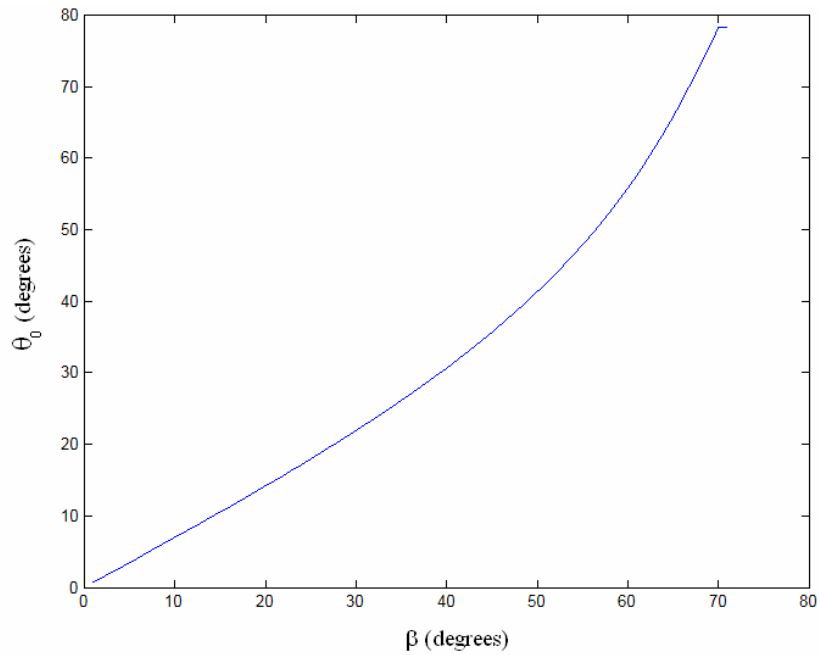


Figure 17: Deflection of beam about neutral axis, θ_0 , v/s input displacement β

Then the values of γ and C_θ that gives the minimum relative error (0.05%) for the largest range of different guess of γ are found for maximum range of motion.

C_θ is the parametric angle co-efficient, defined as the ratio of the maximum range of motion obtained, Θ_{max} , in the pseudo-rigid body model to the ratio of the deflection of the beam about the neutral axis, θ_0 .

The γ and C_θ obtained for all the simulations of various aspect ratios and arc lengths are plotted in Figure 18 and Figure 19 and in Figure 20 the maximum range of motion for the PRBM for the respective values of γ and C_θ .

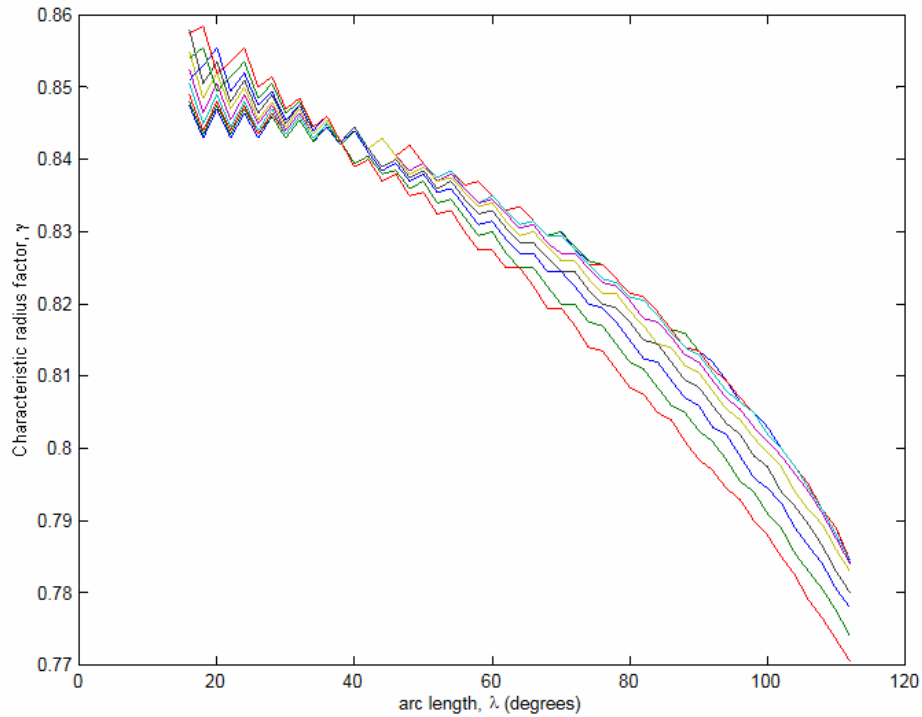


Figure 18: γ v/s Arc-lengths showing various colors for aspect ratios

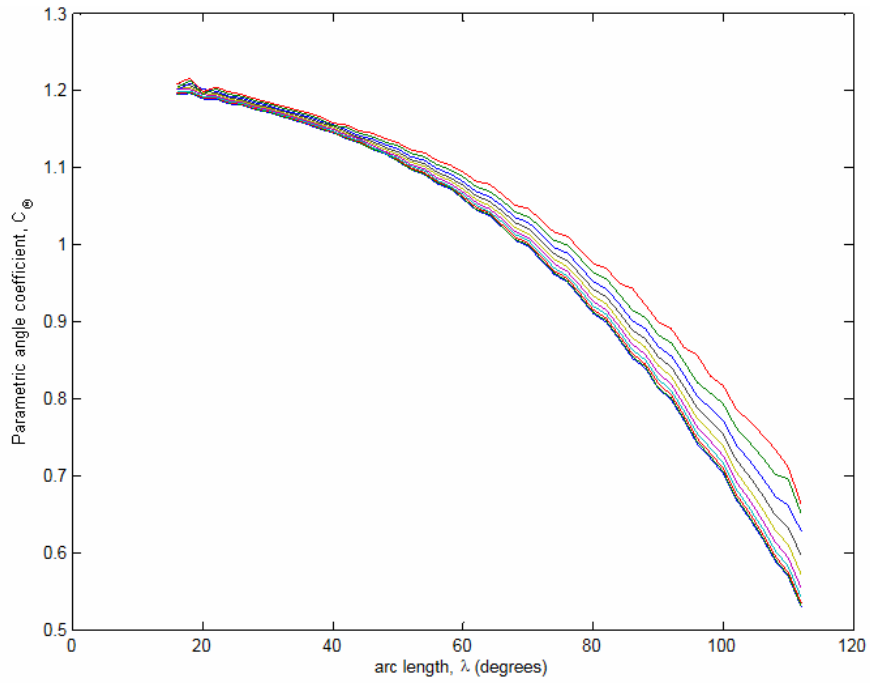


Figure 19: C_θ v/s Arc-lengths showing various colors for aspect ratios

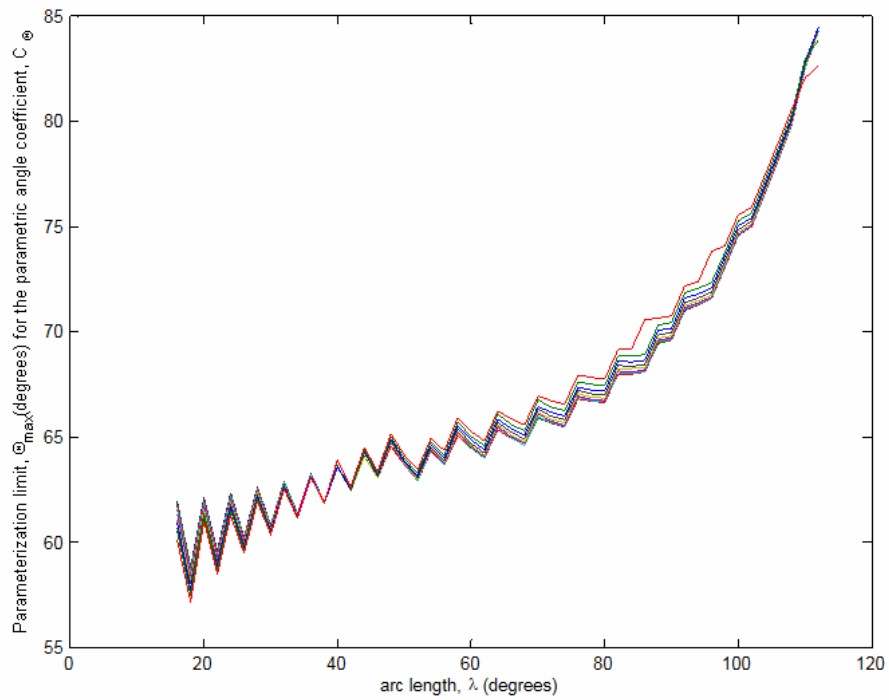


Figure 20: θ_{max} v/s Arc-lengths showing various colors for aspect ratios

These are graphs that are plotted for simulations which were run to obtain outputs at every one degree of the input displacement, β , that is, if the beam was given a total input displacement of 90 degrees then 90 load-steps of one degree were solved. As a consequence not enough data points were obtained when the total input displacement, β was a small value, for example, if the beam was given a total input displacement of just 10 degrees then only 10 load-steps were solved. Thus, the algorithm to process the outputs obtained from the simulations failed to process the data for arc-lengths ranging from 4 to 14 because the total input displacement, β , is given such that it is equal to the arc-length. Hence, the number of data points at an arc-length, were limited to the value of arc-length in degrees, that is, only 4 data points were obtained for an arc-length of 4 degrees.

Moreover, from the graphs it can be seen that there is a lot of 'bouncing' that is there is a 'noise' in the data. This clearly indicates that more data points are required to capture the behavior of the curved beams.

Based on the inference of these graphs the simulations were re-run such that 200 load-steps are solved irrespective of the value of the input displacement, that is, for an input displacement of 4 degrees the beam was analyzed at an input displacement, β , of every 4/200 degrees. These simulations were run for aspect ratios $h/b=0.1, 0.4$

and 0.7. These are then again plotted as shown in Figure 21, Figure 22 and Figure 23.

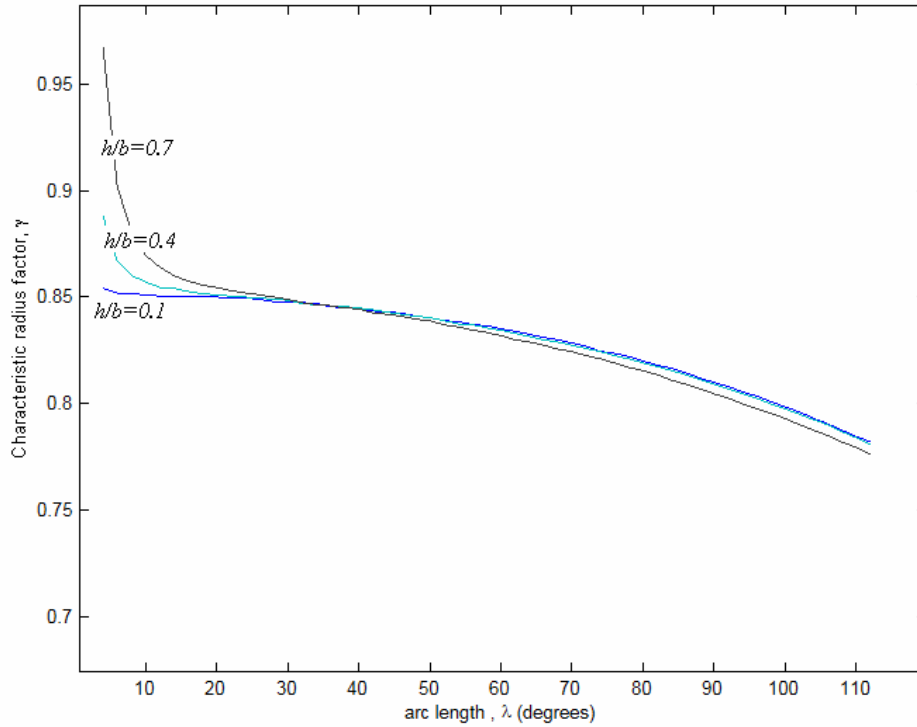


Figure 21: γ v/s Arc-lengths, for 200 load-steps of input displacement

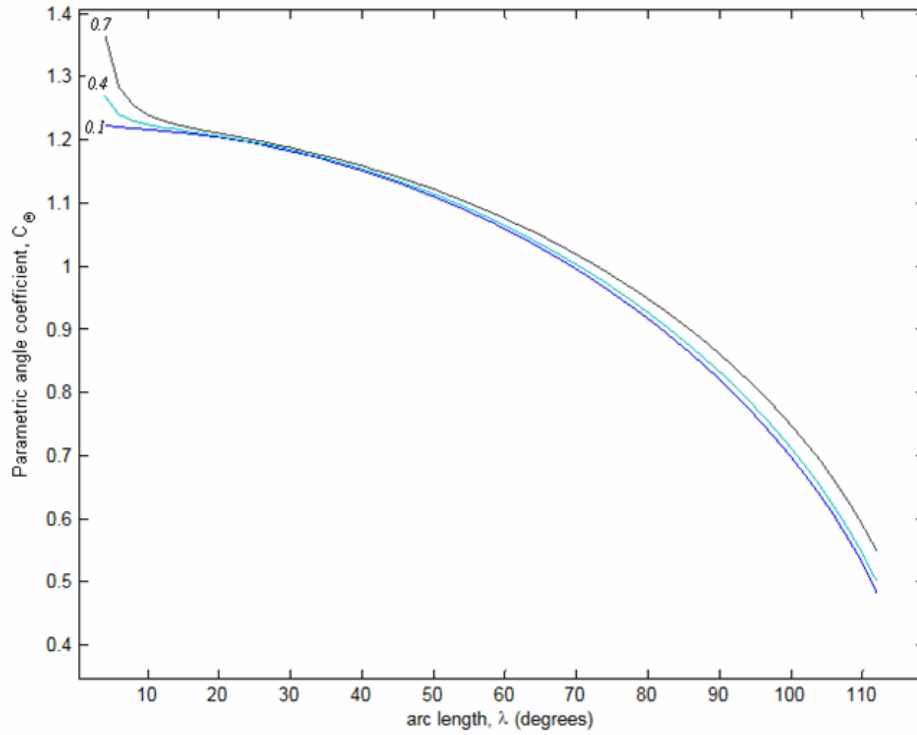


Figure 22: C_θ v/s Arc-lengths, for 200 load-steps of input displacement

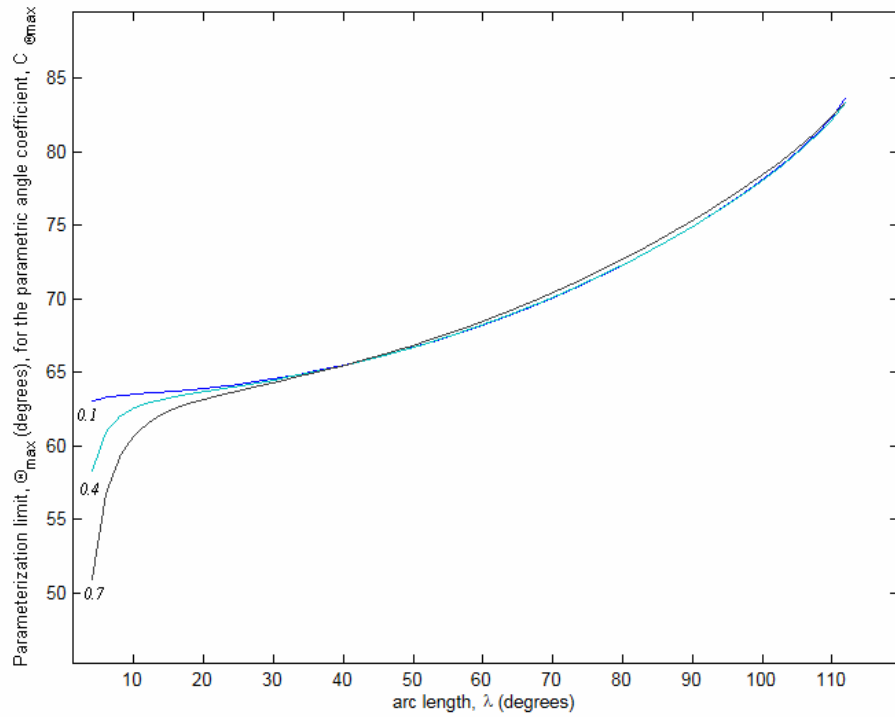


Figure 23: θ_{max} v/s Arc-lengths, for 200 load-steps of input displacement

From Figures 21, 22 and 23 we see that there is no 'bouncing' or 'noise' in the data, smooth curves are obtained. It is observed that this data is suitable to approximate the motion of the beam. An equation is fitted to the curve for the characteristic radius factor γ , and can be used to approximate the motion of a curved beam with the equivalent of vertical end load. A trend-line of second order polynomial for arc-lengths ranging from 16 to 112 is fit individually for aspect ratios $h/b=0.1$, 0.4 and 0.7 and their equations are shown in Figure 24, Figure 25 and Figure 26.

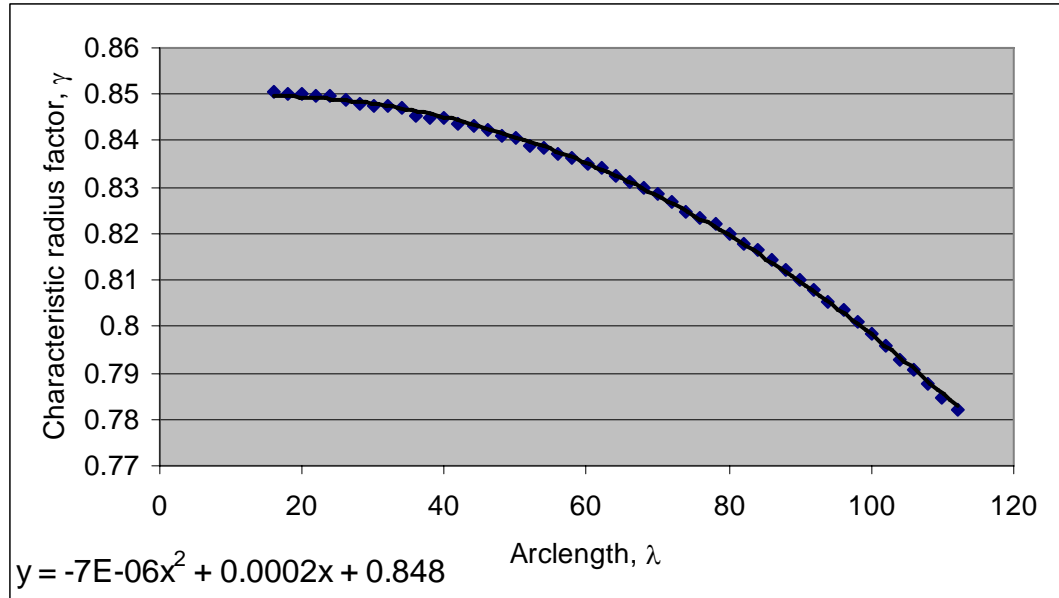


Figure 24: Trend-line of γ , for aspect ratio 0.1

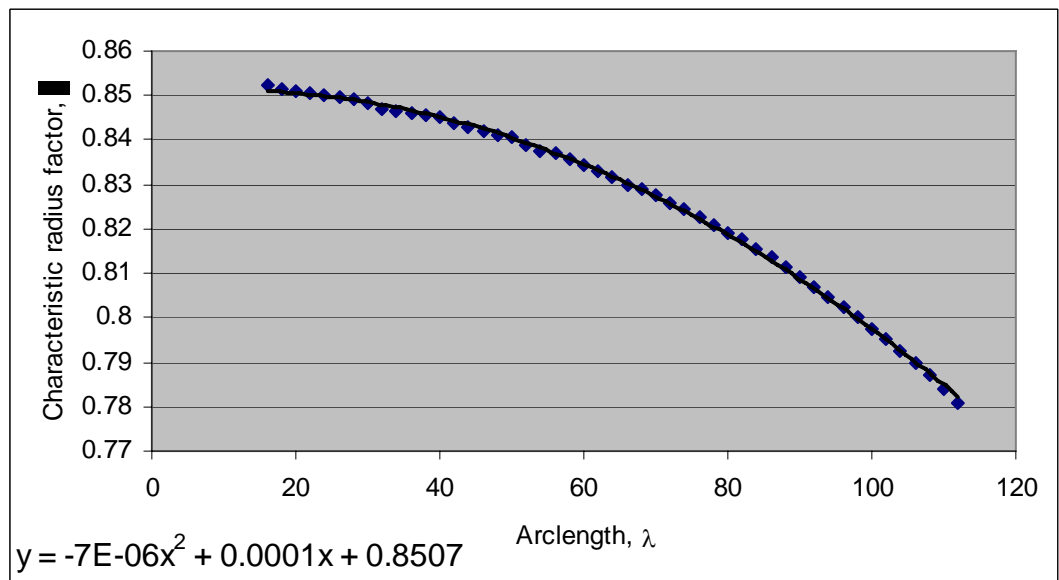


Figure 25: Trend-line of γ , for aspect ratio 0.4

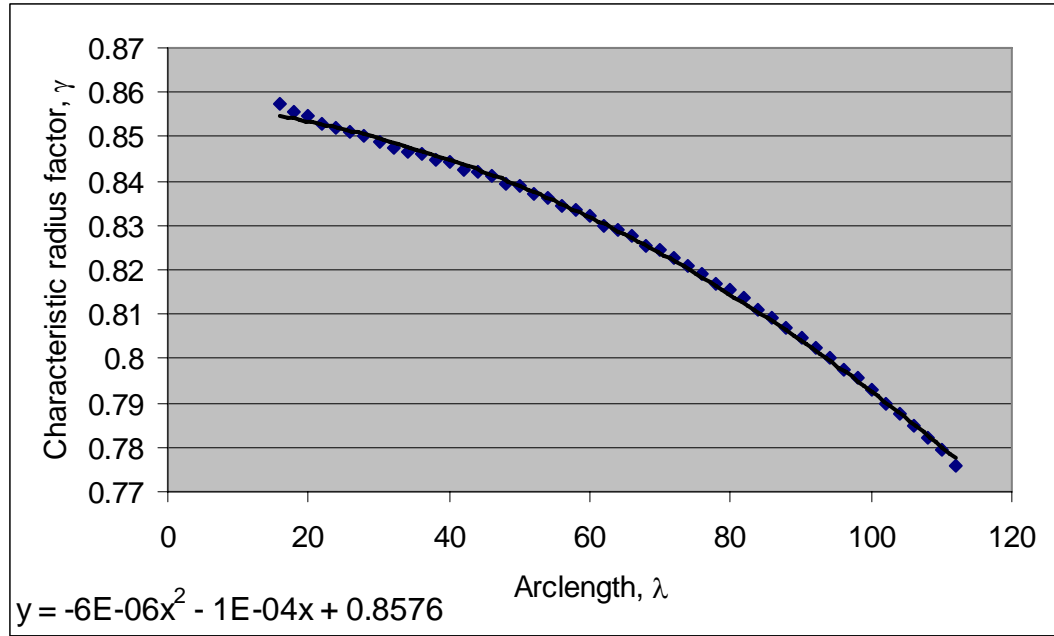


Figure 26: Trend-line of γ , for aspect ratio 0.7

Thus, at a given aspect ratio h/b and arc-length λ of curved beam we can substitute the values in the respective equation to find the corresponding characteristic radius factor γ for the spherical PRBM that best approximates the motion of the curved flexible beam.

6. Conclusion

The first Pseudo-Rigid-Body Model (PRBM) for spherical mechanisms has been developed. The kinematics of a compliant curved beam and its rigid body equivalent were described. The procedure for analyzing the curved compliant beams in a FEM program was developed. Pseudo-rigid body parameters were calculated from FEA results. These parameters are the characteristic radius factor, γ , the parametric angle co-efficient C_θ and the parameterization limit Θ_{\max} . These values approach the values found in the planar case for small arc lengths, λ .

References

- 1) Ananthasuresh, G.K., 1994, "A New Design Paradigm for Micro-Electro-Mechanical Systems and Investigations on the Compliant Mechanism Synthesis," Ph.D. dissertation, University of Michigan, Ann Arbor, MI.
- 2) Ananthasuresh, G. K., and Kota, S., 1995, "Designing of Compliant Mechanisms," *Mechanical Engineering*, Vol. 117, No.11, pp. 93-96.
- 3) Ananthasuresh, G.K., Kota, S., and Gianchandani, Y., 1994, "A Methodical Approach to the Design of Compliant Micro-mechanisms," *Solid-State Sensor and Actuator Workshop*, Hilton Head Island, SC, pp. 189-192.
- 4) ANSYS 10.0, *ANSYS University Advanced Release 10.0*.
- 5) Baker, M.S., Lyon, S.M., and Howell L.L., 2000, "A Linear Displacement Bistable Micromechanism," *Proceedings of the 26th Biennial Mechanisms and Robotics Conference, 2000 ASME Design Engineering Technical Conferences*, DETC2000/MECH-14119.
- 6) Boettama.O. and Roth, B., 1979, *Theoretical Kinematics* Dover, New York.
- 7) Broukett W. R. and Stokes A., 1991 "On the Synthesis of Compliant Mechanisms"
- 8) Cannon J.R., Lusk C.P. and Howell, L.L., 2005 "Compliant Rolling-Contact Element Mechanisms", *ASME Mechanisms and Robotics Conference 2005*.
- 9) Chiang, C. H., 1992, *Spherical kinematics in contrast to planar kinematics*, National Taiwan University, Taipei, Taiwan, Mech Mach Theory v 27 n 3 May 1992 p 243-250.

- 10) Crane, N.B., Howell L.L., and Weight, B. L., 2000, "Design and Testing of a Compliant Floating-Opposing Arm (FOA) Centrifugal Clutch," *Proceedings of 8th International Power Transmission and Gearing Conference*, 2000 ASME Design Engineering Technical Conferences DETC2000/PTG-14451.
- 11) Dado M. H, 2001 "Variable Parametric Pseudo-Rigid Body Model for Large Deflection Beams with End Loads" *International Journal of Non-linear Mechanics*, 2001.
- 12) Derderian, J.M., 1996, "The Pseudo-Rigid Body Model Concept and its Application to Micro Compliant Mechanisms," M.S. thesis, Brigham Young University, Provo, UT.
- 13) Erdman, A.G., and Sandor, G.N., 1997, *Mechanism Design: Analysis and Synthesis*, Vol. 1, 3rd Ed., Prentice Hall, Upper Saddle River, NJ.
- 14) Frankel, T., 1997 *The Geometry of Physics*, Cambridge University Press, pp21-22.
- 15) Frisch-Fay, R., 1962, *Flexible Bars*, Butterworth, Washington DC.
- 16) Guerinot A. E., Magleby S. P., and Howell, L. L., 2004 "Preliminary Design Concepts for Compliant Mechanism Prosthetic Knee Joints", *ASME Mechanisms and Robotics Conference* 2004.
- 17) Her, I., and Midha, A., 1987, "A Compliance Number Concept for Compliant Mechanisms, and Type Synthesis." *Journal of Mechanisms, Transmissions, and Automation in Design*, Trans. ASME, Vol. 109, No. 3, pp. 348-355.
- 18) Her, I., 1986, "Methodology for Compliant Mechanisms Design," Ph.D dissertation, Purdue University, West Lafayette, IN.
- 19) Henderson, D. W., 1998 *Differential Geometry*, Prentice Hall Upper Saddle River, NJ.
- 20) Hill, T.C., and Midha, A., 1990, "A graphical user-driven Newton-Raphson Technique for use in the Analysis and Design of Compliant Mechanisms." *Journal of Mechanical Design*, Trans ASME, Vol. 112, No. 1, pp. 123-130.

- 21) Howell L. L., 2001, *Compliant Mechanisms*, John Wiley and Sons, Inc, NY.
- 22) Howell, L. L., 1991, "The Design and Analysis of Large Deflection Members in Compliant Mechanisms," M.S. thesis, Purdue University, West Lafayette, IN.
- 23) Howell, L. L., and Midha, A., 1993, "Compliant Mechanisms," Section 9.10 in *Modern Kinematics: Developments in the Last Forty Years*, (A. G. Erdman, ed.), Wiley, New York, pp. 422-428.
- 24) Howell, L. L., and Midha, A., 1994, "The development of Force Deflection Relationships," *Machine elements and Machine Dynamics: Proceedings of the 1994 ASME Mechanisms conference*, DE-Vol. 71, pp. 501-508.
- 25) Howell, L. L., and Midha, A., 1995, "Parametric Deflection Approximations for End-Loaded, Large Deflection Beams in Compliant Mechanisms," *Journal of Mechanical Design*, ASME, Vol. 117, No.1, pp. 156-165.
- 26) Howell, L. L., and Midha, A., 1995, "Determination of the Degrees of Freedom of Compliant Mechanisms using the Pseudo-Rigid Body Model Concept," *Proceedings of the 9th World Congress on the Theory of Machines and Mechanisms*, Milano, Italy, Vol. 22, pp. 1537-1541.
- 27) Howell, L.L., Rao, S.S., and Midha, A., 1994, "The Reliability Based Optimal Design of a Bistable Compliant Mechanism," *Journal of Mechanical Design*, Trans. ASME, Vol. 116, No. 4, pp. 1115-1121.
- 28) Howell, L.L., and Midha, A., 1995, "Parametric Deflection Approximations for End-Loaded, Large-Deflection Beams in Compliant Mechanisms," *Journal of Mechanical Design*, Trans. ASME, Vol. 71, pp. 156-165.
- 29) N.B. Hubbard, L.L. Howell, 2005 "Design and Characterization of a Dual-stage, Thermally Actuated Nanopositioner", *Journal of Micromechanics and Microengineering*, 2005.

- 30) Jensen, B.D., Howell L.L., Gunyan, D.B., and Salmon, L.G., 1997, "The Design and Analysis of Compliant MEMS Using the Pseudo-Rigid-Body Model," *Micromechanical Systems (MEMS)*, at the 1997 ASME International Mechanical Engineering Congress and Exposition, DSC-Vol. 62, pp. 119-126.
- 31) Jensen, B.D., Howell L.L., and Salmon, L.G., 1999, "Design of Two-Link, In-plane, Bi-stable Compliant Micro-mechanisms," *Journal of Mechanical Design*, Trans. ASME, Vol. 121, No. 3, pp. 93-96.
- 32) Lai, M.W., Rubin, D, Krempl, E, 1993 *Introduction to Continuum Mechanics 3rd ed* Pergamon, Pr.
- 33) Merriam-Webster Dictionary, 2006, *Merriam-Webster Online*. "<http://www.m-w.com/cgi-bin/dictionary?book=Dictionary&va=great%20circle>".
- 34) Midha, A., Her, I., and Salamon, B.A., 1992, "A Methodology for Compliant Mechanisms Design, Part I: Introduction and Large-Deflection Analysis," in *Advances in Design Automation*, D.A Hoeltzel, ed., 18th ASME Design Automation Conference, DE-Vol. 44-2, pp. 29-38.
- 35) Midha, A., and Howell, L.L., 2000, "Limit Positions of Compliant Mechanism using the Pseudo-rigid body Model", *Mechanism and Machine Theory*, Vol. 35, No. 1, pp. 99-115.
- 36) McCarthy, J., 2000 *Geometric Design of Linkages* Springer, NY.
- 37) Millar A. J., Howell L L and Leonard J N, 1996 "Design and Evaluation of Compliant Constant Force Mechanisms".
- 38) Roach, G.M., and Howell, L. L., 2000, "Compliant Overrunning clutch with centrifugal Throw out," U.S. patent 6,148,979, Nov 21.
- 39) Salamon, B.A., 1989, "Mechanical Advantage Aspects in Compliant Mechanisms Design," in *Advances in Design Automation*, D.A Hoeltzel, ed., 18th ASME Design Automation Conference, DE-Vol44-2, pp. 47-51.

- 40) Saggere L. and Kota S., 1997 "Synthesis of Distributed Compliant Mechanisms for Adaptive Structure application: An Elasto-Kinematic Approach" *Proceedings of the ASME Design Engineering Technical Conferences*, 1997.
- 41) Salmon, L.G., Gunyan, D.B., Derderian, J.M., Opdahl, P.G., and Howell L.L., 1996, "Use of the Pseudo-Rigid Body Model to Simplify the Description of Compliant Micromechanisms," 1996 *IEEE Solid-State and Actuator Workshop*, Hilton Head Island, SC, pp. 136-139.
- 42) Saxena, A. and Kramer, S.N., 1998, "A Simple and Accurate Method for Determining Large Deflections in Compliant Mechanisms Subjected to End Forces and Moments," *Journal of Mechanical Design*, Trans. ASME, Vol. 120, No.3, pp. 392-400, erratum, Vol. 121, No. 2, p.194.
- 43) Sevak, N.M., and McLarman, C.W., 1974, "Optimal Synthesis of Flexible Link Mechanisms with large Static Deflections," ASME Paper 74-DET-83.
- 44) Spiegel M. R., 1968 *Schaums Outlines of Theory and Problems Of Mathematical Handbook Of Formulas And Tables*.
- 45) WordNet , "longitude". *WordNet 1.7.1*. Princeton University, 2001. *Answers.com*, 14 Nov. 2006.
<http://www.answers.com/topic/longitude>.
- 46) Wolfram, Mathworld, 2006,
<http://mathworld.wolfram.com/SphericalTriangle.htm>.

Appendices

Appendix A Spherical Triangles and Napier Rules

Spherical Triangles

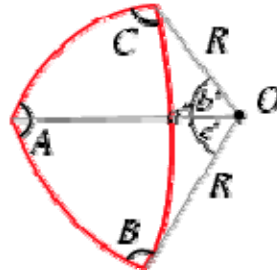


Figure 27: Spherical triangles

A spherical triangle is a figure formed on the surface of a sphere by three great circular arcs intersecting pair-wise in three vertices. The spherical triangle is the spherical analog of the planar triangle, and is sometimes called an Euler triangle (Wolfram, 2006). Let a spherical triangle have angles A , B , and C (measured in radians at the vertices along the surface of the sphere) and let the sphere on which the spherical triangle sits have radius R (Wolfram, 2006)

Napier Rules

Napier's rules are used to derive the parameters required to analyze the bending of curved beam.

Appendix A (Continued)

The derivation of parameters can be easily obtained from two simple rules discovered by John Napier (1550-1617), the inventor of logarithms. (<http://www.angelfire.com/nt/navtrig/B2.html>). As the right angle does not enter into the formulas, only five parts are considered. These are a , b , and the complements of A , B , and C (or $90-A$, $90-B$, $90-C$) which can be written A' , B' , and c' .

If these five parts are arranged in the order in which they occur in the triangle, any part may be selected and called the middle part; then the two parts next to it are called adjacent parts, and the other two are called opposite parts.

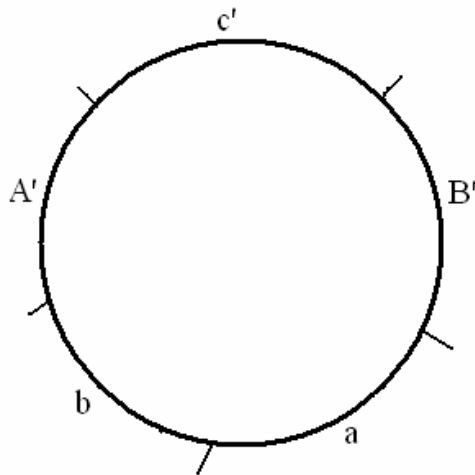


Figure 28: Five parts arranged in order of occurrence

Napier's rules are as follows: 1. The sine of the middle part equals the product of the tangents of the adjacent parts.

Appendix A (Continued)

2. The sine of the middle part equals the product of the cosines of the opposite parts.

The right spherical triangle for the PRBM has the sides, $\gamma\lambda$, β and η . The right angle lies between the 'sides' β and η . Θ is the pseudo-rigid-body angle. ' η' ' is the angle opposite to η as shown in Figure 24

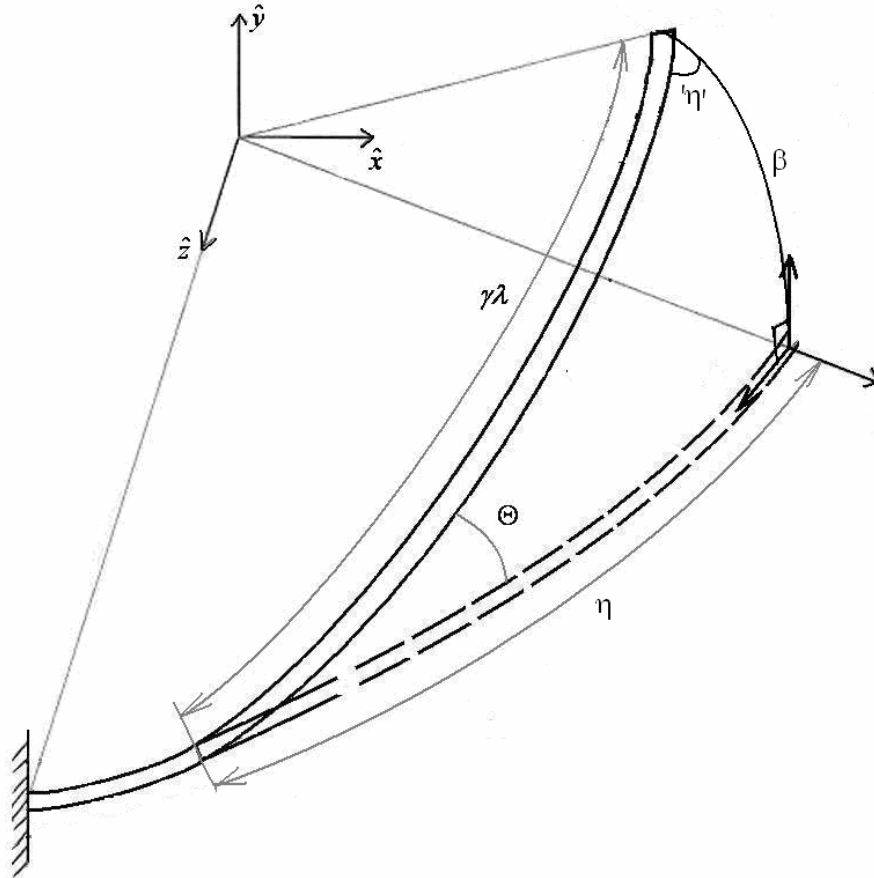


Figure 29: Spherical right triangle

Appendix A (Continued)

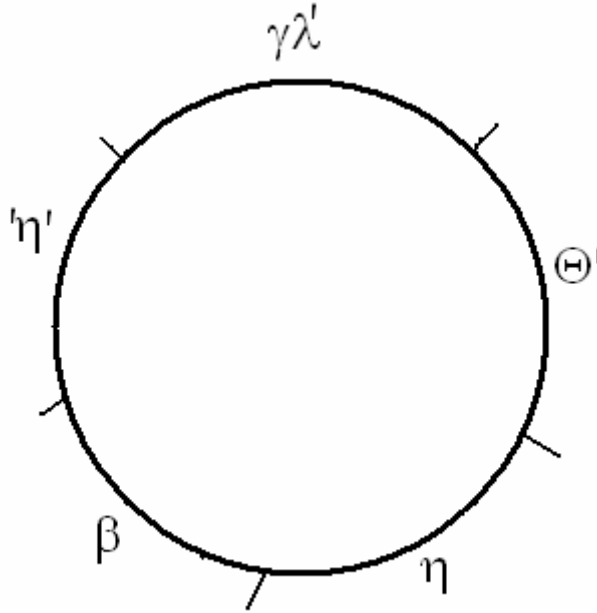


Figure 30: Five parts for PRBM right spherical triangle.

Using Napier Rules the following equations can be obtained.

$$\sin(90 - \Theta) = \tan \eta \tan(90 - \Theta)$$

Where $\eta = (\lambda - \phi) - (\lambda - \gamma\lambda)$

and $\alpha = \lambda - \phi$

To get

$$\Theta = \tan^{-1} \left[\frac{\tan \beta}{\sin[\alpha - \lambda(1 - \gamma)]} \right]$$

Appendix A (Continued)

At $\beta=90^\circ$ this equation fails to give a value of pseudo-rigid body angle, Θ , to overcome this, Θ is also expressed in an alternate form.

From Napier Rules we get

$$\sin \Theta = \frac{\sin \beta}{\sin \gamma \lambda}$$

and

$$\cos \Theta = \tan \eta \cot \gamma \lambda$$

To get

$$\Theta = \tan^{-1} \left[\frac{\sin \beta / \sin \gamma \lambda}{\tan \eta \cot \gamma \lambda} \right]$$

Appendix B Manual for FEA

The following figures (31-54) show a step by step process to run a single simulation for a single load step.

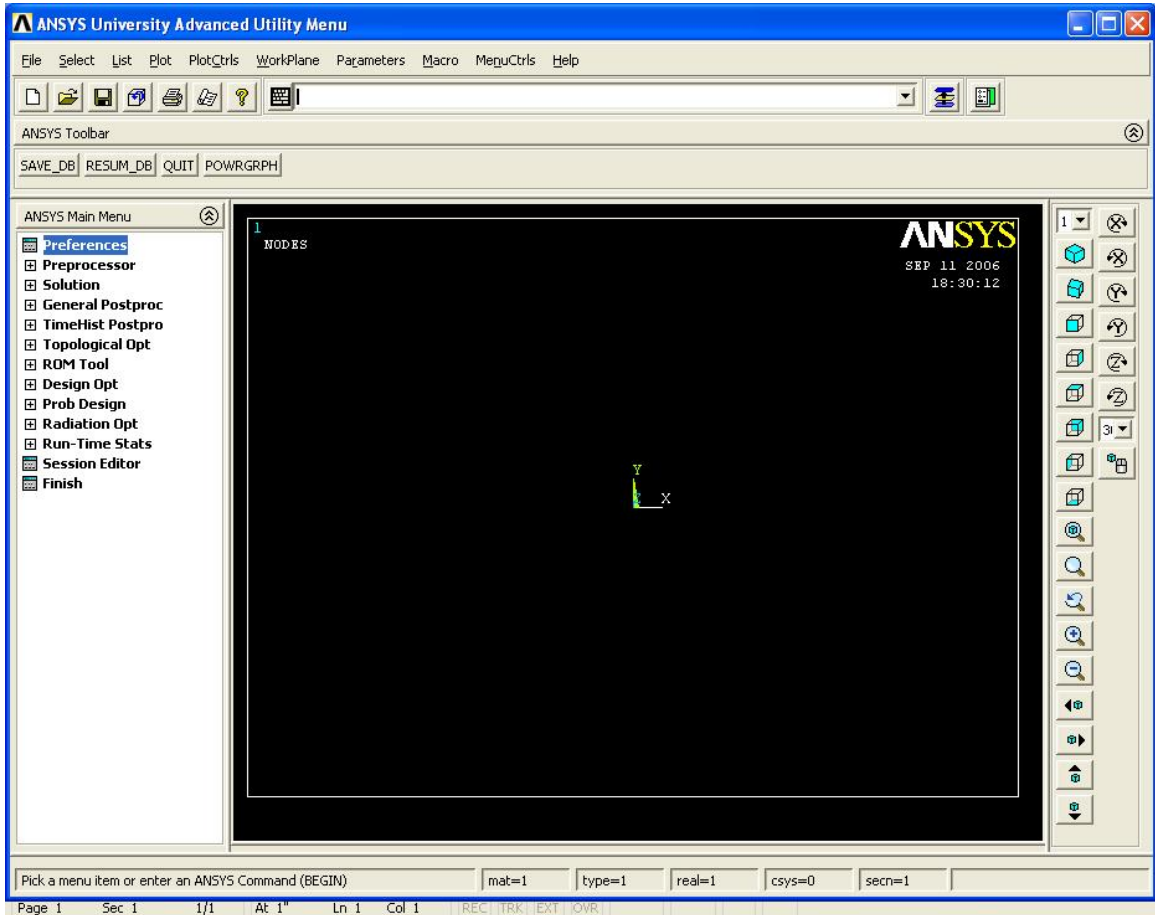


Figure 31: Activating Graphical User Interface (GUI)

Appendix B (Continued)

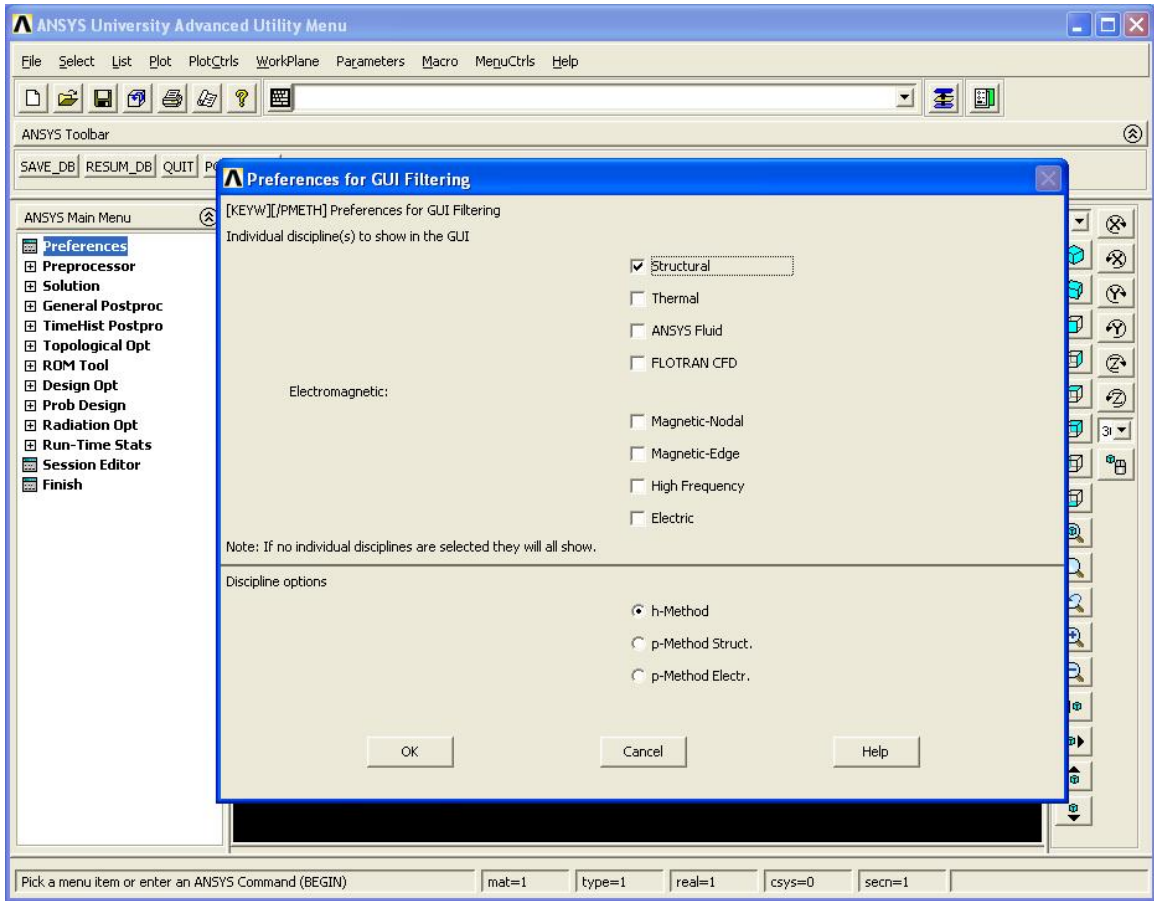


Figure 32: Limiting the GUI options to structural preferences

Appendix B (Continued)

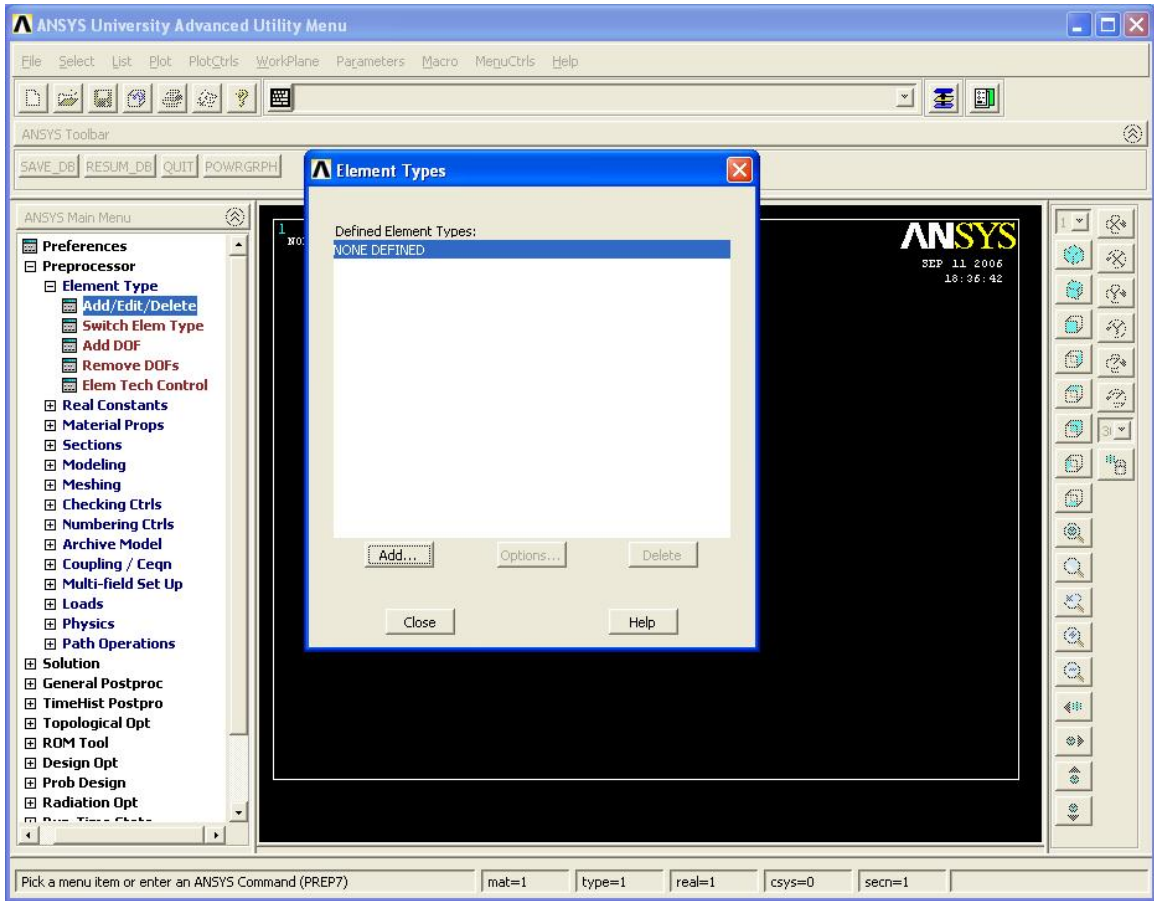


Figure 33: Adding or defining new element types

Appendix B (Continued)

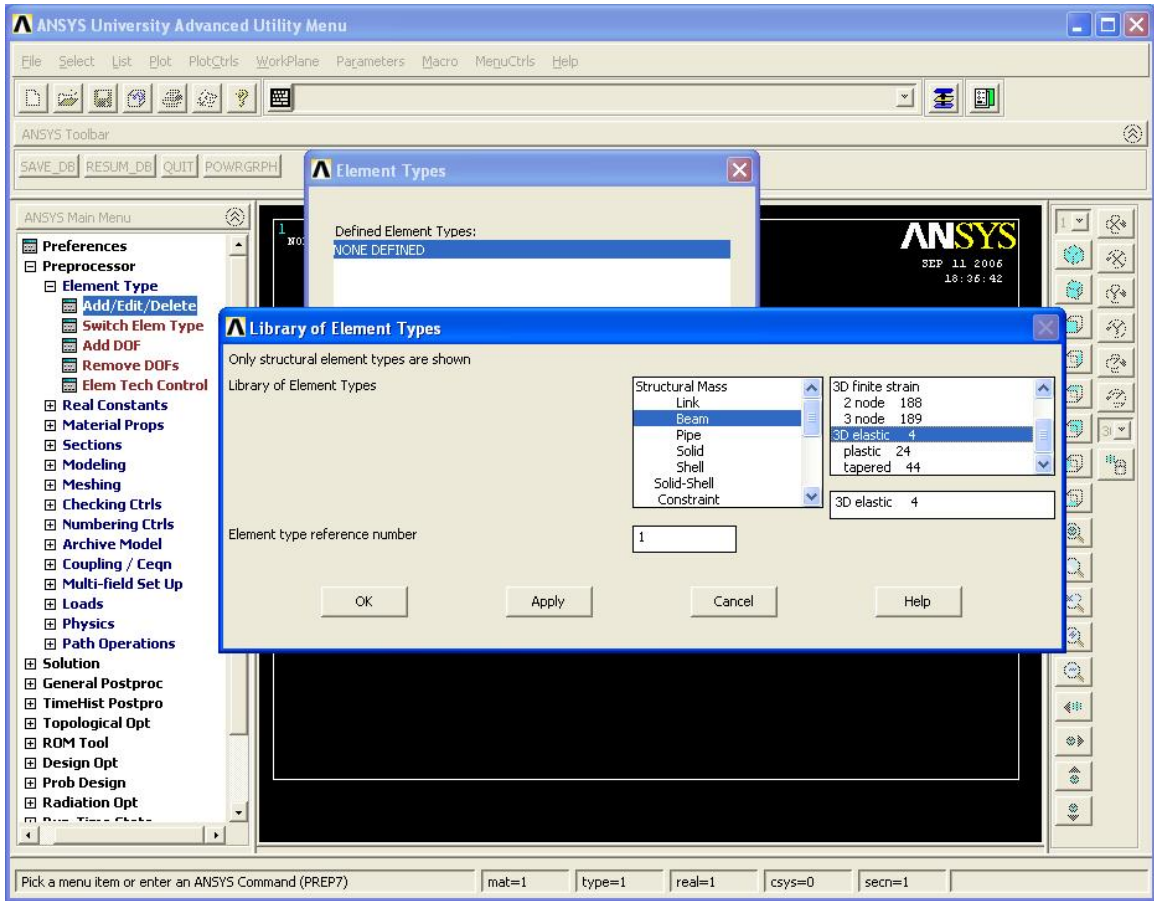


Figure 34: Beam elements

Appendix B (Continued)

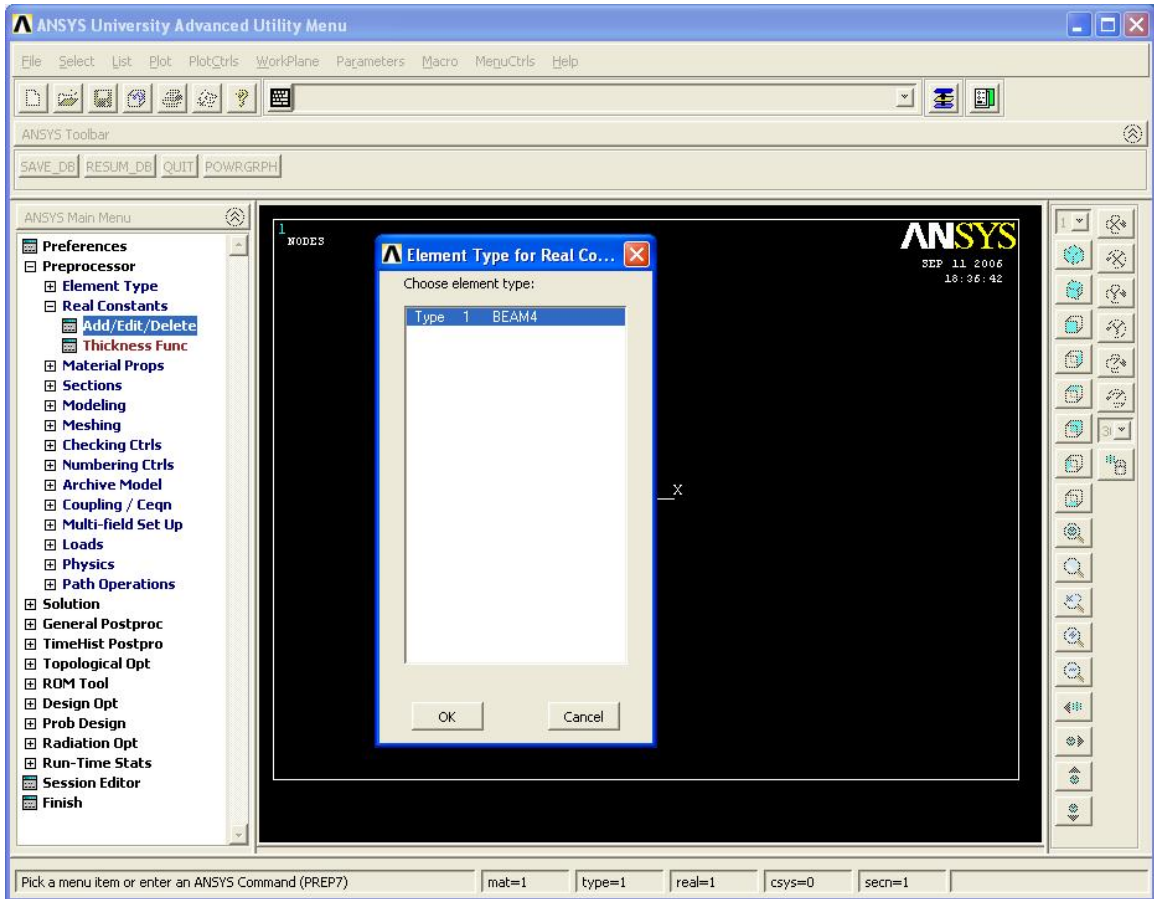


Figure 35: Defining real constants for respective elements

Appendix B (Continued)

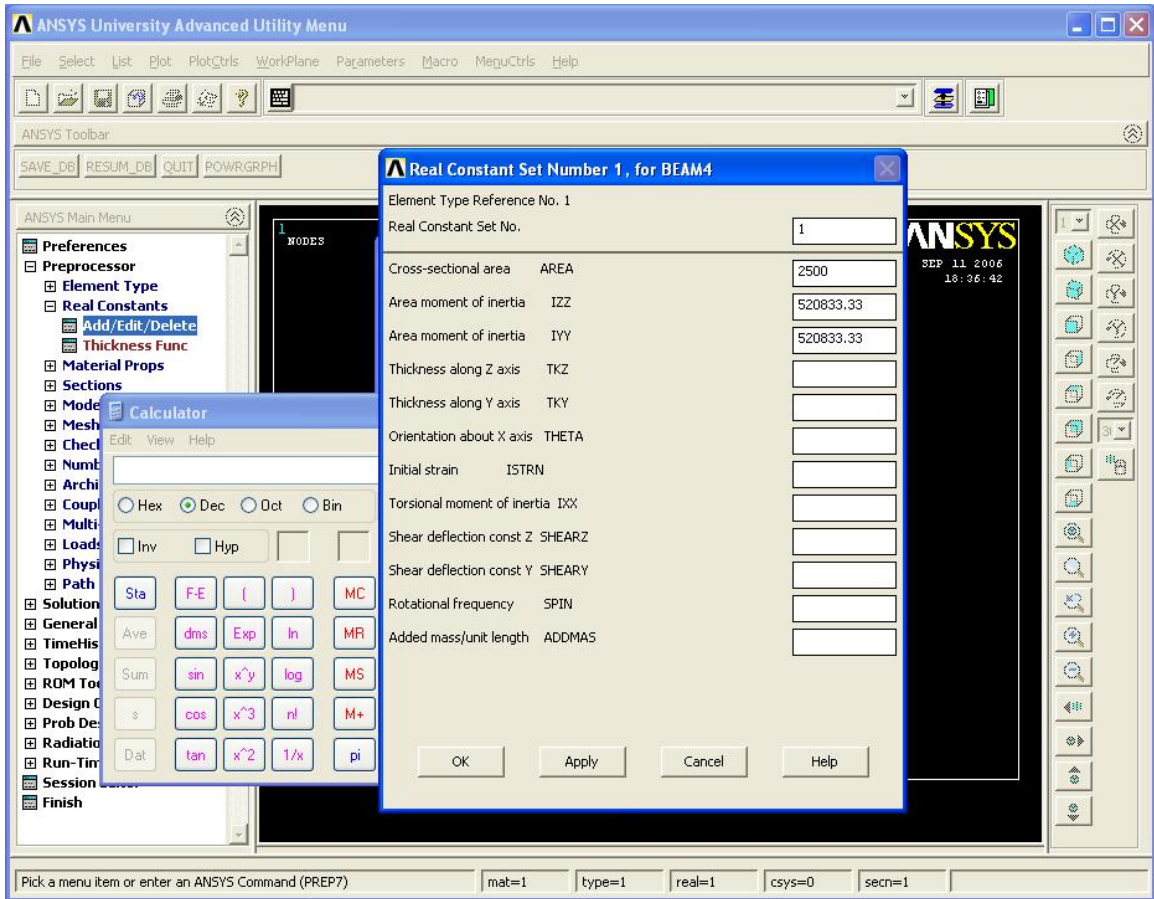


Figure 36: Inputting area and moment of inertia values to elements

Appendix B (Continued)

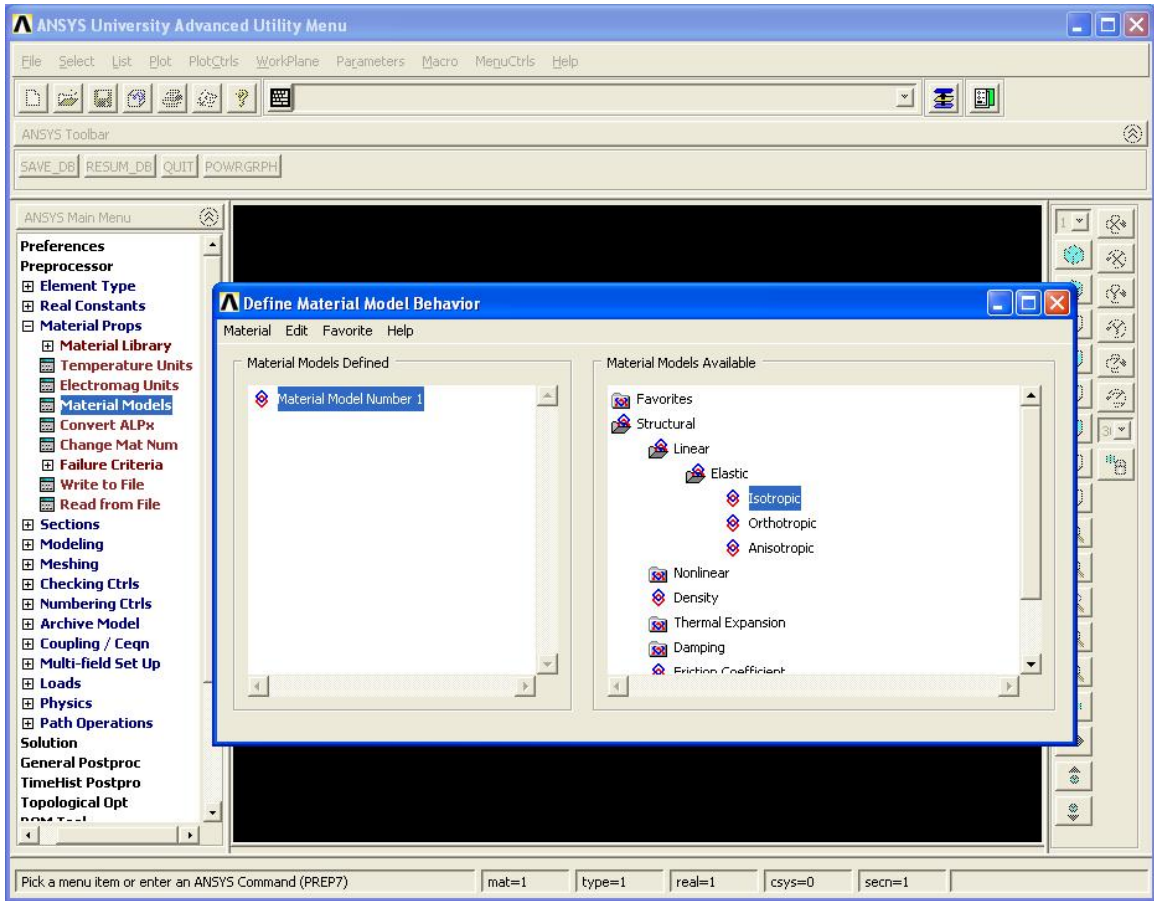


Figure 37: Defining material properties

Appendix B (Continued)

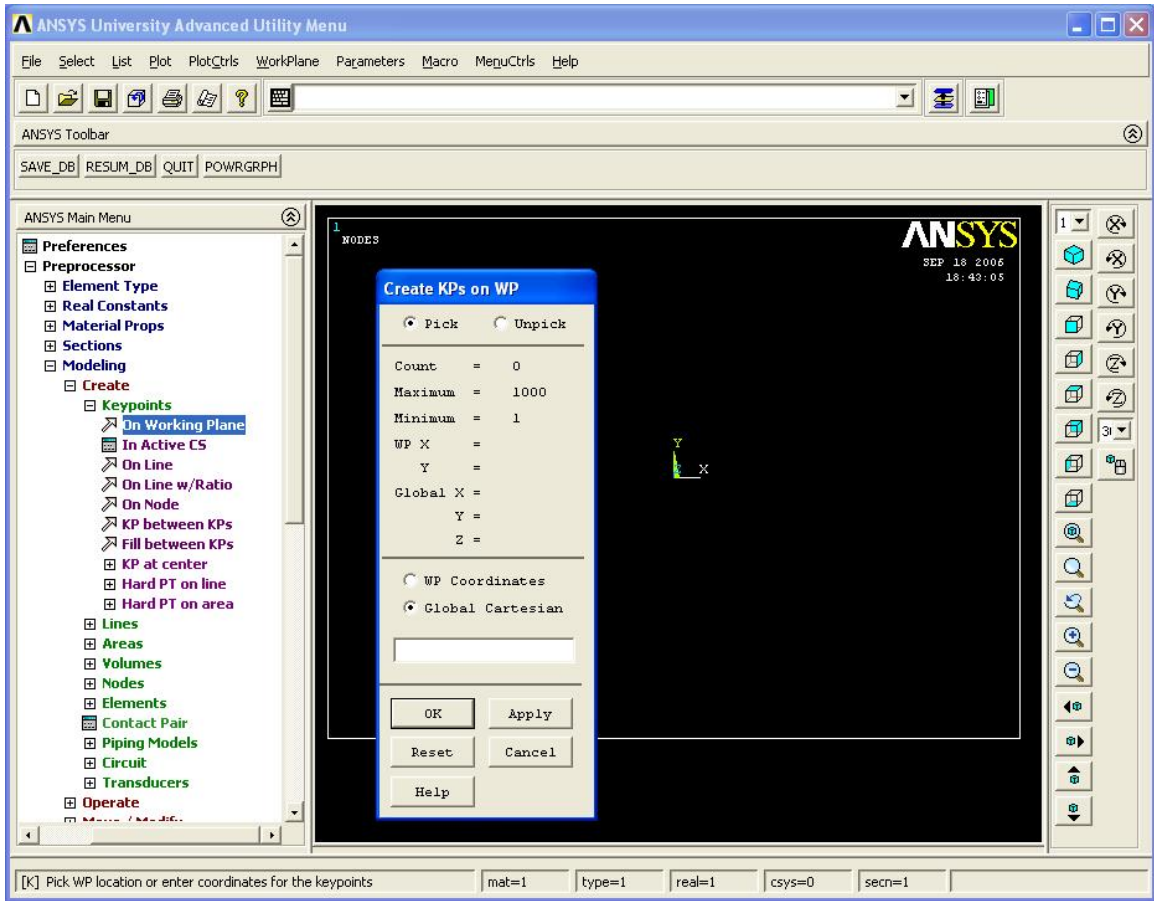


Figure 38: Creating key-points on work-plane through GUI

Appendix B (Continued)

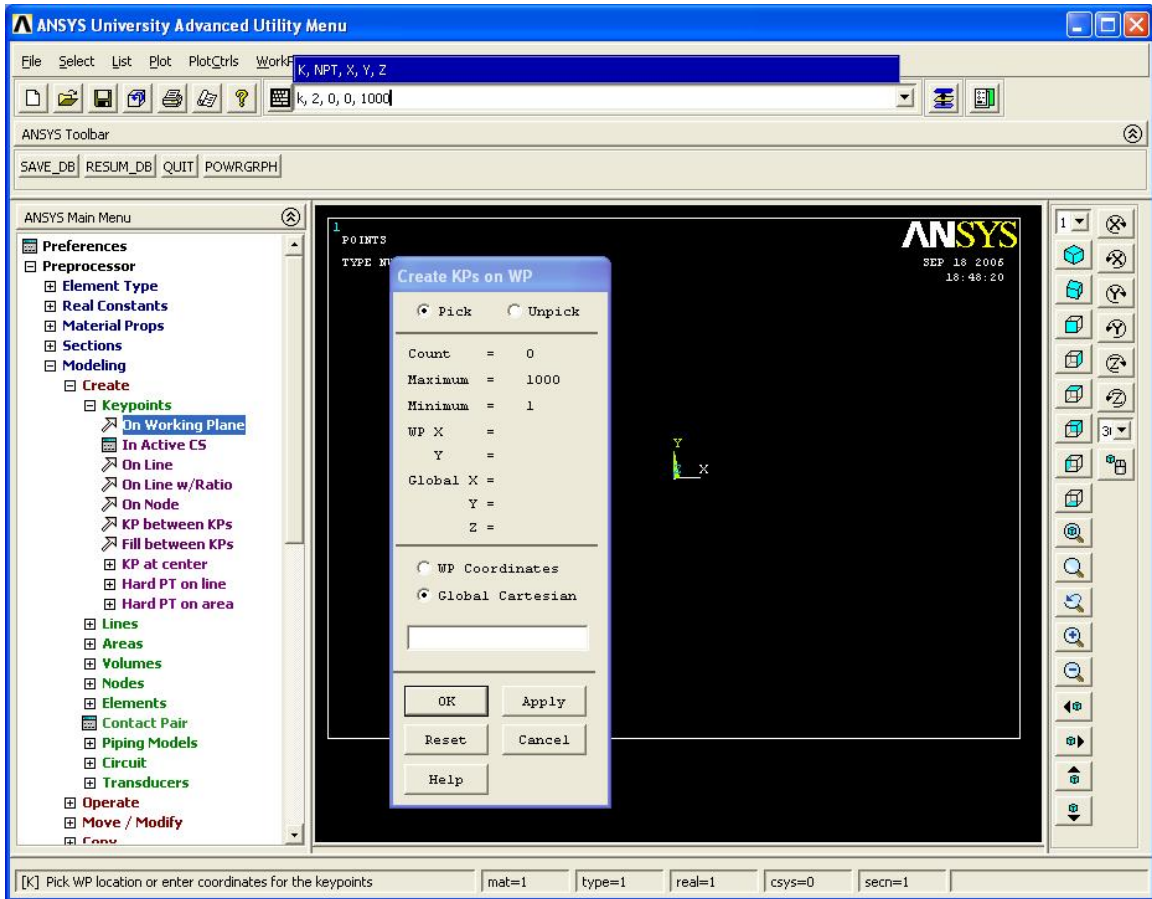


Figure 39: Creating key-points using command line

Appendix B (Continued)

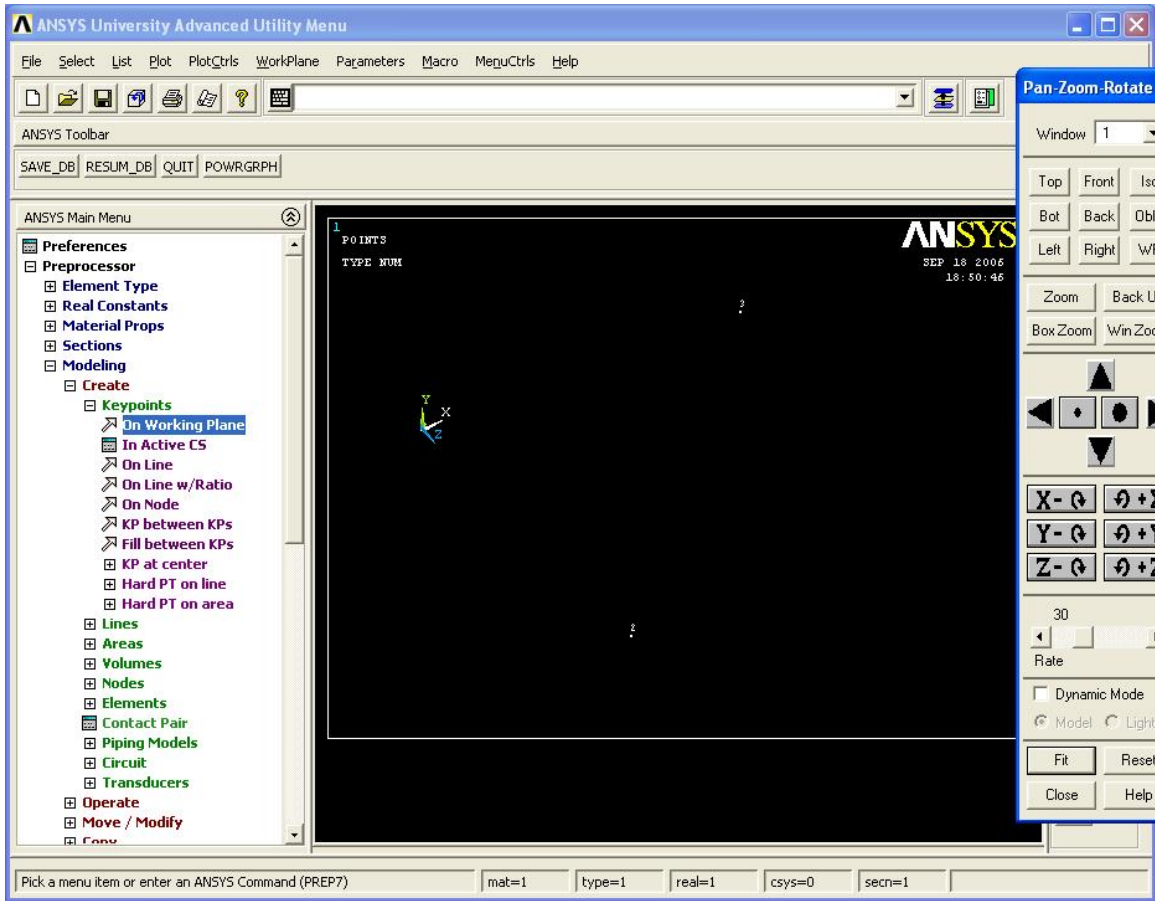


Figure 40: Pan, zoom, rotate

Appendix B (Continued)

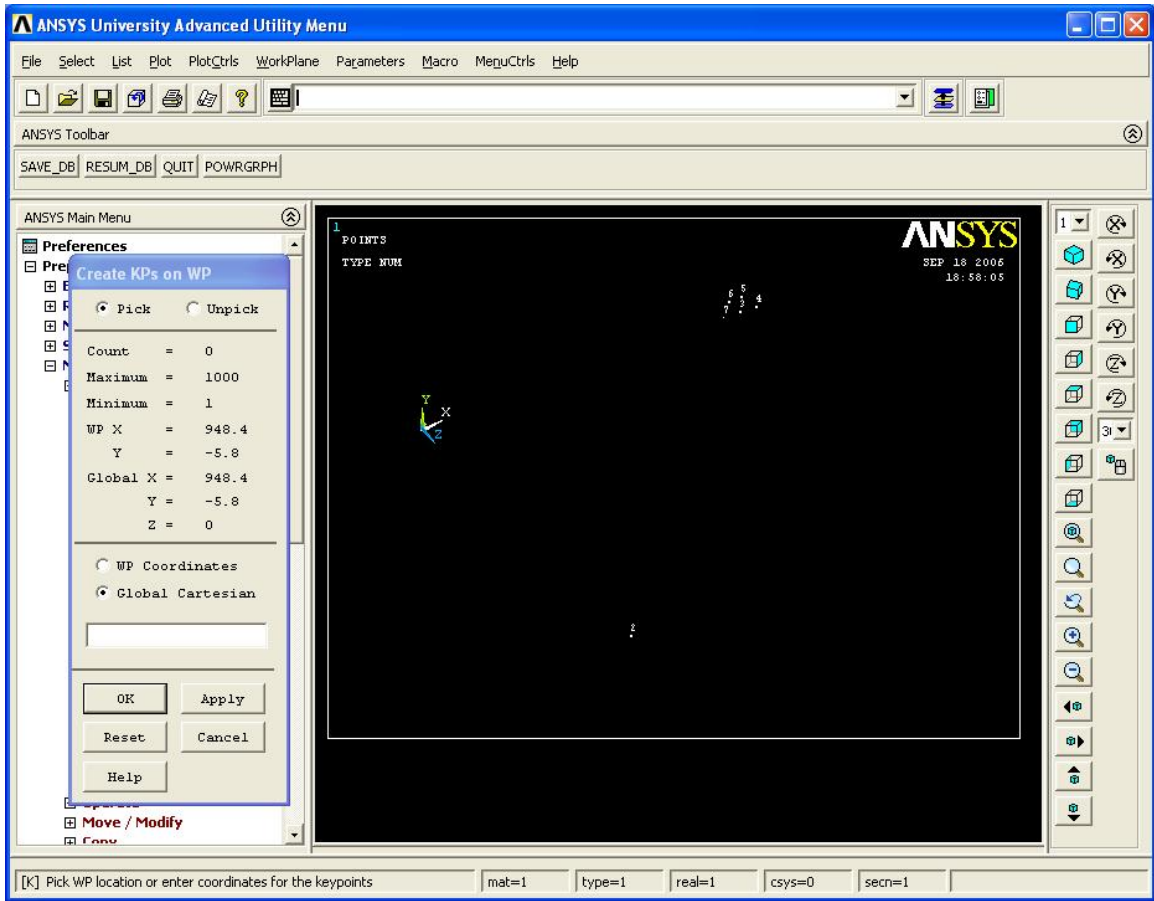


Figure 41: Defining of orthogonal triad at beam end

Appendix B (Continued)

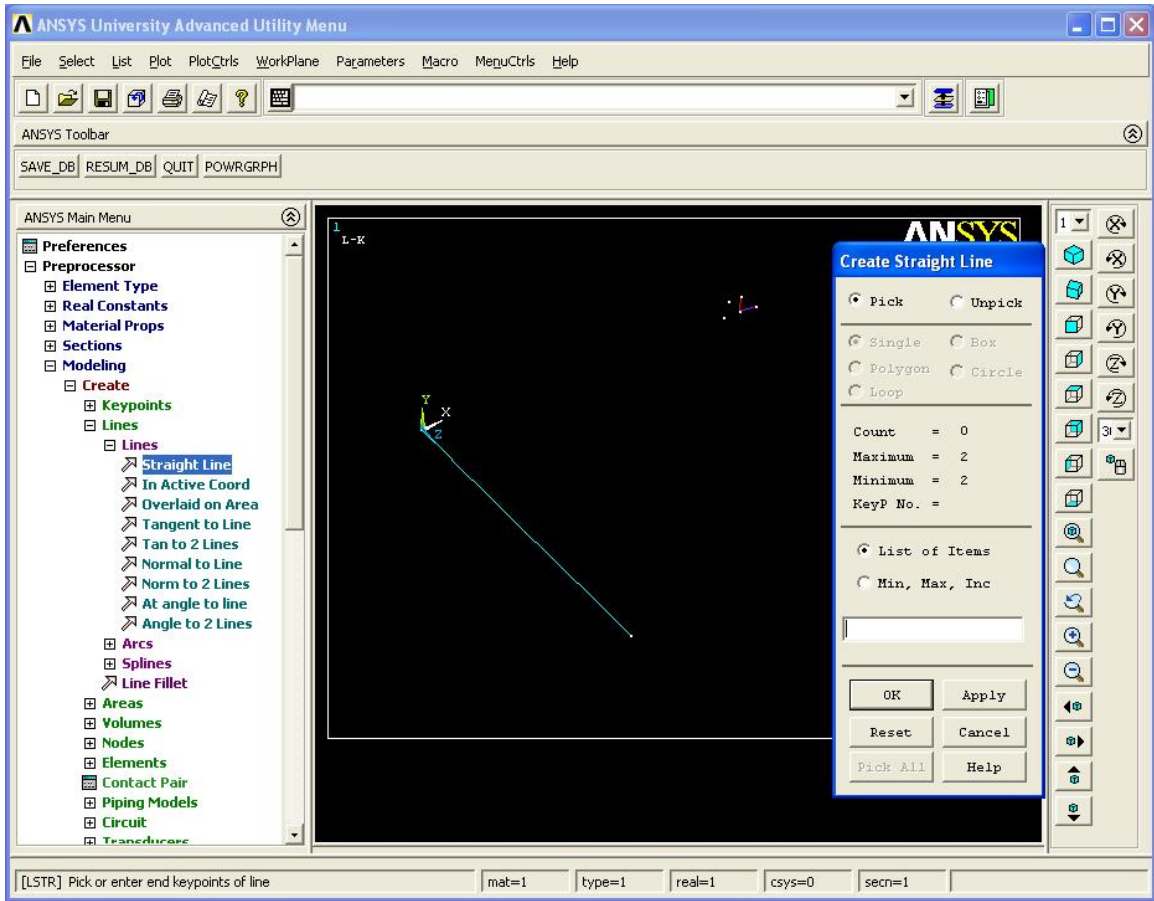


Figure 42: Creating lines

Appendix B (Continued)

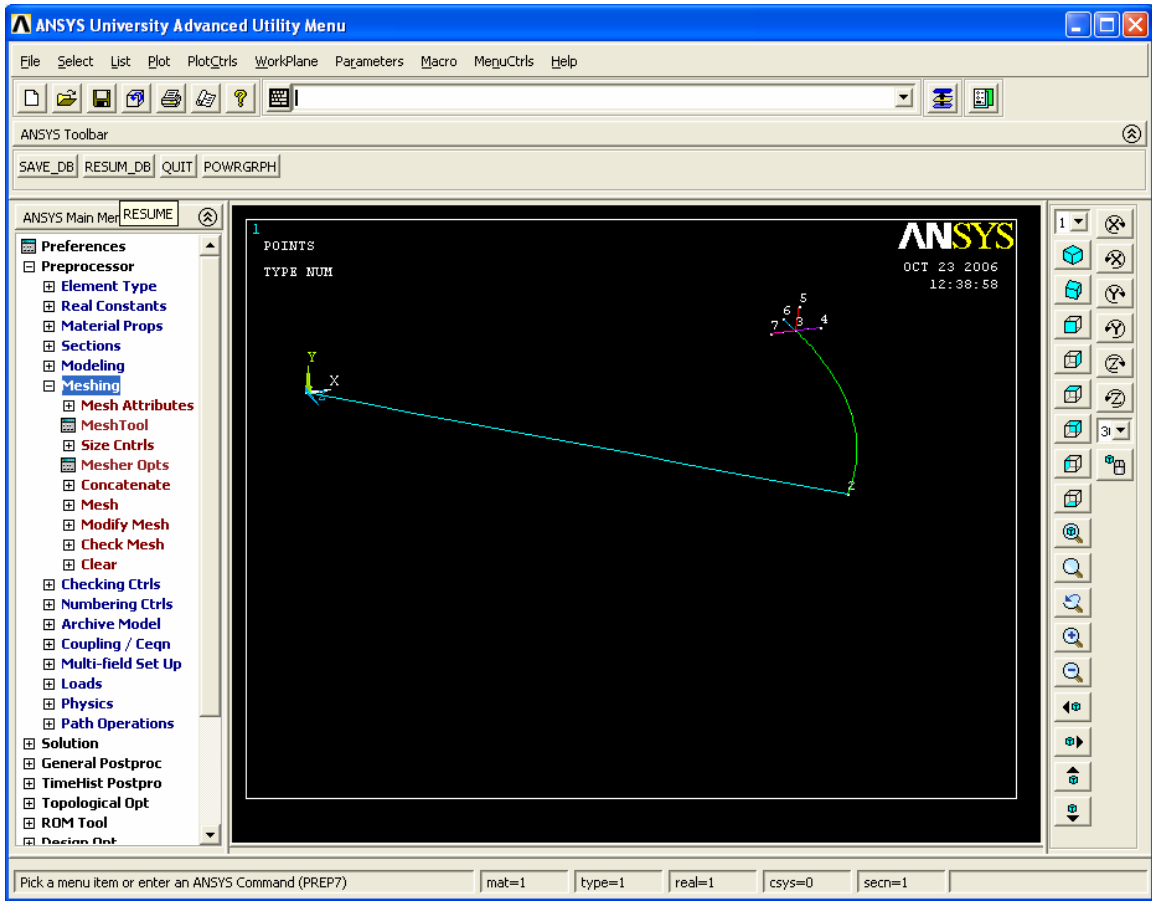


Figure 43: Creating arcs

Appendix B (Continued)

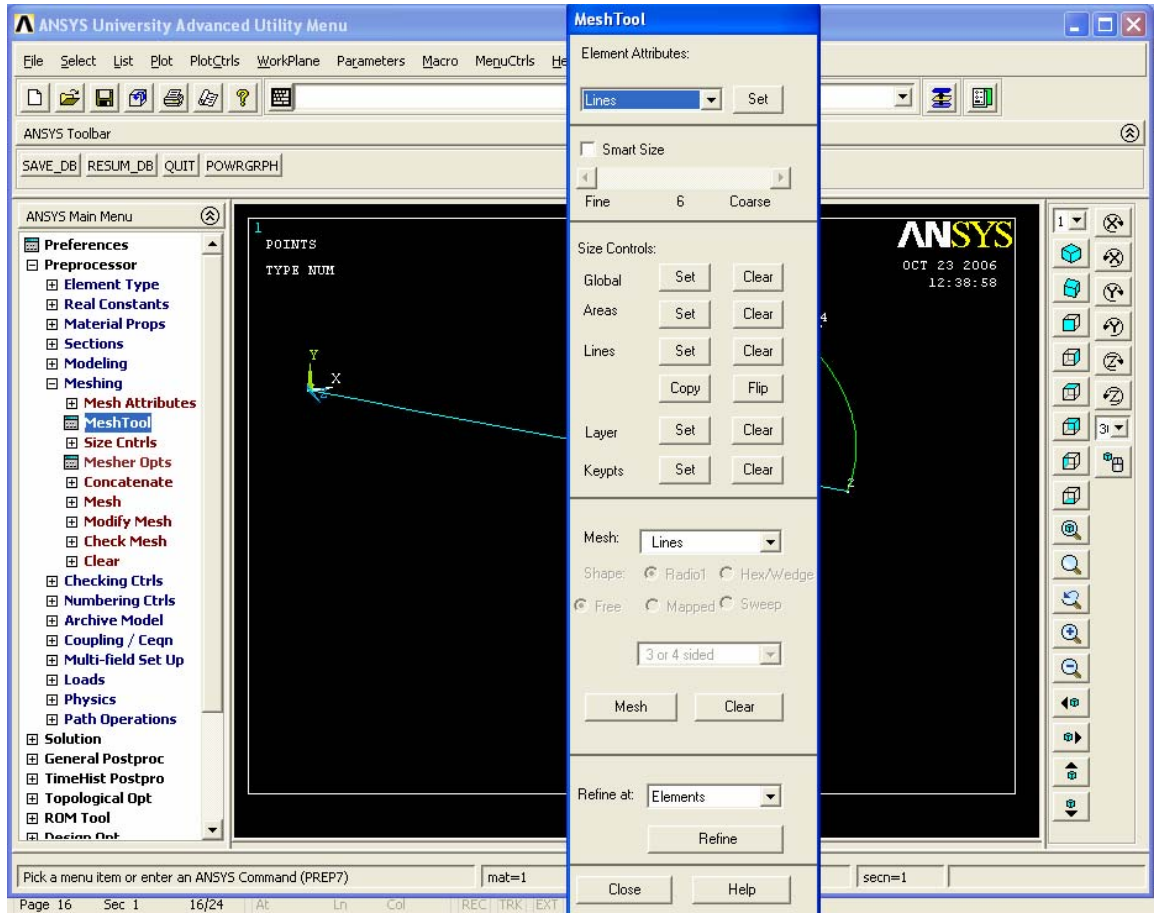


Figure 44: Meshing

Appendix B (Continued)

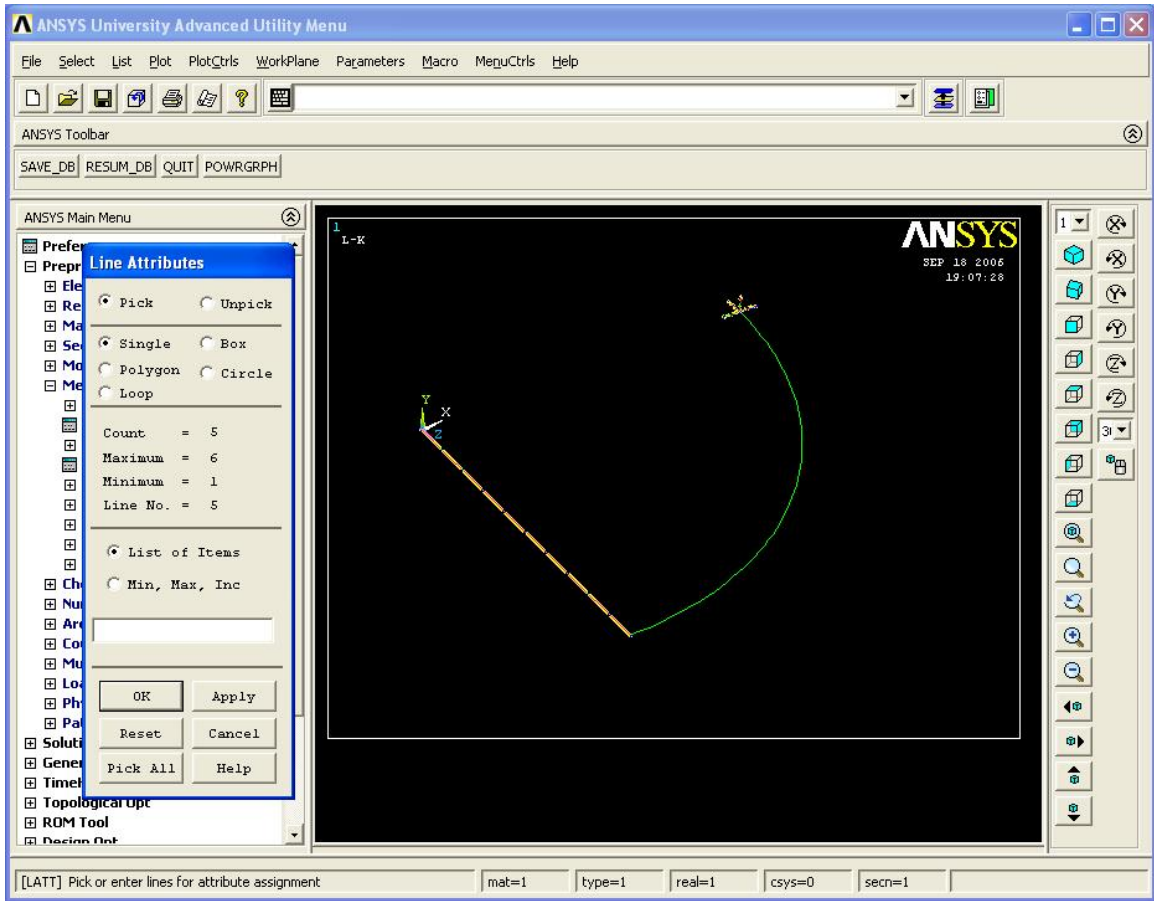


Figure 45: Mesh attributes for line

Appendix B (Continued)

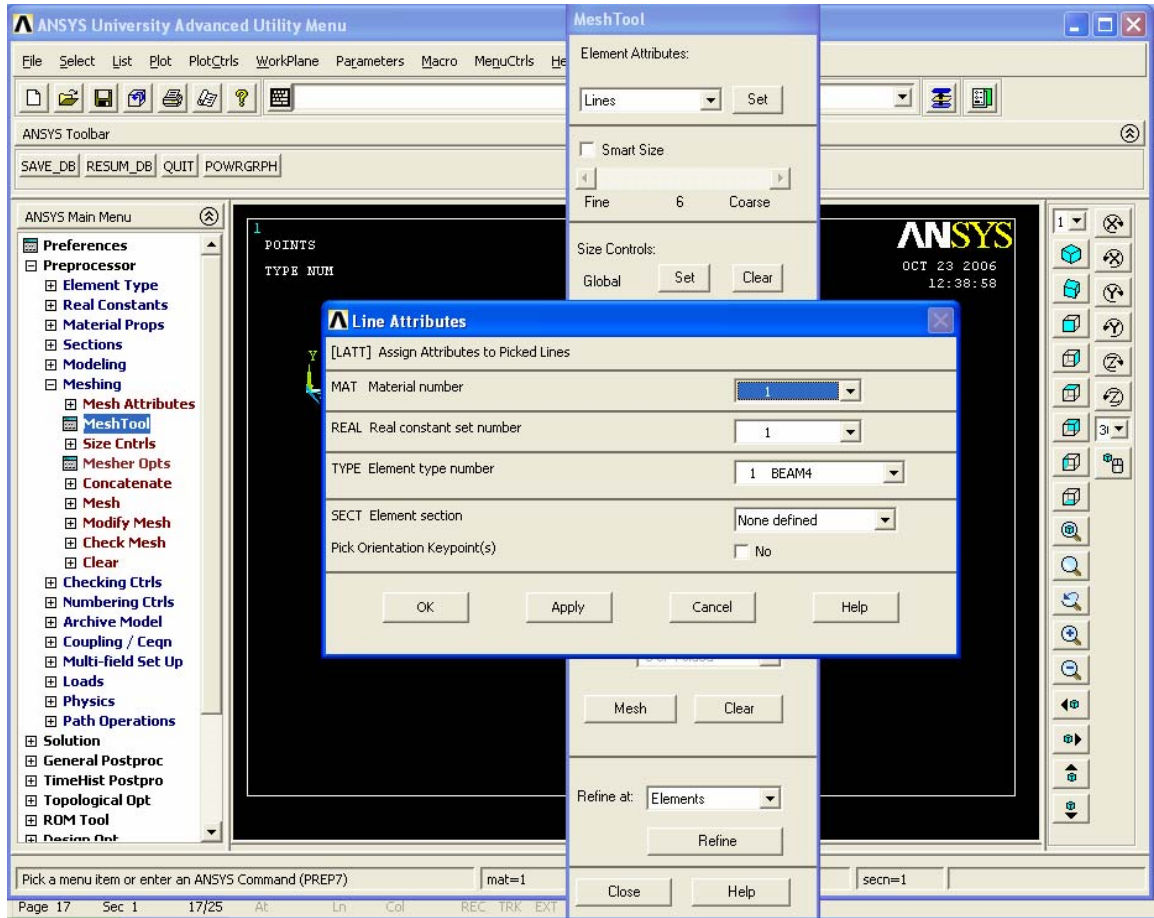


Figure 46: Allocating specific material to mesh (elements)

Appendix B (Continued)

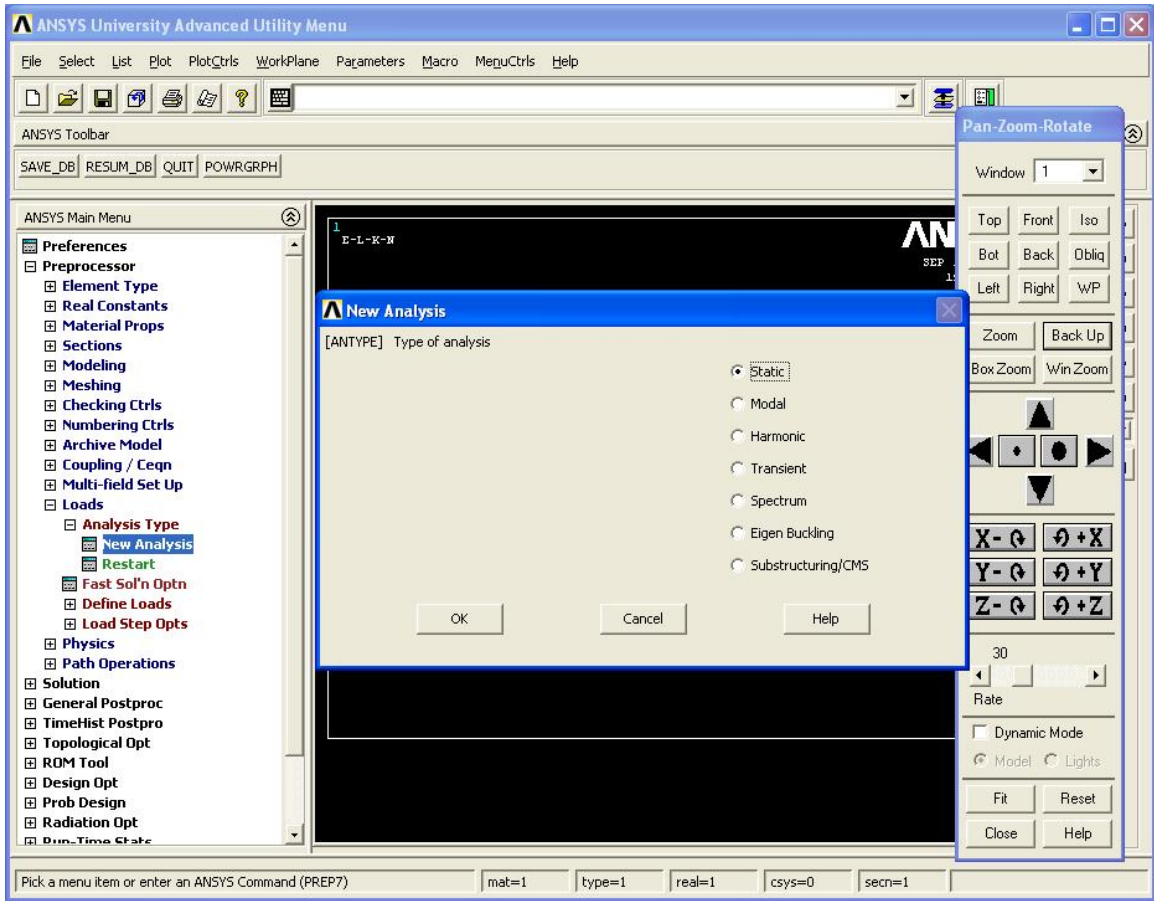


Figure 47: Selecting analysis type

Appendix B (Continued)

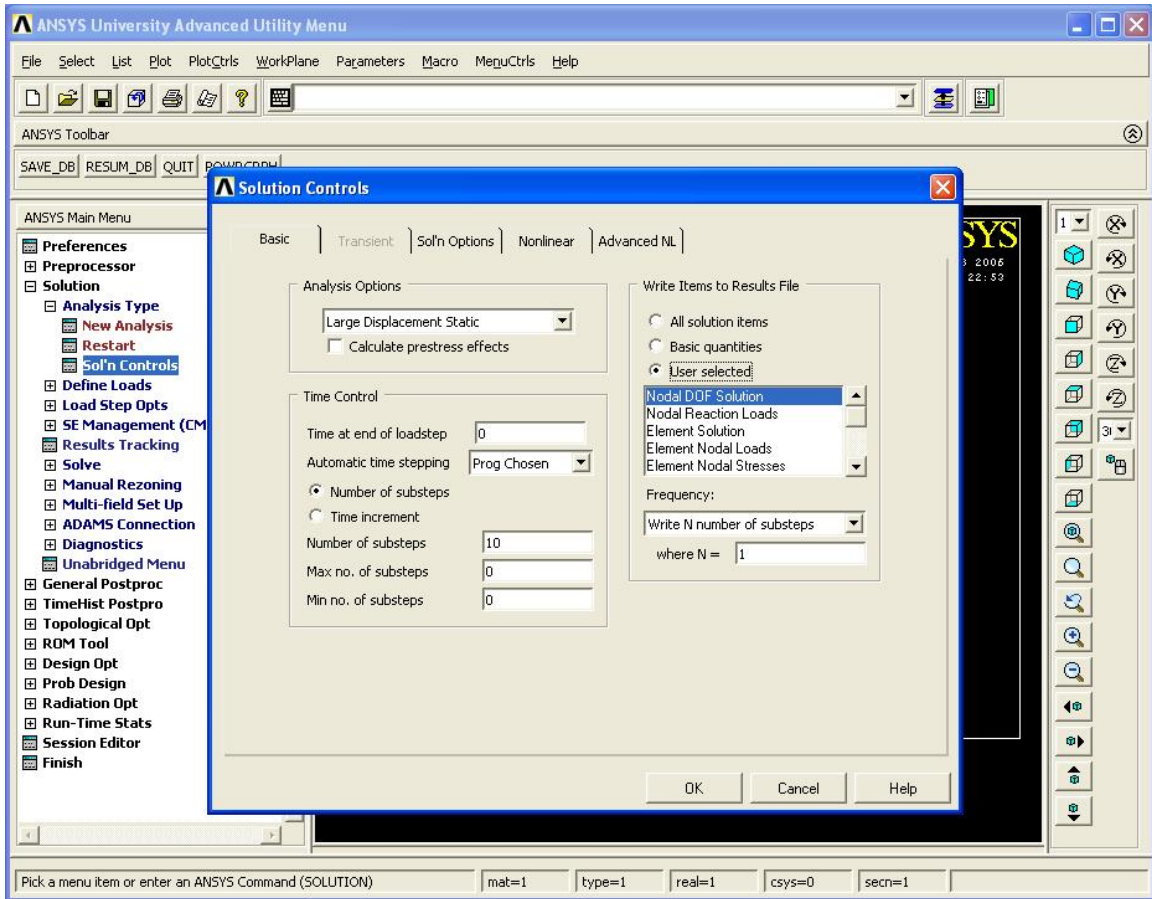


Figure 48: Large displacement analysis selected

Appendix B (Continued)

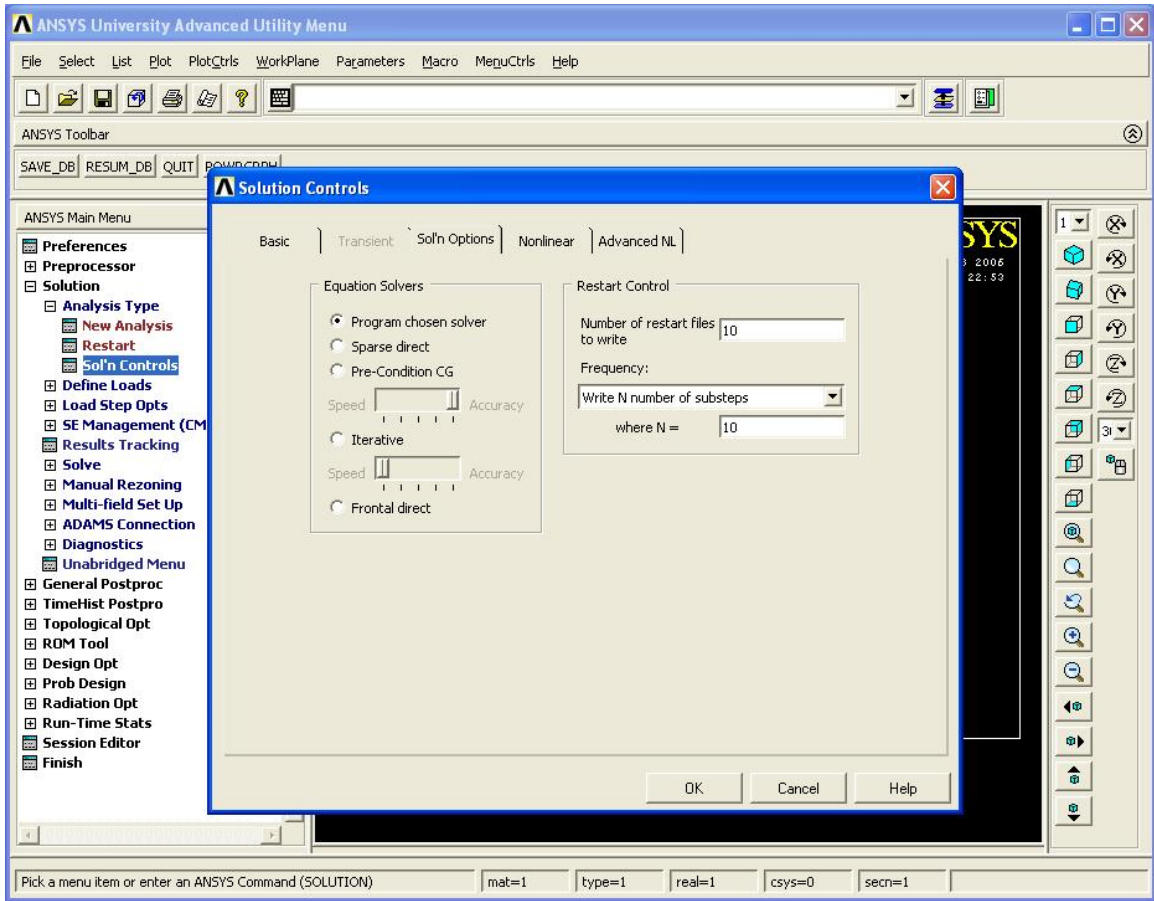


Figure 49: Equation chosen solvers

Appendix B (Continued)

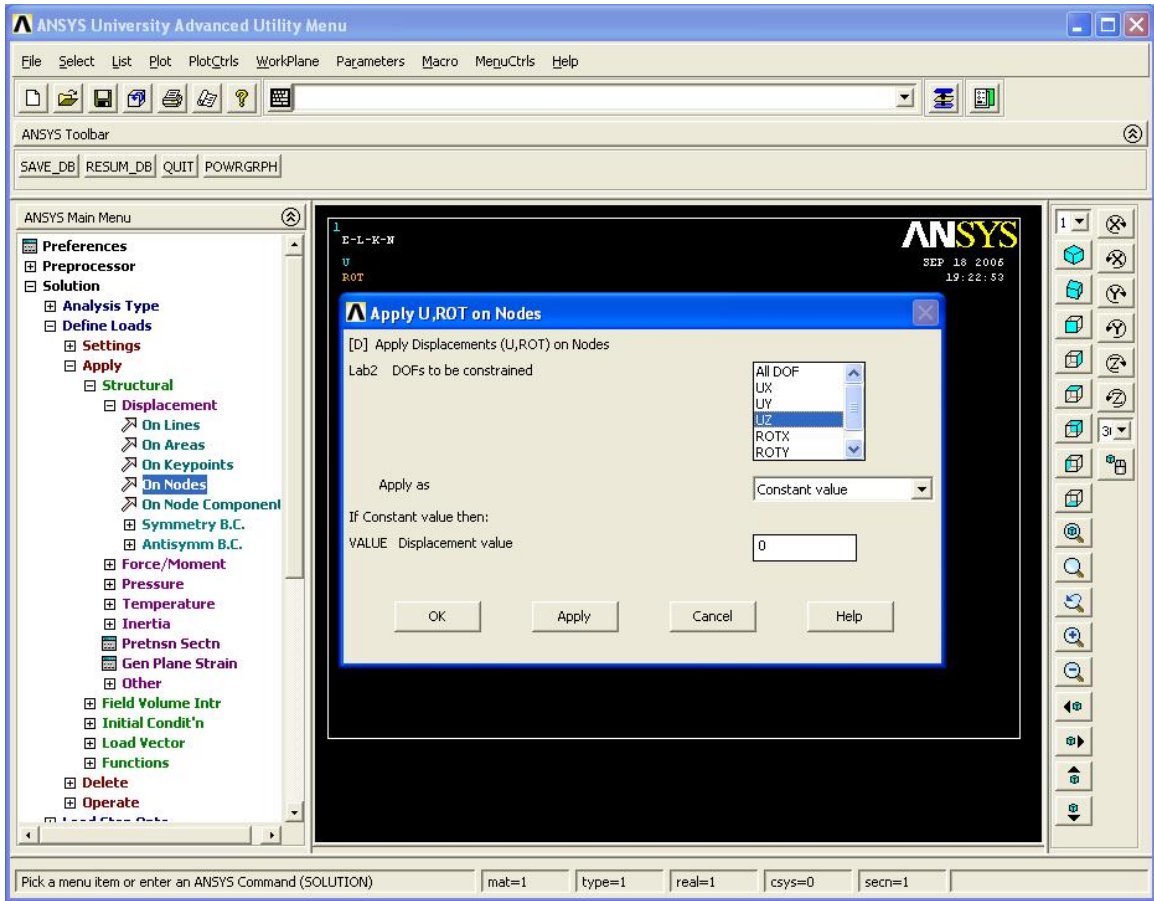


Figure 50: Applying loads to the beam

Appendix B (Continued)

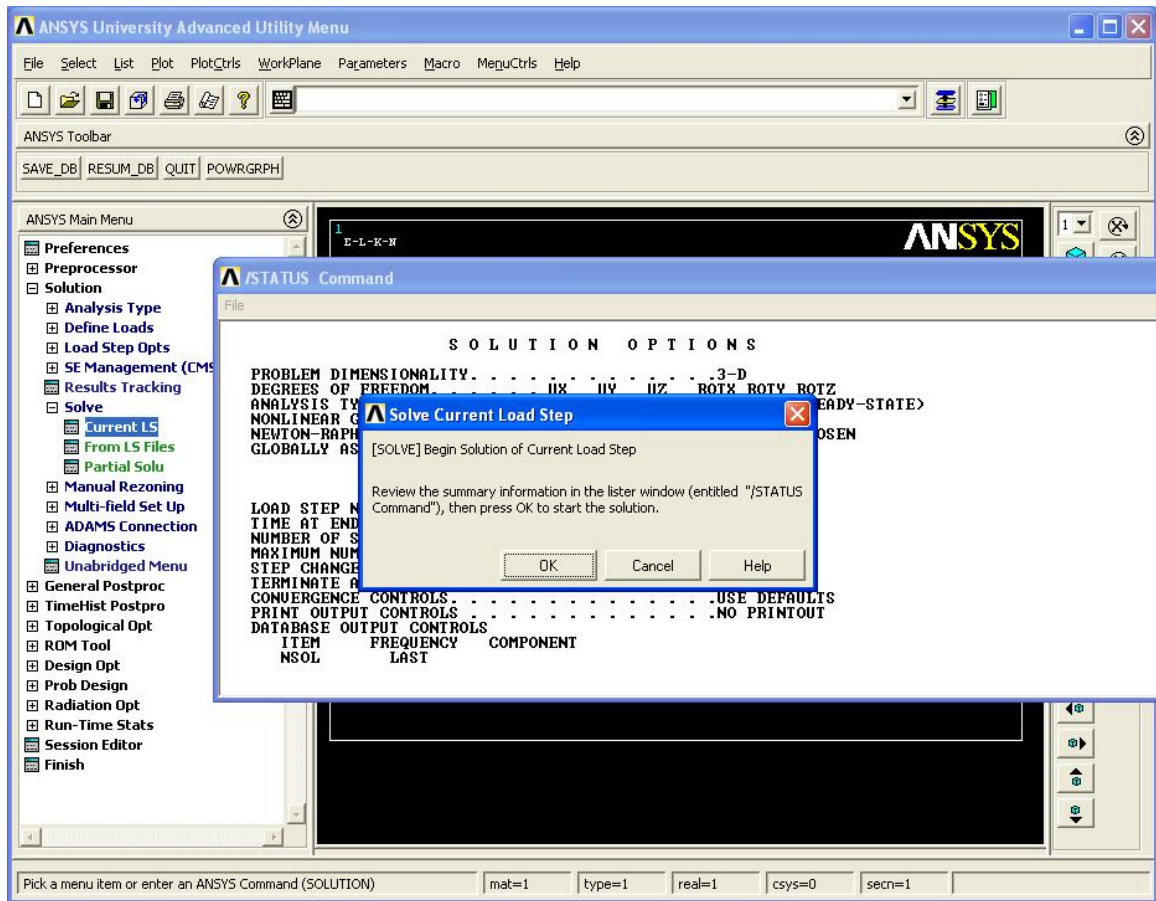


Figure 51: Solve

Appendix B (Continued)

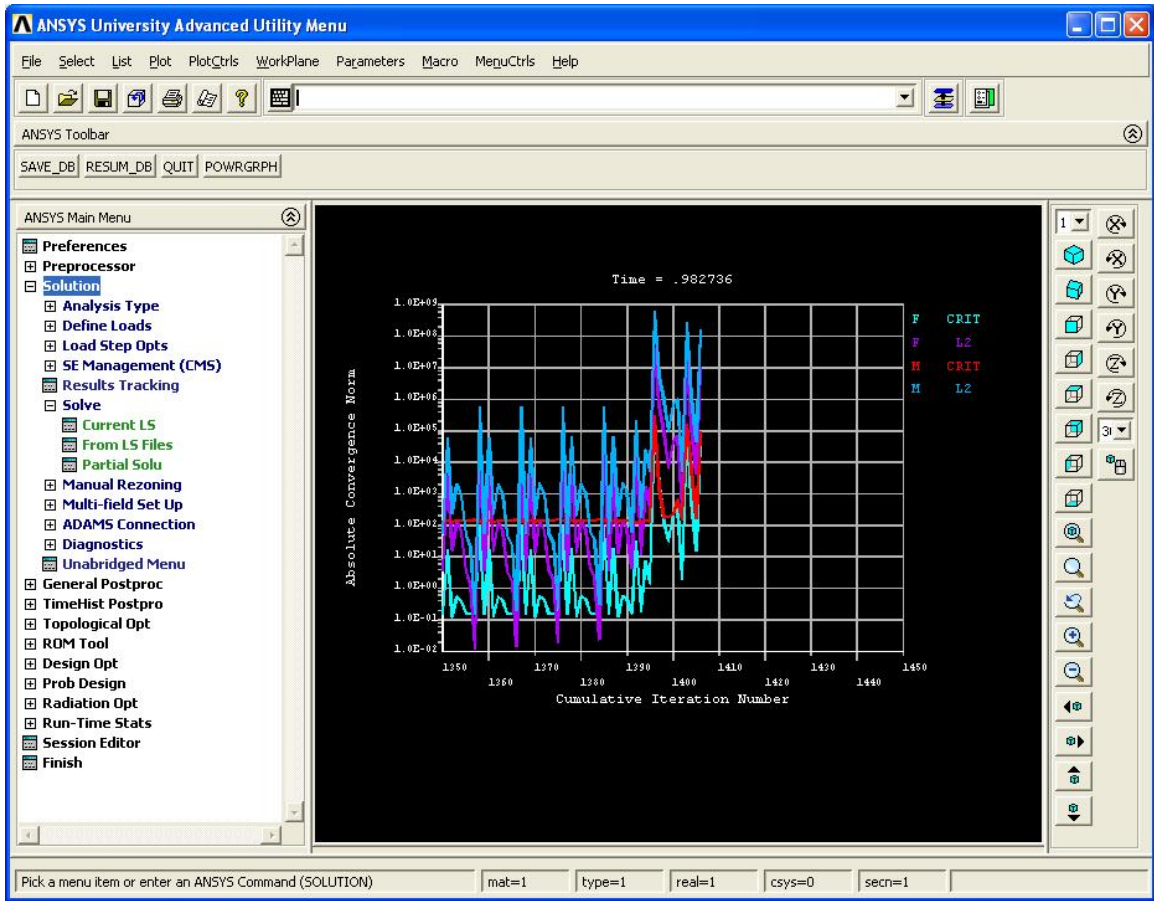


Figure 52: During solve

Appendix B (Continued)

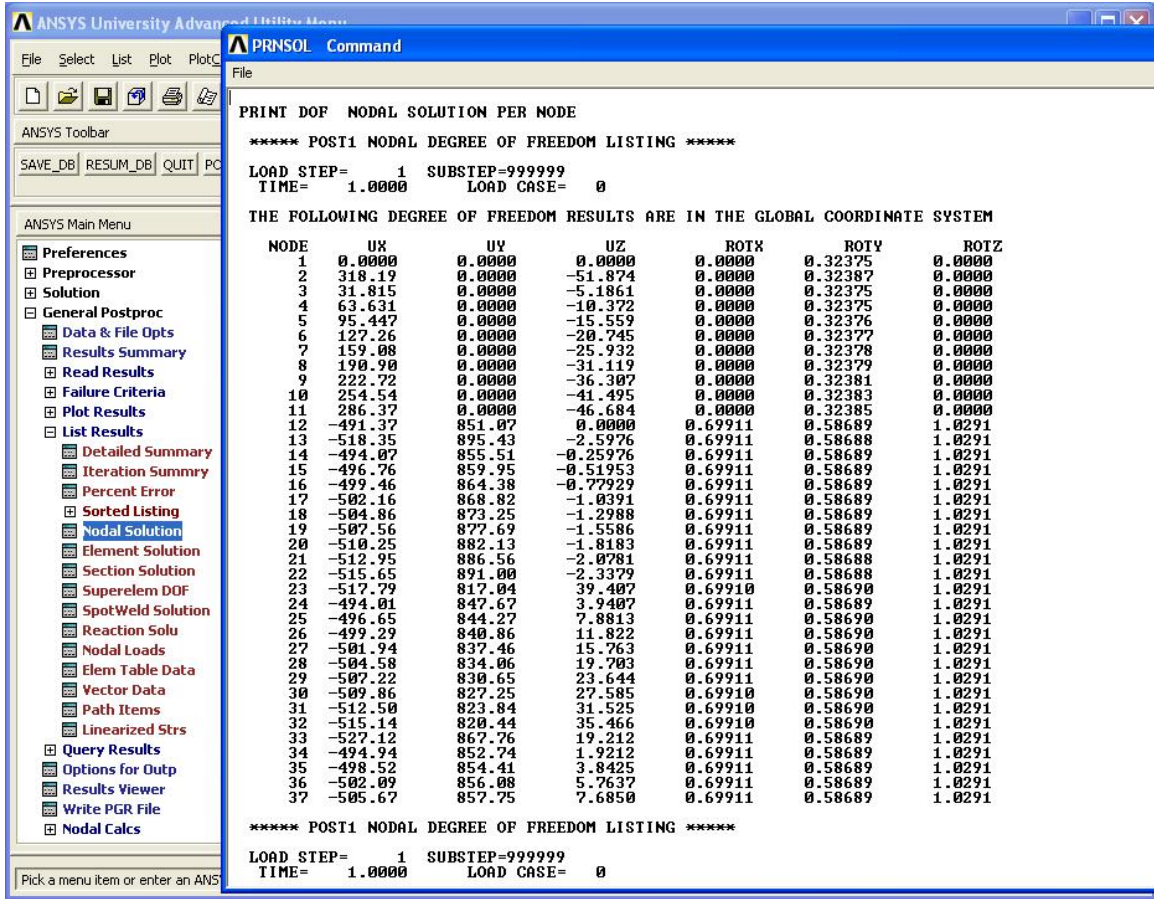


Figure 53: Output

Appendix B (Continued)

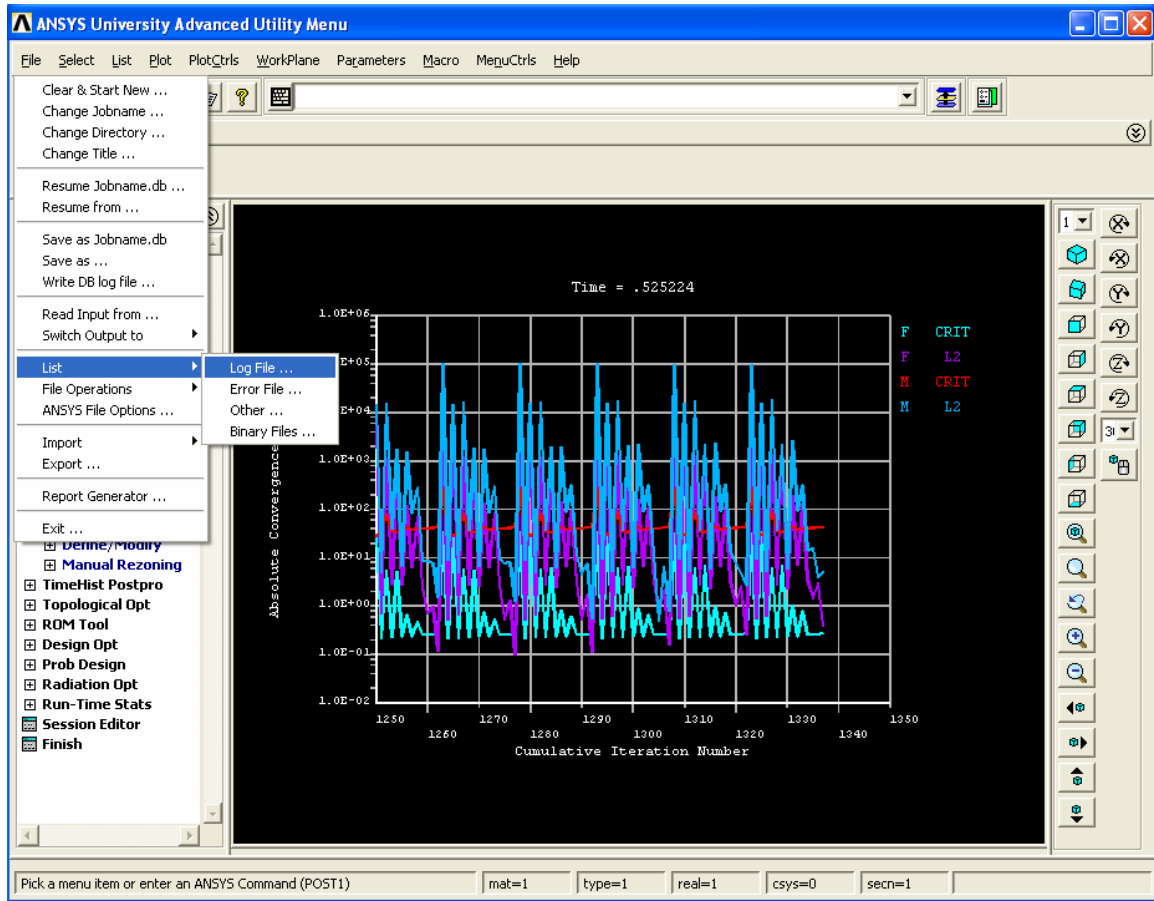


Figure 54: To get the log-file

A log file is obtained and is modified to solve for 200 load steps at a given aspect ratio and arc-length as follows:

```
!*****
/CONFIG,NRES,10000
/CWD,'C:\Documents and
Settings\sjagirda\Directory200steps\arc90_asp0.1'
/NOPR
/PMETH,OFF,0
```


Appendix B (Continued)

KEYW,PR_SET,1

KEYW,PR_STRUC,1

/GO

!*****

/PREP7

R=1000

PI=acos(-1.)

!*****

A1=2500.0

Iy1=520833.333

Iz1=520833.333

E1=300000

!*****

A2= 250.0000037252903

Iy2= 520.8333566163981

Iz2= 52083.33410943548

E2= 300

!*****

ET,1,BEAM4

!*

ET,2,BEAM4

Appendix B (Continued)

!*
/

R,1,A1,Iy1,Iz1, , , ,

RMORE, , , , , ,

!*
/

R,2,A2,Iy2,Iz2, , , ,

RMORE, , , , , ,

!*
/

!*
/

MPTEMP, , , , , , , ,

MPTEMP,1,0

MPDATA,EX,1,,E1

MPDATA,PRXY,1,,0.35

MPTEMP, , , , , , , ,

MPTEMP,1,0

MPDATA,EX,2,,E2

MPDATA,PRXY,2,,0.35

!*****

K,1,0,0,0,

!*****

arclength=90

xcoor=R*cos(arclength*PI/180)

Appendix B (Continued)

zcoor=R*sin(arclength*PI/180)

K,2,xcoor,0,zcoor,

!*****

K,3,1000,0,0,

K,4,1050,0,0,

K,5,1000,50,0,

K,6,1000,0,-50,

/USER, 1

/FOC, 1, 538.256940599 , -110.688686131 , 475.000000000

/REPLO

/VIEW, 1, -0.246365419055 , 0.245754775350 ,

0.937501291032

/ANG, 1, -1.91248212175

/REPLO

/VIEW, 1, -0.378438950955 , 0.367160066605 ,

0.849692559630

/ANG, 1, -4.76219842328

/REPLO

K,7,950,0,0,

/FOC, 1, 427.888273403 , -68.9410891494 , 407.804103704

/REPLO

Appendix B (Continued)

/FOC, 1, 456.194825599 , -81.6519820718 , 425.903867008

/REPLO

/VIEW, 1, -0.455467710156 , 0.439135756168 ,

0.774408776203

/ANG, 1, -7.33131293670

/REPLO

LSTR, 1, 2

LSTR, 3, 4

LSTR, 3, 5

LSTR, 3, 6

LSTR, 3, 7

!*

LARC,2,3,1,1000,

FLST,5,5,4,ORDE,2

FITEM,5,1

FITEM,5,-5

CM,_Y,LINE

LSEL, , , ,P51X

CM,_Y1,LINE

CMSEL,S,_Y

!*

Appendix B (Continued)

```
!*  
  
CMSEL,S,_Y1  
  
LATT,1,1,1, , , ,  
  
CMSEL,S,_Y  
  
CMDELE,_Y  
  
CMDELE,_Y1  
  
!*  
  
FLST,5,1,4,ORDE,1  
  
FITEM,5,1  
  
CM,_Y,LINE  
  
LSEL, , , ,P51X  
  
CM,_Y1,LINE  
  
CMSEL,,_Y  
  
!*  
  
LESIZE,_Y1, , , ,10, , , , ,1  
  
!*  
  
FLST,5,4,4,ORDE,2  
  
FITEM,5,2  
  
FITEM,5,-5  
  
CM,_Y,LINE  
  
LSEL, , , ,P51X
```

Appendix B (Continued)

```
CM,_Y1,LINE
CMSEL,,_Y
!*
LESIZE,_Y1,,,,,1,,,,,1
!*
FLST,2,5,4,ORDE,2
FITEM,2,1
FITEM,2,-5
LMESH,P51X
GPLOT
CM,_Y,LINE
LSEL,,,,,6
CM,_Y1,LINE
CMSEL,S,_Y
!*
!*
CMSEL,S,_Y1
LATT,2,2,2,,,,,
CMSEL,S,_Y
CMDELE,_Y
CMDELE,_Y1
```

Appendix B (Continued)

```
!*  
  
FLST,5,1,4,ORDE,1  
  
FITEM,5,6  
  
CM,_Y,LINE  
  
LSEL, , , ,P51X  
  
CM,_Y1,LINE  
  
CMSEL,,_Y  
  
!*  
  
LESIZE,_Y1, , ,100, , , ,1  
  
!*  
  
LMESH, 6  
  
FINISH  
  
/SOL  
  
ANTYPE,0  
  
NLGEOM,1  
  
NSUBST,10,0,0  
  
OUTRES,ERASE  
  
OUTRES,NSOL,-10  
  
RESCONTRL,DEFINE,ALL,-10,1  
  
FLST,2,1,1,ORDE,1  
  
FITEM,2,1
```

Appendix B (Continued)

```
!*  
  
!*****  
  
/GO  
  
D,1, ,0, , , , UX,UY,UZ,ROTX,ROTZ,  
  
FLST,2,1,1,ORDE,1  
  
FITEM,2,2  
  
!*  
  
/GO  
  
D,2, ,0, , , , UY, , , , ,  
  
FLST,2,1,1,ORDE,1  
  
FITEM,2,12  
  
!*  
  
!*****  
  
/GO  
  
!*****  
  
loadsteps=200  
  
*DO,step,1,loadsteps,1  
  
theta=step*arclength/200  
  
/GO  
  
DDELE,12,ALL  
  
!*****
```


Appendix B (Continued)

```
D,12, ,0, , , ,UZ, , , , ,
FLST,2,1,1,ORDE,1
FITEM,2,12

disp $x$  = -(R-(R*cos(theta*PI/180)))
disp $y$  = R*sin(theta*PI/180)

D,12, ,disp $x$ , , , ,UX, , , , ,
FLST,2,1,1,ORDE,1
FITEM,2,12

!*
/GO

D,12, ,disp $y$ , , , ,UY, , , , ,
FLST,2,1,1,ORDE,1
FITEM,2,12

!*
/GO

D,12, ,theta*PI/180, , , ,ROTZ, , , , ,
LSWRITE,step
*ENDDO

LSSOLVE,1,loadsteps
```

Appendix B (Continued)

```
/STATUS,SOLU

FINISH

!*****

SAVE,'arc90_asp0.1','db','C:\DOCUME~1\SJAGIRDA\Directory200steps
\arc90_asp0.1'

!*****

*do,i,1,200,1,

/POST1

/OUTPUT,arc90_asp0.1,txt,,APPEND

SET,,,,i,,,

FLST,5,6,1,ORDE,4

FITEM,5,1

FITEM,5,-2

FITEM,5,12

FITEM,5,-15

NSEL,S,,P51X

PRNSOL,DOF,

/OUT

*ENDDO

*do,i,1,200,1,

/POST1
```

Appendix B (Continued)

```
/OUTPUT,arc90_asp0.1,m,,APPEND  
SET,,,,i,,  
FLST,5,6,1,ORDE,4  
FITEM,5,1  
FITEM,5,-2  
FITEM,5,12  
FITEM,5,-15  
NSEL,S,, ,P51X  
PRNSOL,DOF,  
/OUT  
*ENDDO  
*do,i,1,200,1,  
/POST1  
/OUTPUT,arc90_asp0.1BETA,txt,,APPEND  
SET,,,,i,,  
FLST,5,6,1,ORDE,4  
NSEL,S,, ,12  
PRNSOL,ROT,Z  
/OUT  
*ENDDO  
*do,i,1,200,1,
```

Appendix B (Continued)

```
/POST1  
  
/OUTPUT,arc90_asp0.1DISPX,txt,,APPEND  
  
SET,,,,i,,,  
  
FLST,5,4,1,ORDE,2  
  
FITEM,5,12  
  
FITEM,5,-15  
  
NSEL,S,, ,P51X  
  
PRNSOL,U,X  
  
/OUT  
  
*ENDDO  
  
*do,i,1,200,1,  
  
/POST1  
  
/OUTPUT,arc90_asp0.1DISPY,txt,,APPEND  
  
SET,,,,i,,,  
  
FLST,5,4,1,ORDE,2  
  
FITEM,5,12  
  
FITEM,5,-15  
  
NSEL,S,, ,P51X  
  
PRNSOL,U,Y  
  
/OUT  
  
*ENDDO
```

Appendix B (Continued)

```
*do,i,1,200,1,  
  
/POST1  
  
/OUTPUT,arc90_asp0.1DISPZ,txt,,APPEND  
  
SET,,,,i,,,  
  
FLST,5,4,1,ORDE,2  
  
FITEM,5,12  
  
FITEM,5,-15  
  
NSEL,S,, ,P51X  
  
PRNSOL,U,Z  
  
/OUT  
  
*ENDDO  
  
*do,i,1,200,1,  
  
/POST1  
  
/OUTPUT,arc90_asp0.1PHI,txt,,APPEND  
  
SET,,,,i,,,  
  
NSEL,S,, ,2  
  
PRNSOL,ROT,Y  
  
/OUT  
  
*ENDDO  
  
FINISH  
  
/EOF
```

Appendix B (Continued)

The respective parameters affected by change in aspect ratio like real constants are then changed in this log file and run separately to obtain respective outputs. The outputs are also limited to the Nodes of interest.

Appendix C Algorithms to Find γ

Algorithm to find γ for load-steps at every one degree

MATLAB Program is as follows.

```
clear all

start=16;

finish=112;

for arclength=start:2:finish

    counter=(arclength+2-start)/2;

    for aspect=0.1:0.1:1

        countas=round(10*aspect);

        %Input

        str1 = [];

        if round(aspect)==aspect,

            str1='.0';

        end

        string =

        ['\arc',num2str(arclength),'_asp',num2str(aspect),str1,'ex.txt'];
```

Appendix C (Continued)

```
fid = fopen(['C:\Documents and
Settings\sjagirda\output\arc',num2str(arclength),string]);

A = fread(fid);

fclose(fid);

G = native2unicode(A)';

s_i = findstr('ROTZ', G);

s_f = findstr('MAXIMUM', G);

cr = native2unicode(10);

space = native2unicode(9);

for j = 1:length(s_i)

    M = strtrim(G(s_i(j)+4:s_f(j)-1));

    M = strrep(M, cr, space);

    M = str2num(M);

    beta(j) =M(3,7);

    PHI(j) =M(2,6);

    B = [ cos(beta(j)) sin(beta(j)) 0 ; -sin(beta(j))
cos(beta(j)) 0 ; 0 0 1 ];

    newcs = [ 50 0 0 ; 0 50 0 ; 0 0 -50 ];

    dispatbeta=[ M(3,2)    M(3,3)    M(3,4) ;

                M(4,2)    M(4,3)    M(4,4) ;
```


Appendix C (Continued)

```
M(5,2)    M(5,3)    M(5,4) ;
M(6,2)    M(6,3)    M(6,4) ];
orgcoord = [ 1000 0 0; 1050 0 0; 1000 50 0;
1000 0 -50];

Finalcoord=dispatbeta+orgcoord;

node12=[
Finalcoord(1,1:3);Finalcoord(1,1:3);Finalcoord(1,1:3);Finalcoord(1,1:
3)];

position_vectorbeta=Finalcoord - node12;
position_vectorbeta(1,:) = [];
A = B*newcs*inv(position_vectorbeta);
thetaobeta(j)=acos(A(2,2));

end

%plot(PHI)
beta(j) =M(3,7);
PHI(j) =M(2,6);
lambda=arclength*pi/180;

BG=zeros(arclength,151);
```

Appendix C (Continued)

```
Beta=0;
for countk=1:1:301
    for countBETA=1:1:arclength
        oldbeta=Beta;
        newbeta=beta(1,countBETA);
        if newbeta==oldbeta
            countBETA=countBETA-1;
            break;
        else
            Beta=newbeta;
            gamma=(countk/2000+.7495);
            gamma_l = gamma*lambda;
            phi=PHI(1,countBETA);
            captheta = atan(tan(Beta)./sin((lambda-phi)-
(lambda-gamma_l)));
            abs_epsilon_e = sqrt((cos(Beta).*cos(phi)-
ones(size(Beta))).^2+(sin(Beta)).^2.*(cos(phi)).^2+(sin(phi)).^2);
            epsilon_ex = cos(Beta).*cos(phi)-1;
            epsilon_ey = sin(Beta);
            epsilon_ez = cos(Beta).*sin(phi);
```

Appendix C (Continued)

```
epsilon_ax = (cos(gamma_l)).^2.*(1-  
cos(capheta))+cos(capheta)-1;  
epsilon_ay = sin(capheta).*sin(gamma_l);  
epsilon_az = sin(gamma_l).*cos(gamma_l).*(1-  
cos(capheta));  
error = sqrt((epsilon_ex-epsilon_ax).^2  
+(epsilon_ey-epsilon_ay).^2 +(epsilon_ez-epsilon_az).^2);  
rel_error = error./abs_epsilon_e;  
  
capheta1(countBETA,countk)=capheta;  
abs_epsilon_e1(countBETA,countk) =  
abs_epsilon_e;  
  
epsilon_ex1(countBETA,countk) = epsilon_ex;  
epsilon_ey1(countBETA,countk) = epsilon_ey;  
epsilon_ez1(countBETA,countk) = epsilon_ez;  
epsilon_ax1(countBETA,countk) = epsilon_ax;  
epsilon_ay1(countBETA,countk) = epsilon_ay;  
epsilon_az1(countBETA,countk) = epsilon_az;  
error1(countBETA,countk)=error;  
rel_error1(countBETA,countk)=rel_error;  
if rel_error <= 0.005
```

Appendix C (Continued)

```
error1(countBETA,countk)=error;
rel_error1(countBETA,countk)=rel_error;
BG(countBETA,countk)=countBETA*countk;
betamax(countk) = Beta;
maxfortheta(countk,countBETA)=Beta;

    else
        break
    end
end
end
end

[y,i] = max(betamax);
gammastar = (i/2000+.7495);
gammastar_l=lambda*gammastar;
[p,q]=max(maxfortheta);
[r,s]=max(q);
Beta=beta(1,s);
phi=PHI(1,s);
thetaostar=thetaobeta(1,s);
```

Appendix C (Continued)

```
capthetastar = atan(tan(Beta)./sin((lambda-phi)-(lambda-  
gammastar_l)));
```

```
CTHETAstar=capthetastar/thetaostar;
```

```
GAMMA_MATRIX(counter,countas)=gammastar;
```

```
CAPTHETA_MATRIX(counter,countas)=capthetastar;
```

```
CTHETA_MATRIX(counter,countas)=CTHETAstar;
```

```
end
```

```
end
```

```
GAMMA_MATRIX;
```

```
CTHETA_MATRIX;
```

```
CAPTHETA_MATRIX;
```

```
figure(1)
```

```
plot(GAMMA_MATRIX)
```

```
figure(2)
```

```
plot(CTHETA_MATRIX)
```

```
figure(3)
```

```
plot(CAPTHETA_MATRIX)
```

Appendix C (Continued)

Algorithm to find γ for 200 load-steps.

```
clear all

start=4;

finish=112;

for arclength=start:2:finish

    arclength

    counter=(arclength+2-start)/2;

    asp=[0.1 0.4 0.7];

    for i=1:3

        aspect=asp(i);

        aspect;

        countas=round(10*aspect);

        %Input

        str1 = [];

        if round(aspect)==aspect,

            str1='.0';

        end

        string =

        ['arc',num2str(arclength),'_asp',num2str(aspect),str1];
```

Appendix C (Continued)

```
fid1 = fopen(['C:\Documents and
Settings\sjagirda\Directory200steps\',string,'\ ',string,'BETA.txt']);

ABT = fread(fid1);

fclose(fid1);

GBT = native2unicode(ABT)';

s_iB = findstr('ROTZ', GBT);

s_fB = findstr('MAXIMUM', GBT);

cr = native2unicode(10);

space = native2unicode(9);

for j = 1:length(s_iB)

    BT = strtrim(GBT(s_iB(j)+4:s_fB(j)-1));

    BT = strrep(BT, cr, space);

    BT = str2num(BT);

    beta(j) =BT(1,2);

end

string =

['arc',num2str(arclength),'_asp',num2str(aspect),str1];

fid2 = fopen(['C:\Documents and
Settings\sjagirda\Directory200steps\',string,'\ ',string,'PHI.txt']);

APH = fread(fid2);
```

Appendix C (Continued)

```
fclose(fid2);

GPH = native2unicode(APH)';
s_iP = findstr('ROTY', GPH);
s_fP = findstr('MAXIMUM', GPH);
cr = native2unicode(10);
space = native2unicode(9);

for j = 1:length(s_iP)
    PH = strtrim(GPH(s_iP(j)+4:s_fP(j)-1));
    PH = strrep(PH, cr, space);
    PH = str2num(PH);
    PHI(j) =PH(1,2);
end

PHI(j);

fid3 = fopen(['C:\Documents and
Settings\sjagirda\Directory200steps\',string,'\ ',string,'DISPX.txt']);

DISPXA = fread(fid3);

fclose(fid3);

DISPXG = native2unicode(DISPXA)';
s_iX = findstr('UX', DISPXG);
s_fX = findstr('MAXIMUM', DISPXG);
```


Appendix C (Continued)

```
fid4 = fopen(['C:\Documents and
Settings\sjagirda\Directory200steps\',string,'\ ',string,'DISPY.txt']);
DISPYA = fread(fid4);
fclose(fid4);
DISPYG = native2unicode(DISPYA)';
s_iY = findstr('UY', DISPYG);
s_fY = findstr('MAXIMUM', DISPYG);

fid5 = fopen(['C:\Documents and
Settings\sjagirda\Directory200steps\',string,'\ ',string,'DISPZ.txt']);
DISPZA = fread(fid5);
fclose(fid5);
DISPZG = native2unicode(DISPZA)';
s_iZ = findstr('UZ', DISPZG);
s_fZ = findstr('MAXIMUM', DISPZG);

cr = native2unicode(10);
space = native2unicode(9);

for j = 1:length(s_iX)
```

Appendix C (Continued)

```
M = strtrim(DISPXG(s_iX(j)+4:s_fX(j)-1));
```

```
M = strrep(M, cr, space);
```

```
M = str2num(M);
```

```
NODE12DISPX =M(1,2);
```

```
NODE13DISPX =M(2,2);
```

```
NODE14DISPX =M(3,2);
```

```
NODE15DISPX =M(4,2);
```

```
N = strtrim(DISPYG(s_iY(j)+4:s_fY(j)-1));
```

```
N = strrep(N, cr, space);
```

```
N = str2num(N);
```

```
NODE12DISPY =N(1,2);
```

```
NODE13DISPY =N(2,2);
```

```
NODE14DISPY =N(3,2);
```

```
NODE15DISPY =N(4,2);
```

```
O = strtrim(DISPZG(s_iZ(j)+4:s_fZ(j)-1));
```

```
O = strrep(O, cr, space);
```

```
O = str2num(O);
```

```
NODE12DISPZ =O(1,2);
```

```
NODE13DISPZ =O(2,2);
```

Appendix C (Continued)

NODE14DISPZ =O(3,2);

NODE15DISPZ =O(4,2);

B = [cos(beta(j)) sin(beta(j)) 0 ; -sin(beta(j))
cos(beta(j)) 0 ; 0 0 1];

newcs = [50 0 0 ; 0 50 0 ; 0 0 -50];

dispatbeta=[NODE12DISPX NODE12DISPY
NODE12DISPZ ;

 NODE13DISPX NODE13DISPY

NODE13DISPZ ;

 NODE14DISPX NODE14DISPY

NODE14DISPZ ;

 NODE15DISPX NODE15DISPY

NODE15DISPZ];

orgcoord = [1000 0 0; 1050 0 0; 1000 50 0;
1000 0 -50];

Finalcoord=dispatbeta+orgcoord;

node12=[

Finalcoord(1,1:3);Finalcoord(1,1:3);Finalcoord(1,1:3);Finalcoord(1,1:
3)];

position_vectorbeta=Finalcoord - node12;

Appendix C (Continued)

```
position_vectorbeta(1,:) = [];  
A = B*newcs*inv(position_vectorbeta);  
thetaobeta(j)=acos(A(2,2));  
  
end  
  
lambda=arclength*pi/180;  
  
BG=zeros(arclength,151);  
Beta=0;  
for countk=1:1:501  
    for countBETA=1:1:200  
        oldbeta=Beta;  
        newbeta=beta(1,countBETA);  
        if newbeta==oldbeta  
            countBETA=countBETA-1;  
            break;  
        else  
            Beta=newbeta;  
            gamma=(countk/2000+.7495);  
            gamma_l = gamma*lambda;  
            phi=PHI(1,countBETA);
```

Appendix C (Continued)

```
sincaptheta=sin(Beta)./sin(gamma_l);  
coscaptheta=tan((lambda-phi)-(lambda-  
gamma_l)).*cot(gamma_l);  
%           captheta = atan(tan(Beta)./sin((lambda-phi)-  
(lambda-gamma_l)));  
           captheta = atan2(sincaptheta,coscaptheta);  
  
           abs_epsilon_e = sqrt((cos(Beta).*cos(phi)-  
ones(size(Beta))).^2+(sin(Beta)).^2.*(cos(phi)).^2+(sin(phi)).^2);  
           epsilon_ex = cos(Beta).*cos(phi)-1;  
           epsilon_ey = sin(Beta);  
           epsilon_ez = cos(Beta).*sin(phi);  
           epsilon_ax = (cos(gamma_l)).^2.*(1-  
cos(captheta))+cos(captheta)-1;  
           epsilon_ay = sin(captheta).*sin(gamma_l);  
           epsilon_az = sin(gamma_l).*cos(gamma_l).*(1-  
cos(captheta));  
           error = sqrt((epsilon_ex-epsilon_ax).^2  
+(epsilon_ey-epsilon_ay).^2 +(epsilon_ez-epsilon_az).^2);  
           rel_error = error./abs_epsilon_e;
```

Appendix C (Continued)

```
captheta1(countBETA,countk)=captheta;
abs_epsilon_e1(countBETA,countk) =
abs_epsilon_e;

epsilon_ex1(countBETA,countk) = epsilon_ex;
epsilon_ey1(countBETA,countk) = epsilon_ey;
epsilon_ez1(countBETA,countk) = epsilon_ez;
epsilon_ax1(countBETA,countk) = epsilon_ax;
epsilon_ay1(countBETA,countk) = epsilon_ay;
epsilon_az1(countBETA,countk) = epsilon_az;
error1(countBETA,countk)=error;
rel_error1(countBETA,countk)=rel_error;
if rel_error <= 0.005
    error1(countBETA,countk)=error;
    rel_error1(countBETA,countk)=rel_error;
    BG(countBETA,countk)=countBETA*countk;
    betamax(countk) = Beta;
    maxfortheta(countk,countBETA)=Beta;

else
    break
end
```

Appendix C (Continued)

```
end  
end  
end  
  
[y,i] = max(betamax);  
gammastar = (i/2000+.7495);  
gammastar_l=lambda*gammastar;  
[p,q]=max(maxfortheta);  
[r,s]=max(q);  
Beta=beta(1,s);  
phi=PHI(1,s);  
thetaostar=thetaobeta(1,s);  
  
sincapthetastar=sin(beta)./sin(gammastar_l);  
coscapthetastar=tan((lambda-PHI)-(lambda-  
gammastar_l)).*cot(gammastar_l);  
capthetastar = atan2(sincapthetastar,coscapthetastar);  
% capthetastar =atan2(tan(beta),sin((lambda-PHI)-  
(lambda-gammastar_l)));  
[p2,s2] = polyfit(capthetastar(1:s),thetaobeta(1:s),1);
```

Appendix C (Continued)

```
CTHETAstar=p2(1);

GAMMA_MATRIX(counter,countas)=gammastar;

CAPTHETA_MATRIX(counter,countas)=capthetastar(s)*(180/pi);

CTHETA_MATRIX(counter,countas)=CTHETAstar;

end

%plot([0.1:.1:1],GAMMA_MATRIX(arclength,:));

%drawnow

end

GAMMA_MATRIX;

CTHETA_MATRIX;

CAPTHETA_MATRIX;

figure(1)

plot([4:2:112],GAMMA_MATRIX)

xlabel('arc length , \lambda (degrees)')

ylabel('Characteristic radius factor, \gamma')

figure(2)

plot([4:2:112],CTHETA_MATRIX)

xlabel('arc length, \lambda (degrees)')
```


Appendix C (Continued)

```
ylabel('Parametric angle coefficient, C_\Theta')
```

```
figure(3)
```

```
plot([4:2:112],CAPTHETA_MATRIX)
```

```
xlabel('arc length, \lambda (degrees)')
```

```
ylabel('Parameterization limit, \Theta_{max} (degrees) for the  
parametric angle coefficient, C_\Theta_{max}')
```

Appendix D Summary

Table 1: Spherical PRBM

$\alpha = (1 - \gamma)\lambda + \tan^{-1}(\tan \gamma\lambda \cos \Theta)$
$\beta = \sin^{-1}(\sin \gamma\lambda \sin \Theta)$
$\theta_0 = C_\theta \Theta$
$\Theta = \tan^{-1}\left[\frac{\tan \beta}{\sin[(\lambda - \phi) - (\lambda - \gamma\lambda)]}\right]$
$\varepsilon_e = \{[\cos \beta \cos \phi - 1]^2 + \sin^2 \beta + [\cos \beta \sin \phi]^2\}^{1/2}$
$\varepsilon_a = \{[\cos \gamma\lambda(1 - \cos \Theta) + \cos \Theta]^2 + [\sin \Theta \sin \gamma\lambda]^2 + [\sin \gamma\lambda \cos \gamma\lambda(1 - \cos \Theta)]^2\}^{1/2}$
$error = \{[(\cos \beta \cos \phi - 1) - (\cos \gamma\lambda(1 - \cos \Theta) + \cos \Theta - 1)]^2 + [\sin^2 \beta - \sin \Theta \sin \gamma\lambda][\cos \beta \sin \phi - \sin \gamma\lambda \cos \gamma\lambda(1 - \cos \Theta)]^2\}^{1/2}$
$\frac{error}{ \varepsilon_e } = \frac{[(\cos \beta \cos \phi - 1) - (\cos \gamma\lambda(1 - \cos \Theta) + \cos \Theta - 1)]^2 + [\sin^2 \beta - \sin \Theta \sin \gamma\lambda][\cos \beta \sin \phi - \sin \gamma\lambda \cos \gamma\lambda(1 - \cos \Theta)]^2}{\{[\cos \beta \cos \phi - 1]^2 + \sin^2 \beta + [\cos \beta \sin \phi]^2\}^{1/2}}$

For small angles when the sphere has a very large radius the above formulas can be approximated to the planar case.

Appendix D (Continued)

Table 2: Planar PRBM

$a = l(1 - \gamma(1 - \cos \Theta))$
$b = \gamma l \sin \Theta$
$\theta_0 = C_\theta \Theta$
$\Theta = \tan^{-1} \frac{b}{a - l(1 - \gamma)}$
$\delta_e = \sqrt{(l - a)^2 + b^2}$
$\delta_a = \sqrt{[\gamma l(1 - \cos \Theta)]^2 + (\gamma l \sin \Theta)^2}$
$error = \sqrt{\{(a/l) - [1 - \gamma(1 - \cos \Theta)]\}^2 + [(b/l) - \gamma \sin \Theta]^2}$
$\frac{error}{\varepsilon_e} = \frac{\sqrt{\{(a/l) - [1 - \gamma(1 - \cos \Theta)]\}^2 + [(b/l) - \gamma \sin \Theta]^2}}{\sqrt{(1 - a/l)^2 + (b/l)^2}}$